DYNAMICS OF NEUTRALLY BUOYANT INFLATABLE VISCOELASTIC CANTILEVERS IN THE OCEAN ENVIRONMENT

by

DAVID TAT-SANG POON

B.A.Sc., University of British Columbia, 1974

A THESIS SUBMITTED IN PARTIAL FULFILMENT OF THE REQUIREMENTS FOR THE DEGREE OF MASTER OF APPLIED SCIENCE

in the Department

of

Mechanical Engineering

We accept this thesis as conforming to the required standard

THE UNIVERSITY OF BRITISH COLUMBIA

October, 1976

In presenting this thesis in partial fulfilment of the requirements for an advanced degree at the University of British Columbia, I agree that the Library shall make it freely available for reference and study. I further agree that permission for extensive copying of this thesis for scholarly purposes may be granted by the Head of my Department or by his representatives. It is understood that publication, in part or in whole, or the copying of this thesis for financial gain shall not be allowed without my written permission.

DAVID TAT-SANG POON

Department of Mechanical Engineering

The University of British Columbia,
Vancouver, B.C.,
Canada, V6T 1W5.

Date Nov. 24/76

ABSTRACT

Statics and dynamics of the neutrally buoyant inflated viscoelastic cantilevers constituting a submarine detection system is investigated. Two geometries of the thin-walled beams are considered: uniform circular cylindrical and circular tapered. The static flexural behaviour of the beam is studied using the three parameter viscoelastic solid model which yields material properties for the mylar-polyethylene-mylar plastic film used. Results of a detailed experimental program are also presented to substantiate validity of the analytical model. This is followed by free vibration analyses of the inflated cantilevers in the ocean environment accounting for the added inertia and nonlinear hydrodynamic drag. For the uniform cylindrical beam, thin-shell theories are employed to account for the inflation effects on the free vibration characteristics. A significant feature of the analysis is the reduction of the shell equations (the membrane, Flügge's, and Herrmann-Armenàkas') into a single equation which is similar in form to that for a vibrating beam with rotary inertia effects. The natural frequencies obtained are compared with the experimental results and those predicted by the Rayleigh-Ritz method in conjunction with the Washizu and membrane shell theories. The analyses show, and experimental program confirms, that Flügge's shell equation in the reduced form is capable of predicting free vibration behaviour quite accurately. However, the reduction technique should be applied with care, since

in several cases it leads to misleading results (e.g. in the case of Herrmann-Armenàkas theory). For the tapered case the elementary beam theory is used to predict their natural frequencies. Next, the dynamical response of the uniform and tapered cantilevers to root excitation, at the fundamental wave frequency and its second harmonic, is studied. The governing nonlinear equations are analyzed by taking two terms of the assumed Fourier series solution. Results suggest that for the case of the simple harmonic excitation, the nonlinear hydrodynamic drag introduces no superharmonic components into the response. For low forcing frequencies typical of the ocean environment, an increase in taper ratio tends to reduce the tip amplitudes. However, for frequencies above the fundamental, the response characteristics are completely reversed. The analysis provides valuable information concerning the system parameters leading to critical response and hence should prove useful in the design of inflatable members employed in the submarine detection system.

TABLE OF CONTENTS

Chapter Page

LIST OF ILLUSTRATIONS

FIGURES

Figures

TABLES

ACKNOWLEDGEMENT

The author wishes to thank his colleagues for their valuable suggestions and criticisms. He is particularly grateful to Dr. Arun K. Misra for the selfless sharing of his knowledge and experience. Above all, the author is deeply indebted to Dr. V.J. Modi, his supervisor, for the guidance given throughout the preparation of this thesis. His help and encouragement have made the accomplishment possible.

Finally, to his wife Alice, the author owes his deep gratitude for her unfailing patience and understanding during the many cheerless moments of this undertaking.

The investigation reported herein was supported by the Defence Research Board of Canada, Grant No. 9550-38, and the National Research Council of Canada, Grant No. A-2181.

LIST OF SYMBOLS

A_i	coefficients in the reduced shell Equation (3.7)
A_w	cross-sectional area of water inside an inflated beam
A_{w_r}	cross-sectional area of water inside an inflated beam at root
B_i	nondimensionalizing constants, Equation (3.16)
C	shell bending stiffness, $Eh/(1-\nu^2)$
C_i	coefficients in solution for zero drag, Equations (3.22) and (3.24)
C_d, C_m	drag and added inertia coefficients, respectively
C_{ki}	coefficients in the eigenfunction expansion of $\frac{d^2\Phi_k}{d\xi^2}$, Equation (3.33b)
$\bar{C}_{nj}$	cosine-component of forced response, Equation (4.6a)
C^*_{nj}	cosine-component of excitation, Equation (4.6c)
D	determinant of operator [L], Equation (3.2)
D_{ij}	minors of determinant D
E	Young's modulus
E_1, E_2, ν_2	parameters in linear viscoelastic solid model
$E^*(\omega)$	complex modulus
F	tip load
F_d	hydrodynamic drag force acting on an element of a beam, Equation (3.15)
F_H	total hydrodynamic force acting on an element of a beam, Equation (3.58b)

G	parameter, $\rho a^2(1-\nu^2)/E$
$\bar{G}$	shear modulus
H	amplitudes of forced response, Equation (4.10a)
I	moment of inertia of the beam cross-section
I_i	integrals, Equations (4.8)
I_r	moment of inertia of the beam cross-section at root
$J_s(t)$	creep compliance in shear
K_r	normalizing multiplier, Equation (3.25)
L	length of cantilever beam
L_{ij}	matrix elements of differential operator [L], Equation (3.1)
N_x	axial prestress due to internal pressure, pa/2
N_θ	circumferential prestress due to internal pressure, pa
P	dimensionless pressure, pa/(Eh)
R_{ij}	amplitudes of forced response, Equation (4.10b)
$\bar{S}_{nj}$	sine-component of forced response, Equation (4.6b)
S^*_{nj}	sine-component of excitation, Equation (4.6d)
T	kinetic energy of shell
U	potential energy of shell
a	radius of beam
c_i	tracers, i = 1, 2, 3
d	diameter of beam
d_r	diameter of beam at root
d_t	diameter of beam at tip

e_x, e_θ	axial and circumferential strains of a shell section, respectively, Equations (3.50)
h	thickness of beam
k	taper ratio, $(d_r-d_t)/d_r$
p	internal pressure
s	dimensionless axial co-ordinate, $\tilde{x}/a$, Chapter 3
t	time
$\tilde{t}$	time variable, Equation (3.29)
v	transverse velocity of a beam
w	flexural displacement of beam
$w_{v.e.}$	viscoelastic flexural displacement of beam
x, y, z	orthogonal displacement components in axial, circumferential, and radial directions, respectively, Figure 3-1
$\tilde{x}$	axial co-ordinate for cylindrical shell, Figure 3-1
$\tilde{z}$	distance from the middle surface of a shell section
Γ	potential function
$\Phi_i(\xi)$	eigenfunctions of a cantilever
$\Psi_i(\xi)$	eigenfunctions of a clamped-pinned beam
Ω	dimensionless frequency, Equation (3.57b)
α	damping parameter of beam, Equation (3.17b)
β	mode shape of zero drag solution, Equation (3.22b)
β_{irs}	constant, Equation (3.40b)
$\gamma(\omega)$	dimensionless viscoelastic damping coefficient

$\bar{\gamma}(\omega)$	viscoelastic loss factor, Equation (4.1d)
δ	real part of complex modulus, Equation (4.1c)
ε_x, ε_θ	axial and circumferential middle surface strains, respectively
η	dimensionless transverse displacement, w/d
θ	circumferential co-ordinate, Figure 3-1
κ_x, κ_θ	axial and circumferential curvatures, respectively, Equations (3.52)
λ_i	dimensionless natural frequency of tapered beam, $\left((1+C_m)\rho_w A_{w_r} L^4 \omega_i^2/(EI_r)\right)^{1/2}$
λ, λ', λ''	solutions to frequency equations (3.23)
λ_k^*	principal stretches, k = 1, 2, 3
μ_r	eigenvalues of a cantilever
ν	Poisson's ratio
ξ	dimensionless distance from root (clamped end) of a cantilever
ρ, ρ_w	mass densities of tube wall and water, respectively
σ_x, σ_θ, $\sigma_{x\theta}$	vibratory stresses, Equations (3.47)
σ_x^i, σ_θ^i, $\sigma_{x\theta}^i$	initial stresses due to internal pressure, Equation (3.49)
σ_{ij}	stress tensor
τ	dimensionless time, Equation (3.16)
υ_r	eigenvalues of a clamped-pinned beam
χ_k	integrals, p. 100
ω	frequency

Dots indicate differentiation with respect to τ. Primes, unless otherwise specified, denote differentiation with respect to ξ.

1. INTRODUCTION

1.1 Preliminary Remarks

There has been considerable attention given lately to the behaviour of thin pressure-stabilized shell structures, commonly called inflatable shells. Besides their abilities to resist loads efficiently by normal tensile stresses, inflatable shells have the advantages of being lightweight, compact, and collapsible, implying ease in transportation and erection for service. The state-of-the-art in inflatable shell research is summarized by Leonard[1], who, in his conclusions, recommended more efforts to study:

(i) interaction of the shells to their embedding media;

(ii) material related problems, e.g., determining the best materials from both the strength and the environmental stability aspects.

Inflatable shells have already exhibited their potential in the design of structural components for aerospace and oceanographic systems. Brauer[2] has discussed in considerable details, which include design and performance data, a variety of inflatable structures having aerospace application. They include the propellent tank of the Atlas intercontinental ballistic missile, the gigantic U.S. balloon satellites Echo I and II, and the experimental paragliders as a decelerating device for atmospheric re-entry. On the other hand, neutrally buoyant inflated structures have been proposed for

underwater applications like submarine detection, oceanographic survey, lifting surfaces of hydrofoils, etc.

Of particular interest is the use of sonobuoys in submarine detection systems. Sonobuoys are passive listening devices conventionally housed in a cylinder about 0.9m (3 ft.) long and 12.7 to 15.3 cm (5 to 6 in.) in diameter. The containers are deposited from an aircraft in the area of interest. Upon hitting the water, a hydrophone attached by a cable to the floating container is released. All acoustic signals received at the hydrophone are relayed back to the aircraft via a transmitter. Since the target emits signals on an unknown time-base, at least three or four hydrophones are needed to locate it in two or three dimensions, respectively.

The sonobuoy has a preset lifetime after which it turns itself off and sinks. Extensive research has established that the efficiency of this operation can be improved by using an array of inflatable tubes, each carrying a hydrophone at one end and joined to a pump-equipped central head at the other (Figure 1-1). The target can then be located through processing of signals received by the array, provided the position and orientation of the array are known.

The optimal design of such a submarine detection system requires a knowledge of its response to environmental loads such as ocean currents, waves and other local disturbances. The general

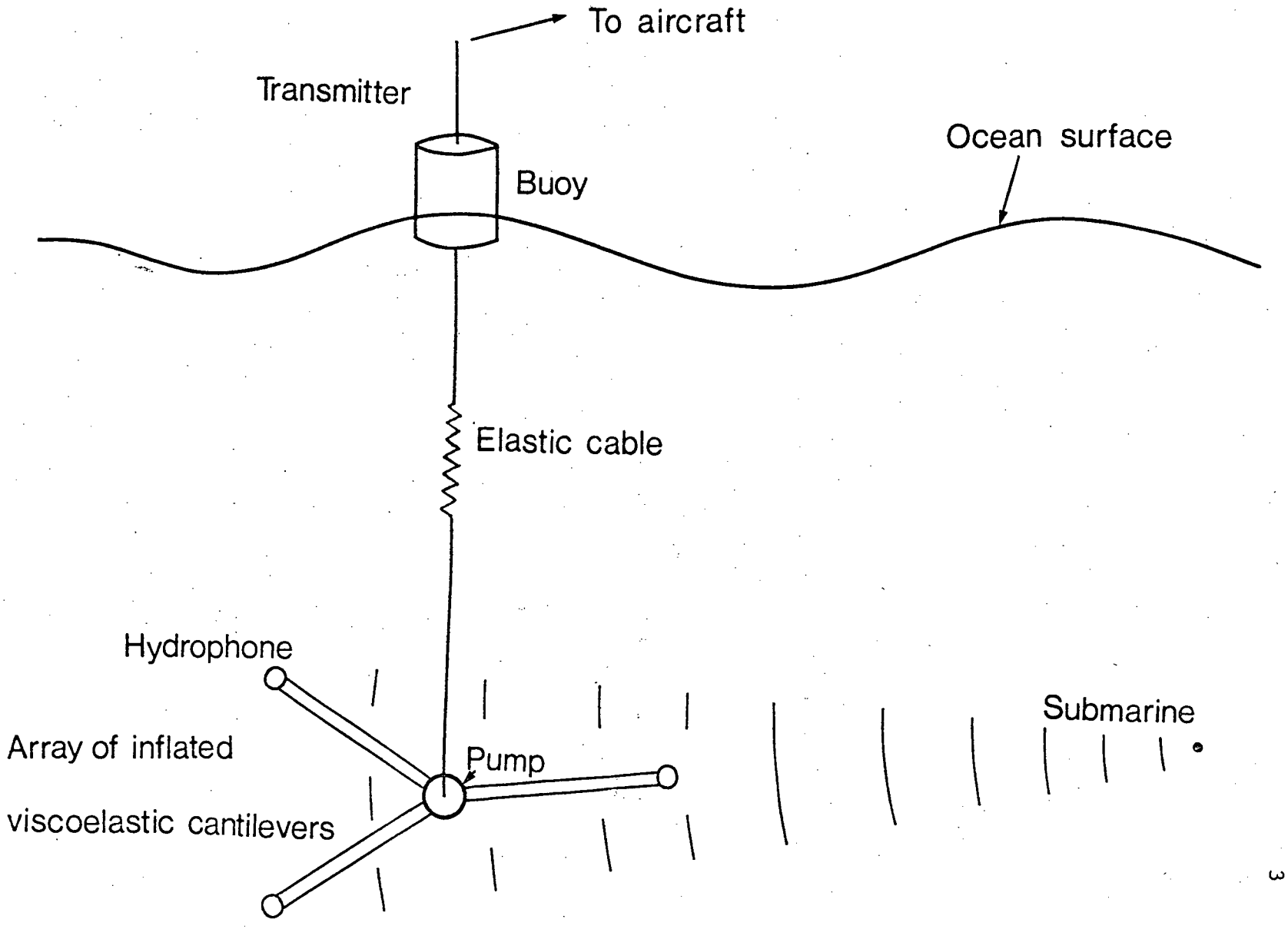

Figure 1-1 Schematic diagram of a submarine detection system using an array of neutrally buoyant inflatable cantilevers

motion of the system is quite complex because of the large number of degrees of freedom involved[3]: the rolling and spatial oscillations of the buoy superimposed on its drifting, three dimensional motion of the flexible cable, and the coupled inplane and out of plane flexural-rotational motions of the array itself.

1.2 Literature Review

The interest in inflatable structures is of relatively recent origin. Leonard, Brooks and McComb[4] were probably the first to calculate the collapse and buckling loads for inflated cylindrical cantilever beams. Buckling in the form of wrinkles occurs when compressive bending stress balances the tensile stress due to internal pressure. As the load is increased the wrinkles progress around the cross section, and collapse occurs when they propagate all the way to the other extreme. Assuming the collapsing root to fold like a plastic hinge, the critical tip load was found to be $F=\pi pa^3/L$, where p is internal pressure, and a and L are the radius and length of the beam, respectively. The test data presented showed good agreement with this equation. Stein and Hedgepeth[5] derived a theory to predict the structural behaviour of wrinkled membranes. It was shown that membrane structures retain much of their stiffness at loads substantially above that at which wrinkling first occurs. Comer and Levy[6] studied the tip deflections and maximum stresses of inflated cylindrical cantilever beams for loads between incipient buckling and final collapse. Topping[7] analyzed the buckling of

inflated plates and columns by deriving a relation between shear stiffness and inflation pressure accounting for beam edge effects. He concluded that the inflation pressure can be treated as an effective shear modulus. All these investigators observed that the flexural stiffness is essentially independent of internal pressure. This is true if the deformation is small and the yield strength of the material is not exceeded.

A theory for the case of small deformation superposed on known finite deformations of a thin, homogeneous, elastic membrane was formulated by Corneliussen and Shield[8]. Small deformations of a circular cylindrical tube subjected to finite homogeneous extension and inflation were considered as an example. A circular membrane shell prestressed by internal pressure and by axial tension has been studied by Huang[9]. The behaviour of the membrane subjected to a radial line load was considered in detail. Using the theory of incremental deformations, Douglas[10] investigated the effect of finite inflation on the subsequent response of a circular cylindrical cantilever to bending loads. The analysis accounted for changing geometry and material properties during inflation. It was observed that for small inflation the pressure and inflation stretch are nearly linearly related. The effect of internal pressure on the influence coefficients of cylindrical shells subjected to axisymmetric edge loads was studied by Narasimhan[11]. Using the stress-deformation equations formulated by Nachbar[12], curves of influence coefficients for various edge loads were obtained. Koga[13] also presented a system of linear constitutive

equations for small strain deformations superimposed upon a known state of finite deformation. The equations were applied to an inflated circular cylindrical membrane subjected to pure bending. These investigations are limited to materials with time-independent properties.

A knowledge of the hydrodynamic forces acting on a vibrating cylinder is essential to the study of its underwater dynamics. A number of model and prototype investigations devoted to force data is summarized by Wiegel[14]. The conventional Morison's type equation, derived independently by Morison et al.[15] and Keulegan and Carpenter[16], assumes that the total hydrodynamic force can be obtained by linearly combining the drag and added inertia components, and is virtually universally used in this class of investigations. Keulegan and Carpenter investigated the drag and inertia coefficients of cylinders in simple sinusoidal currents and correlated them with the period parameter $U_m T/D$, where U_m is the maximum intensity of the sinusoidal current, T is the period of the wave, and D is the diameter of the cylinder. They observed that the drag and mass coefficients show opposite behaviours over the range of the period parameter considered, but the sum of the two forces deviates relatively little from the average value. Stelson and Mavis[17] studied the virtual mass of long circular cylinders oscillating in water and found that for cylinders with large length to diameter ratios the added mass approaches unity, as predicted by potential flow analysis. Jen[18] observed, experimentally,

that the forces exerted by uniform periodic waves in relatively deep water give an average added mass coefficient of 1.04. Laird et al.[19] and Toebes et al.[20] assumed a constant mass coefficient and included all its deviations from unity in the variation of the drag coefficient. The forces on cylinders having constant acceleration and deceleration have been measured by Laird et al. Although the drag coefficient was found to change, the variations were not substantial. Toebes et al. measured the hydrodynamic forces on a transversely oscillating cylinder with its axis perpendicular to the mean flow direction. The drag coefficient was observed to deviate substantially from the theoretical value if the vibrational frequency was close to the Strouhal frequency. However, the deviations were small for frequencies far from the Strouhal frequency. Using a similar concept, Protos et al.[21] also considered a fixed apparent mass and studied the variation of the remaining force with the frequency ratio (ratio of the natural frequency of the cylinder to the Strouhal frequency). In another study, Laird et al.[22] demonstrated that wave forces on a circular cylinder could be influenced significantly by eddy-shedding from neighbouring cylinders.

In contrast to the extensive literature on apparent mass effects for a rigid cylinder in a fluid, the corresponding studies for a flexible cylinder are relatively scarce. Landweber[23,24] and Warnock[25] investigated dynamics of an elastic cylinder in an incompressible, inviscid fluid to determine the apparent mass effects. However, the potential flow assumed discounted any hydrodynamic damping forces. The flexural vibration of an inflated cylindrical

cantilever in air has been studied by Douglas[26], and Corneliussen and Shield[8]. Misra[3], on the other hand, investigated an inflated viscoelastic cantilever vibrating in water. In the study a detailed analysis of the cylindrical cantilever in the presence of hydrodynamic drag and a tensile follower force was given. However, the elementary beam theory employed does not account for the circumferential stress induced by the internal pressure. Modifications of the Timoshenko beam equations for thin-walled tubes to account for normal pressure and Poisson ratio effects were made by Simmonds[27]. The study was confined to open-ended tubes as there was no axial initial stress terms present.

To fully account for the stresses arising due to internal pressure, one has to resort to thin shell theory. However, only a small portion of the vast amount of available literature on shell vibrations is concerned with the beam-bending mode of interest here. The reason may be that, as pointed out by Forsberg[28], for relatively long shells without internal pressure, the beam-bending mode analysis can be considerably simplified without much loss of accuracy by considering the shell as a thin-walled beam and applying the beam theory. Kornecki[29] has shown that, for the beam-bending mode of shells without internal pressure, the Goldenveizer shell equations[30] reduce to an equation very similar to the one for the transverse vibrations of a beam with rotary inertia included.

Incorporating initial stress effects due to internal pressure

requires a generalization of the equations of motion for thin shells. Various shell equations accounting for initial stresses have been collected and listed in a monograph by Leissa[31]. Because of the relative mathematical simplicity, the vast majority of studies made to date have dealt with shells having their boundaries supported by "Shear-Diaphragms" (SD). Straight-forward methods for handling other edge conditions, including an exact procedure, are available but have been sparingly applied because of the great deal of effort required. Reissner[32] and Vlasov[33] have independently shown that in the case of the SD-SD shells, use of the Donnell-Mushtari theory and neglecting tangential inertia, give rise to simple formulas, which directly relate frequencies for the unloaded and uniformly prestressed shells. Using the Flügge theory, Greenspon[34] also arrived at a relation between the natural frequencies of the pressurized and unloaded shells, and concluded that an internal pressure will always give an increase in natural frequency. This is in variance with the results given by Baron and Bleich[35] for the beam-bending mode. However, for other modes their results approach the values predicted by Greenspon. DiGiovanni and Dugundji[36], using the Washizu shell equations[31], analyzed pressurized SD-SD shells by the exact method. For the beam-bending mode the frequency was found to be virtually independent of internal pressure, especially for short shells. Even for long shells the increase in frequency was very moderate and of minor importance. Fung et al.[37] investigated the effect of pressure on the frequency of vibrations of SD-SD cylindrical shells. The

frequency equation was established on the basis of the Timoshenko-Voss[31] theory. However, for certain ranges of shell parameters and for modes having small number of circumferential waves their results, as claimed by Herrmann and Shaw[38], cannot be relied on to yield more accurate results than those obtained by Reissner[39] using a shallow shell theory. In these investigations, where the shells are supported at both ends by shear-diaphragms (SD-SD), the equations of motion and the end conditions are exactly satisfied by simple displacement functions.

For other boundary conditions the problem is considerably more complicated and relatively few results are available. The exact procedure to determine frequency parameters for clamped-clamped shells was described by Seggelke[40]. Unfortunately, the results presented do not specify the shell theory used, thus making usefulness of the data questionable. Experimental results for clamped-clamped circular cylindrical shells subjected to internal pressure were given by Mixson and Heer[41], Miserentino and Vosteen[42], and Nikulin[43]. The Rayleigh-Ritz method or its equivalent have been used by several investigators to study the motion of shells with various boundary conditions[44-52]. Sewall and Naumann[44] used the Rayleigh-Ritz technique with beam functions and the Goldenveizer-Novozhilov shell theory to obtain frequencies for clamped-free shells and compared them with experimental results. They employed seven terms in the assumed mode shapes to obtain convergence of the Ritz procedure. Results were also obtained by Resnick and Dugundji[45] using an energy method equivalent to Rayleigh-Ritz,

beam functions, and the Sanders shell theory. A good agreement between theory and experiment was found only for modes with more than five circumferential waves. Extensive numerical results for clamped-free shells were obtained by Sharma and Johns[46-48] using the Ritz method and the Flügge shell equations. Displacement functions were assumed to be a combination of the clamped-free and clamped-pinned beam functions. It may be pointed out that the above approximate investigations were confined to the case of zero initial stress.

The energy method was also used by Arya et al.[49] to study the dynamic characteristics of fluid-filled shell containers. Open cylindrical shells clamped at the base and free at the top were studied under the empty condition as well as when filled to varying water depths. The mode shapes and frequencies of free vibration of cantilever cylindrical shells partially or completely filled with fluid were studied by Baron and Skalak[50]. Numerically obtained virtual mass coefficients were presented as functions of the height of the fluid in a tank. The free vibrations of orthotropic and isotropic fluid-filled cylindrical shells using the Rayleigh-Ritz method were also studied by Jain[51] and Stillman[52].

A number of workers have used shell theories to study the added mass effects of cylindrical shells in a fluid media. Workers like Greenspon[53], Warburton[54], Bleich and Baron[55], Herrmann and Russel[56], and Berger[57] are amongst the interested investigators.

From space consideration, it is attractive to look at the

array configuration, mentioned in the context of submarine detection, consisting of tapered inflatable cantilevers. Hence a brief review of the literature on tapered beams, which have interested researchers for a long time, would be appropriate. Conway et al.[58] calculated the frequencies for truncated-cone cantilever bars for a number of different boundary conditions. The first three natural frequencies and the corresponding modes of vibration of cantilever beams for numerous different tapers were presented by Housner and Keightley[59]. Gaines and Volterra[60] derived approximate formulas for upper and lower values of the three lowest natural frequencies for transverse vibrations of cantilever bars of variable cross sections. Other investigations on the free vibrations of taper cantilever beams include those by Cranch and Adler[61], Siddall and Isakson[62], and Pinney[63]. All these workers made use of elementary beam theory and effects of initial stress were not considered.

If the initial stress effects are to be included, shell theory has to be used. In this case the tapered cantilever beam becomes a conical shell, the analysis of which is far from simple. Weingarten[64] investigated the case of the simply-supported conical shell frustum subjected to internal and external pressures. The Galerkin method was applied to reduce the Donnell conical shell equations to the form of a frequency determinant. The agreement between theoretical and experimental frequencies was poor for modes with a small number of circumferential waves, mainly due to the nature of the Donnell theory used.

Goldberg et al.[65,66] developed a general numerical integration computer program and demonstrated its applicability to the problem of the clamped-clamped conical shell subjected to pressure. Unfortunately whether the pressure was internal or external was not indicated.

The inflatable members of the array under study are generally made of plastic films which are viscoelastic and exhibit time-dependent behaviour. This internal damping effect has received little attention in the past while studying the dynamic characteristics of inflated beams. The forced lateral vibration of a uniform cantilever Timoshenko beam with internal damping was studied by Lee[67]. On the other hand, Leissa and Hwee[68] investigated the problem of forced vibrations of simply-supported Timoshenko beams with viscous damping. Numerical results showed that the amplitude responses for the Timoshenko beam to be considerably larger than the corresponding simple beam predictions. Baker et al.[69] introduced various internal and external damping forces into the equations for free vibration of elementary beams. Solutions to the equations were obtained by energy methods in conjunction with a digital computer. The free vibration of a cantilever was also studied by Paidoussis and des Trois Maisons[70], who represented the viscoelastic effects by the two parameter Kelvin-Voigt model. Finally, the steady-state vibration of beams with nonlinear material damping was analyzed by Fu[71] using a perturbation technique. Numerical results obtained were compared to the ones given by Pisarenko[72].

Under operating conditions the submarine detection system will

be continually disturbed by the marine environment. The buoy at the water surface is excited by wind, surface waves, and currents. The cable and the hydrophone array are perturbed by currents, sub-surface turbulence, and internal waves. Each subsystem responds to these disturbances with drift motion together with translational and rotational oscillations. The cable subsystem also suffers from mechanical deformation. The general response of the whole assembly is governed by interactions between the coupled subsystems. The equilibrium configurations and dynamical behaviour will be similar to those of a towed vehicle system although the drifting velocity is usually much lower. The towed vehicle problem has drawn considerable interest for the last two decades. Applications of this system range from mooring of buoys to towing of glider aircrafts. A variety of techniques have been employed in studying these systems -- methods of characteristics, linearization procedures, equivalent lumped mass approach, finite element method, etc. A survey of these analytical methods for the dynamic simulation of cable-buoy systems is given by Choo and Casarella[73]. An interesting description on the advances in Canadian towed system research is presented by Eames and Drummond[74]. The fairing of the cable to reduce drag and its associated problems are discussed in depth. An extensive literature review on cable dynamics and towed systems is given by Misra[3].

The configuration of the towed body in the submarine detection system under consideration is more complicated than previous studies

due to coupling of the array of flexible viscoelastic tubes. The flexibility of the array legs is an important parameter in the analysis and can affect the stability of the system considerably.

1.3 Purpose and Scope of the Study

In the dynamical study of any system, a knowledge of the stiffness and response characteristics of the constituent members necessarily forms a prerequisite. With this in mind and because of the complex nature of the problem, a small subsystem is selected. An effort is made to investigate in detail the static and dynamical behaviour of the neutrally buoyant, inflated, viscoelastic beams forming the hydrophone array. Two geometries of the thin-walled viscoelastic beams are considered: uniform circular cylindrical and circular tapered. The static solutions of the elastic, inflated cantilevers are first extended to the viscoelastic case for moderately large inflation. This is followed by free vibration analyses of the inflated cantilever members in the ocean environment. For the uniform cylindrical beam, the shell theory is used to account for the internal pressure effects on the statics and free vibration characteristics. For the tapered case elementary beam theory is used to predict their natural frequencies. Next, the dynamical response of the viscoelastic, inflated cantilevers (uniform cylindrical and tapered) to root excitation is studied. The governing nonlinear equations are analyzed by taking two terms of the assumed Fourier series solution. Experimental results are obtained to substantiate the static and free vibration analyses.

Figure 1-2 illustrates schematically the plan of study.

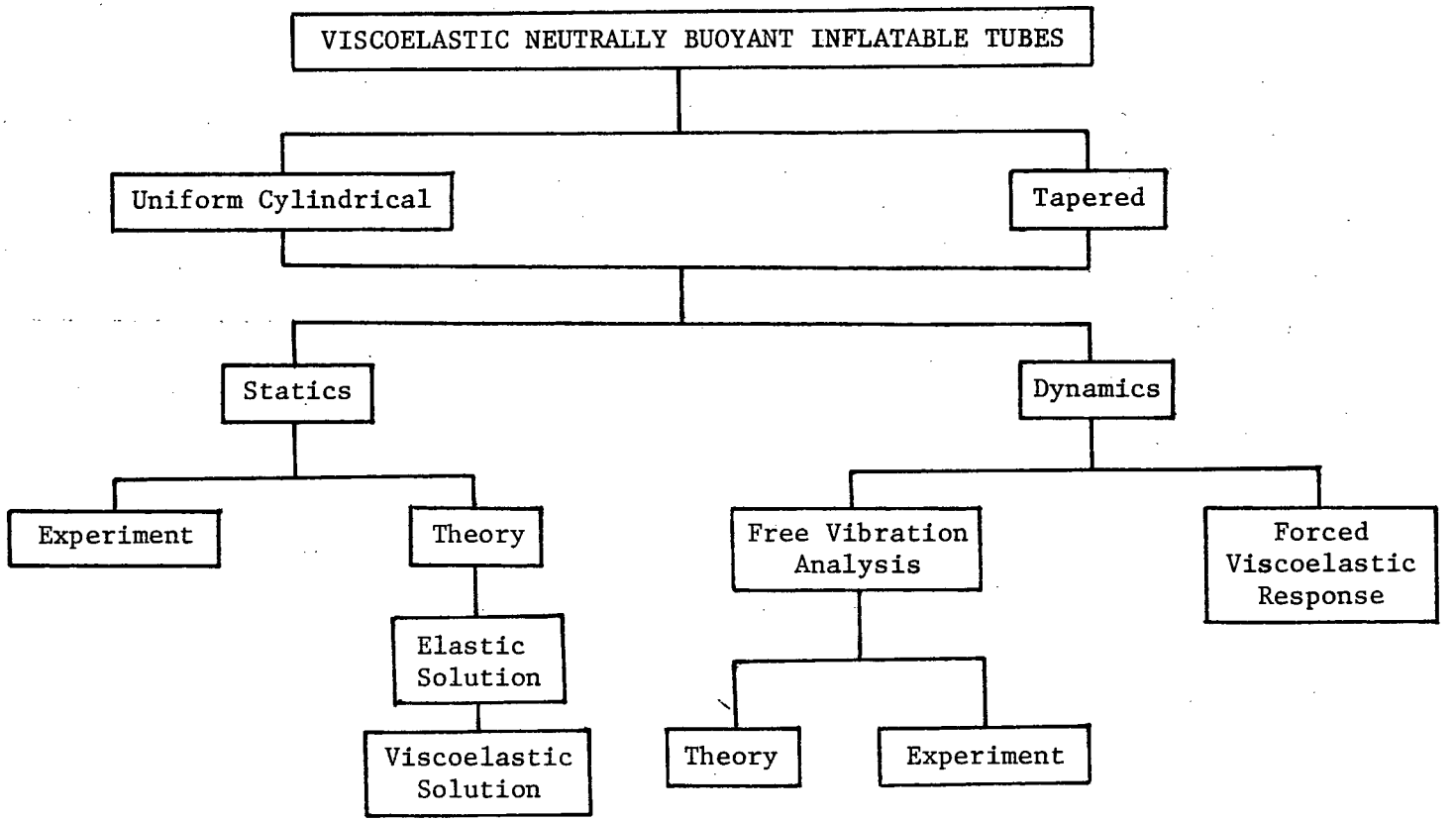

Figure 1-2 Schematic diagram of the proposed plan of study

2. STATICS OF NEUTRALLY BUOYANT INFLATED VISCOELASTIC CANTILEVERS

The present chapter investigates static deflections of neutrally buoyant inflated viscoelastic circular beams. It is assumed that internal pressure effects are relatively small such that the change in material properties is insignificant[7]. Consequently only geometrical variations due to inflation are treated. The viscoelastic deflections are obtained using the three parameter solid model in conjunction with the correspondence principle. The analysis is substantiated through an experimental program employing a large number of uniform and tapered beam models made of mylar-polyethylene sandwiched films.

The objectives of this chapter are:

(i) to predict static deflections of circular cylindrical uniform and tapered beams made from plastic films;

(ii) to obtain information concerning material constants for the specified mylar-polyethylene sandwiched films;

(iii) to investigate the internal pressure effects on the static behaviour of the inflated cantilevers.

2.1 Theoretical Analysis

2.1.1 Uniform Cylindrical Beam

Consider a thin-walled inflated circular cylindrical cantilever

(Figure 2-1) of initial length L_0, diameter d_0, wall thickness h_0, and internal pressure p. The dimensions at any instant during inflation are related to their initial values by the principal stretches as follows,

$$L = \lambda_1^* L_0 \quad , \quad d = \lambda_2^* d_0 \quad \text{and} \quad h = \lambda_3^* h_0 \quad . \tag{2.1}$$

As the bulk modulus of the materials under study is relatively large, incompressibility can be safely assumed, and hence,

$$\lambda_1^* \lambda_2^* \lambda_3^* = 1 \quad . \tag{2.2}$$

The principal stresses for the cylindrical beam can be shown to be[10]

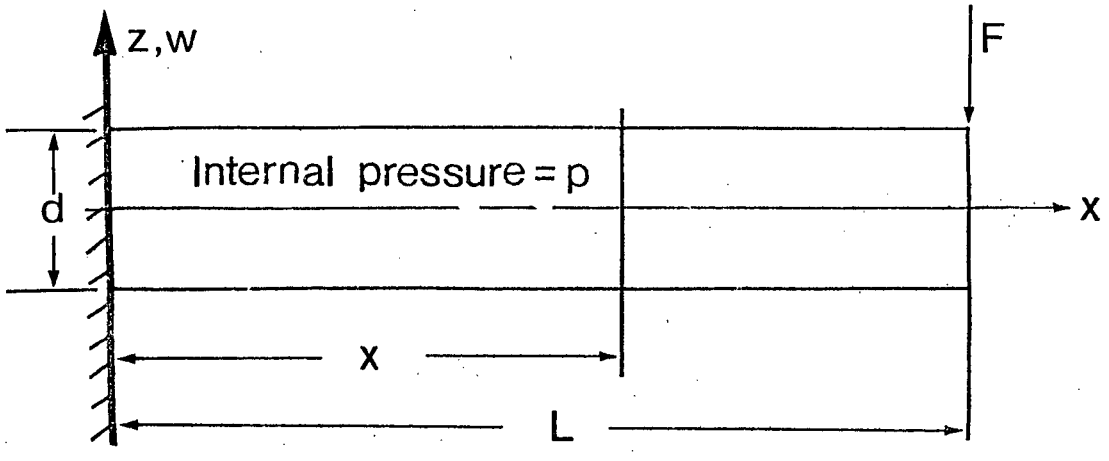

Figure 2-1 Geometry of flexure of an inflated circular cylindrical beam

$$\sigma_{11} = \phi_0+\phi_1\lambda_1^{*2}+\phi_{-1}\lambda_1^{*-2} = pd/4h \quad , \tag{2.3a}$$

$$\sigma_{22} = \phi_0+\phi_1\lambda_2^{*2}+\phi_{-1}\lambda_2^{*-2} = pd/2h \quad , \tag{2.3b}$$

$$\sigma_{33} = \phi_0+\phi_1\lambda_3^{*2}+\phi_{-1}\lambda_3^{*-2} = 0(p) \quad , \tag{2.3c}$$

where ϕ_i are scalar functions of the diagonal stretch matrix. Note that σ_{33} is small compared to σ_{11} and σ_{22} (the ratio being of the order of h/d). Setting σ_{33} to zero, Misra[3] has shown that, for moderate stretches up to 40% increase in diameter,

$$\lambda_1^* = 1 \quad , \tag{2.4a}$$

$$\lambda_2^* = (1-pd_0/2\bar{G}h_0)^{-1/4} \quad , \tag{2.4b}$$

$$\lambda_3^* = 1/\lambda_2^* \quad , \tag{2.4c}$$

where $\bar{G}$ is the shear modulus of the undeformed material. As $pd_0/2\bar{G}h_0 << 1$, the expressions for λ_2^* and λ_3^* can be simplified to get

$$\lambda_2^* = 1+pd_0/8\bar{G}h_0 \quad , \tag{2.5a}$$

$$\lambda_3^* = 1-pd_0/8\bar{G}h_0 \quad . \tag{2.5b}$$

In actual practice, a change in length will be small compared to

changes in diameter and thickness. Hence Equations (2.4) represent a good approximation to changes in dimensions due to inflation.

To account for the time dependent properties of the material, Equations (2.5) can be modified using a concept similar to the correspondence principle[75],

$$\lambda_2^*(t) = 1+pd_0J_s(t)/8h_0 \quad , \tag{2.6a}$$

$$\lambda_3^*(t) = 1-pd_0J_s(t)/8h_0 \quad , \tag{2.6b}$$

where p is the step pressure applied at t=0 and $J_s(t)$ is the shear creep compliance of the material. The dimensions after a long time are thus given by

$$L_f = L_0 \quad , \tag{2.7a}$$

$$d_f = d_0[1+pd_0J_s(\infty)/8h_0] \quad , \tag{2.7b}$$

$$h_f = h_0[1-pd_0J_s(\infty)/8h_0] \quad . \tag{2.7c}$$

The cantilever beam is now allowed to undergo bending deformations. It is assumed that the internal pressure is sufficiently large to make the resultant stress tensile everywhere so that no wrinkles appear on the beam. The resultant axial stress on an element with coordinates (x,y,z) is obtained by superposing the stresses due

to bending and inflation pressure, i.e.,

$$\sigma_{11} = F(L-x)z/I+pd_f/4h_f \quad , \tag{2.8}$$

where F is the load and I the cross-sectional moment of inertia about a transverse axis,

$$I = \pi d_f^3 h_f/8 \quad .$$

From elementary beam theory the curvature is given by

$$\frac{d^2w}{dx^2} = -F(L-x)/EI \quad . \tag{2.9}$$

Integrating twice and applying the boundary conditions at x = 0, leads to the static deflection expression of an elastic cantilever,

$$w(x) = -(FL^3/6EI)[(x/L)^2(3-x/L)] = W(x)/E \quad . \tag{2.10}$$

For step loads the Laplace transforms of the viscoelastic and elastic deflections are related via the correspondence principle:

$$\bar{w}_{v.e.}(x,s) = \bar{w}(x,s)E/s\bar{E}(s) \quad , \tag{2.11}$$

where $\bar{w}_{v.e.}(x,s)$, $\bar{w}(x,s)$ and $\bar{E}(s)$ are the Laplace transforms of the viscoelastic solution, elastic solution, and the relaxation modulus

of the material, respectively. Noting that

$$\bar{w}(x,s) = W(x)/sE \quad ,$$

from Equation (2.11) one obtains

$$\bar{w}_{v.e.}(x,s) = W(x)/s^2\bar{E}(s) \quad . \tag{2.12}$$

For relatively low stress levels the beam material under study is found to exhibit a small long-time creep and behaves like a linear viscoelastic solid. Hence the three parameter viscoelastic solid model (Figure 2-2) can be used to represent its behaviour fairly well.

For a three parameter solid,

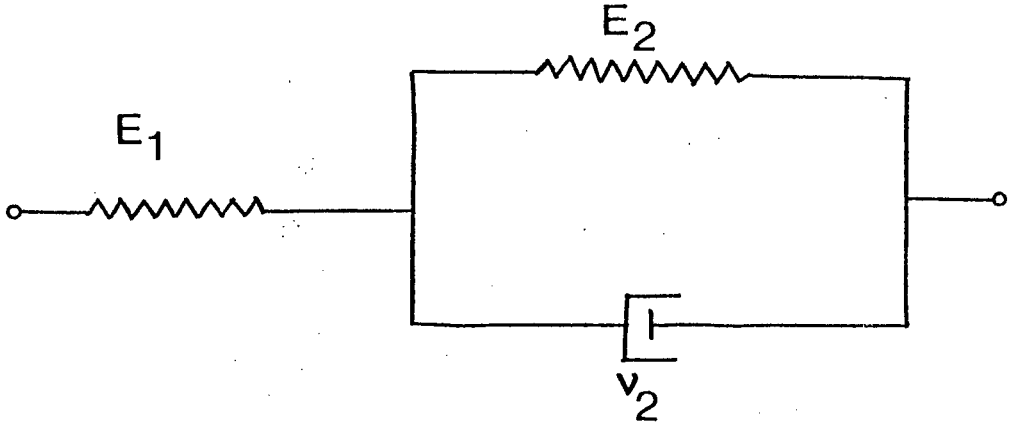

Figure 2-2 Three parameter viscoelastic solid model

$$s^2\bar{E}(s) = sE_1(E_2+\nu_2 s)/(E_1+E_2+\nu_2 s) \quad , \tag{2.13}$$

where E_1, E_2 and ν_2 are the three parameters defining the material behaviour. Substituting Equation (2.13) into Equation (2.12) and inverting into time domain, gives

$$\bar{w}_{v.e.}(x,t) = W(x)J(t) \quad , \tag{2.14}$$

where

$$J(t) = 1/E_1+(1/E_2)[1-\exp(-E_2 t/\nu_2)] \quad ,$$

and W(x) is obtained from Equation (2.10).

2.1.2 Tapered Beam

For a tapered cantilever (Figure 2-3), the diameter and length are linear functions of x, and thus the curvature relation is

$$\frac{d^2w}{dx^2} = -F(L-x)/EI \quad ,$$

where

$$I = I(x) = I_r[1-k(x/L)]^3 \quad ,$$

$$k = \text{taper ratio} = (d_r-d_t)/d_r \quad ,$$

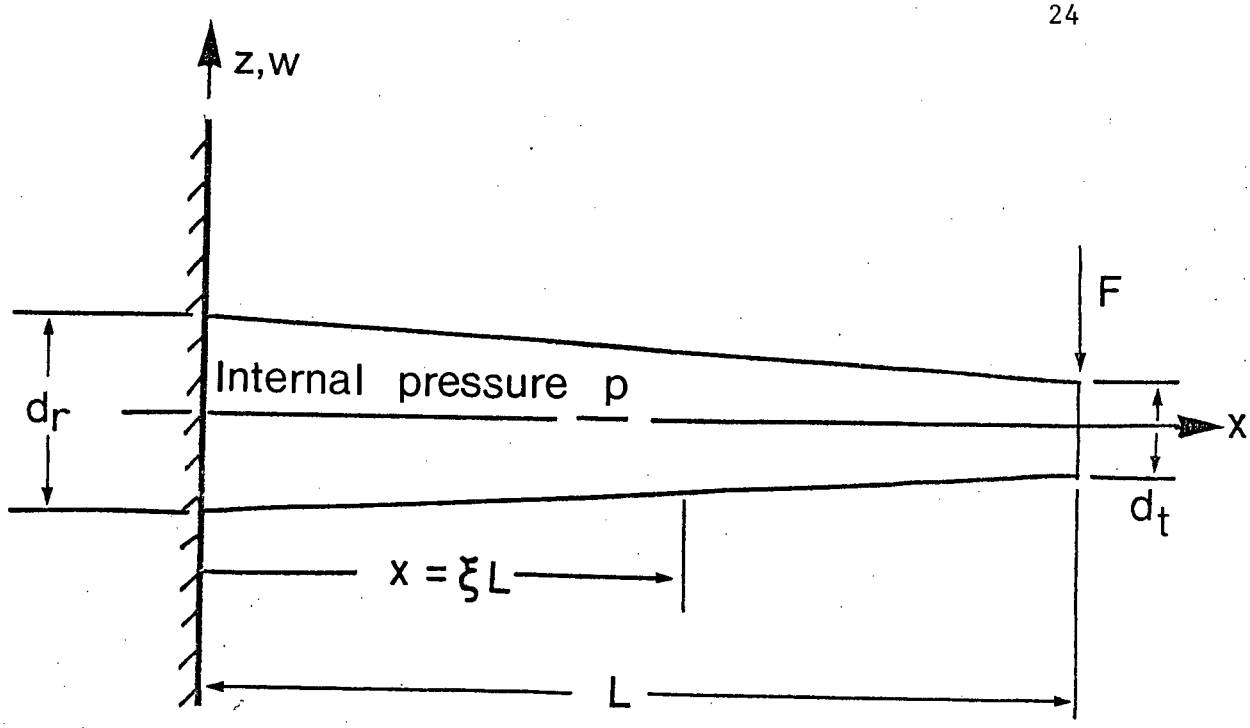

Figure 2-3 Geometry of flexure of an inflated tapered beam

I_r = moment of inertia at root, i.e., at x = 0.

Integrating twice and using the boundary conditions at x = 0, leads to

$$w(x) = W(x)/E \quad , \tag{2.15}$$

where

$$W(x) = -FL^3\{[(k-1)/(1-kx/L)-(k+1)]/2-\ln(1-kx/L)\}/k^3I_r \quad .$$

Analogous to the uniform cylindrical beam, the viscoelastic solution

may be written as

$$w_{v.e.}(x,t) = W(x)J(t) \quad , \tag{2.16}$$

where J(t) and W(x) are given in Equations (2.14) and (2.15), respectively.

2.2 Experimental Program

2.2.1 Test Equipment and Procedures

To assess validity of the analysis and to generate relevant design information, an experimental programme was undertaken. Model test were performed in a 1.83x0.91x1.22m (6'x3'x4') rectangular water tank (Figure 2-4) made of waterproof plywood with front and side plexiglas panels to facilitate observation. A compressed air bottle pressurized an intermediate water tank for inflating a model after the test tank had been filled with water. A pressure gauge in the interconnecting piping indicated the inflation pressure. A trolley system enabled static loading at any desired station along the tube.

As the static deflections are time varying and the measurements at different stations along the tube have to be taken simultaneously, photographic technique was employed to record the time history of a beam undergoing creeping deformation. 35mm pictures were taken, initially 30 seconds apart with the interval gradually increasing to 5 minutes as the creep rate diminished. A thin wire

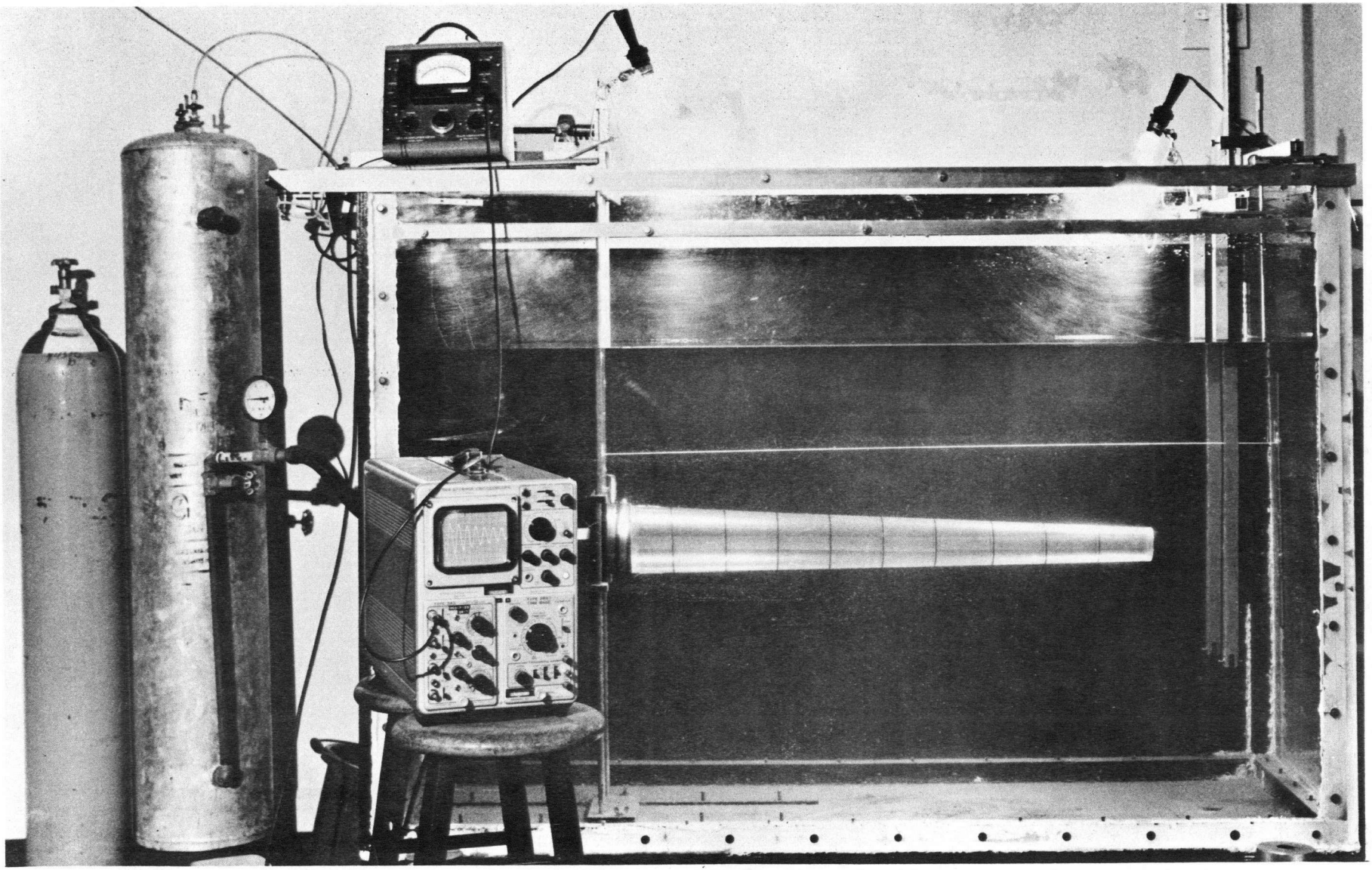

Figure 2-4 Experimental set-up

strung above the beam served as a reference during these measurements. The deflection data were obtained from the projection of the pictures on a screen.

2.2.2 Test Models

A large number of uniform and tapered cylindrical tubes were made from thin sandwiched films of mylar and polyethylene. For the tapered beams only the case of 0.5 taper ratio, i.e., $d_r = 2d_t$, is considered. Two sheets of the commercially available plastic film (Nap-Lam clear laminating film by General Binding Corporation) were pressed together by a heat tacking iron. The heat melted the polyethylene layers and fused them together (Figure 2-5a). The sandwiched sheet was then wrapped around an appropriate cylindrical blank to form the desired cross-section, and the edges sealed with a piece of mylar heat-sealing tape (Schjel-Bond GT-300 Thermoplastic Adhesive by Schjeldahl). One end of the tube was closed using a thin plexiglas cap epoxy-glued to the end (Figure 2-5b). Each tube was divided into 10.16 cm (4 in.) sections at which deflections were measured.

2.3 Results and Discussion

Although a vast amount of experimental information was generated, only a few of the typical results helpful in identifying trends are presented here. Figure 2-6 shows a typical creep-relaxation curve for the sandwiched material under study. An instantaneous deflection followed by creep is apparent. The creep rate decreases and becomes

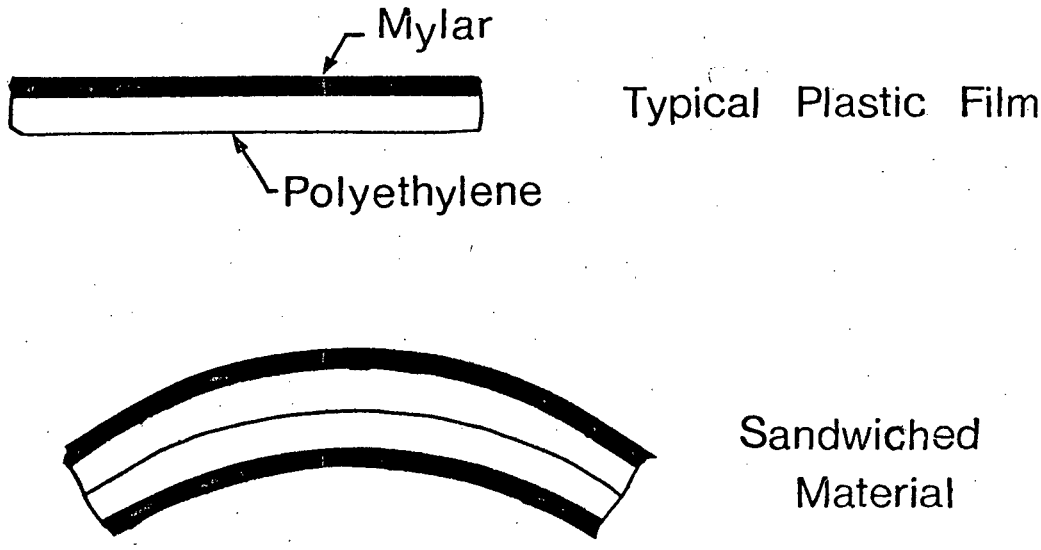

(a) Sandwiched material made from two layers of plastic films

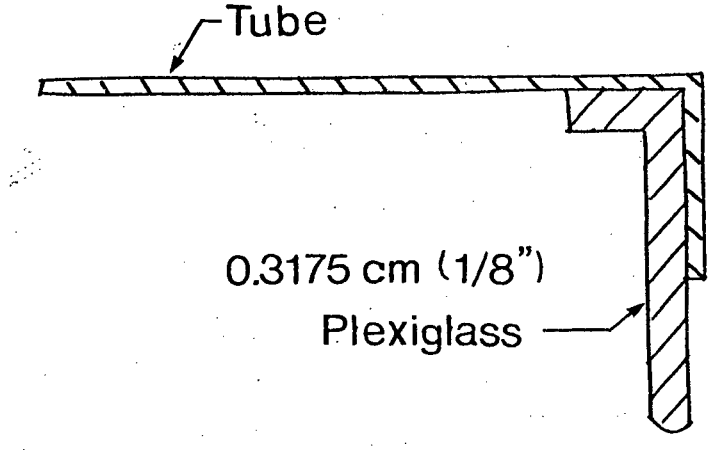

(b) End details

Figure 2-5 Sandwiched material and details of the end cap

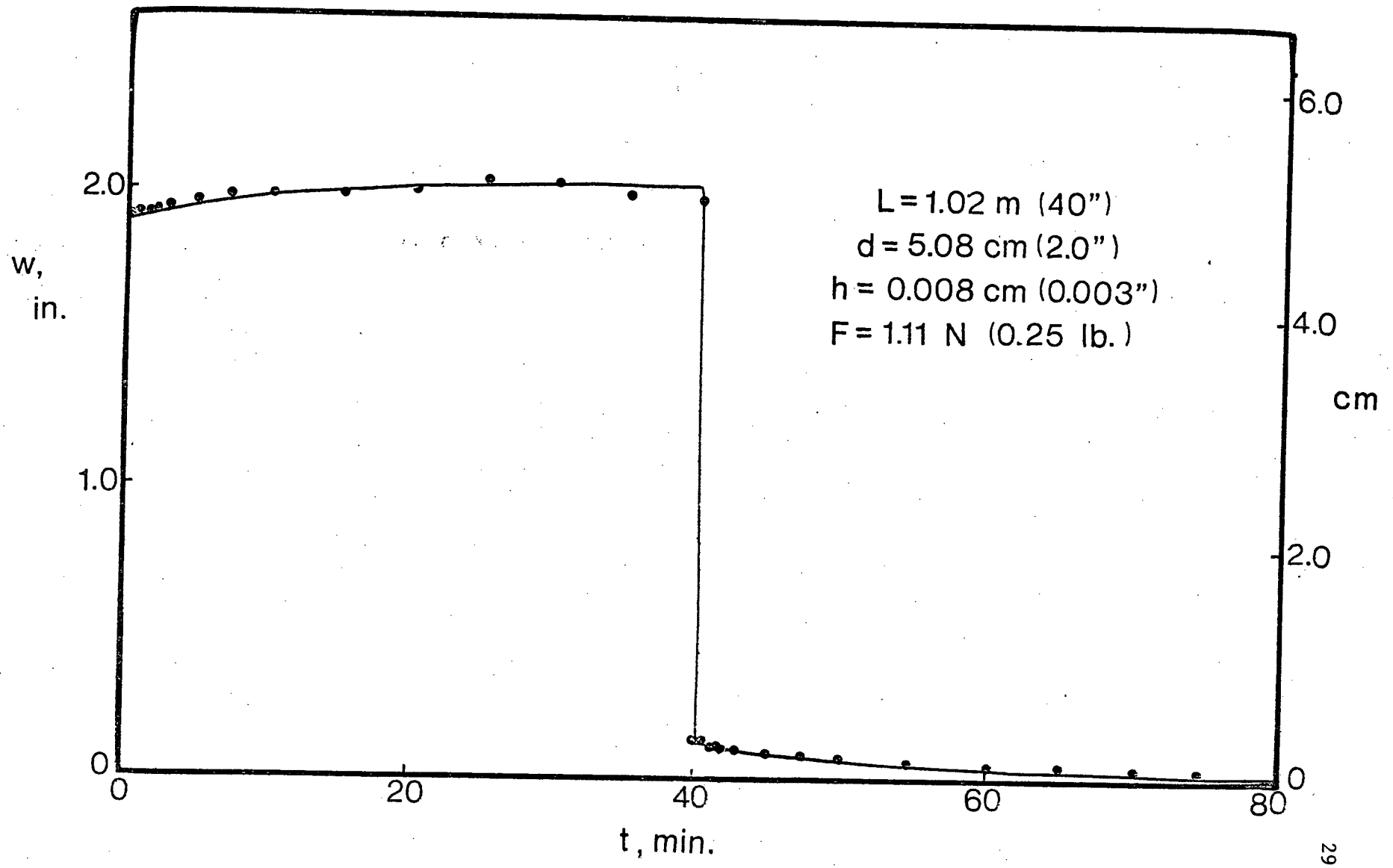

Figure 2-6 A typical creep-relaxation curve for the sandwiched inflated beam

almost negligible after about 40 minutes. Removal of the load causes an instantaneous drop in the deflection, of the magnitude equal to the initial one. The beam asymptotically returns to the original position following essentially the same behaviour as that observed during the loading cycle.

2.3.1 Uniform Cylindrical Beam

Figure 2-7 compares some of the test results with analytical predictions. It is interesting to note that the behaviour can be described very well by the three parameter solid model. Average values of the three material constants, E_1, E_2, and ν_2 have been obtained to give the analytical curves. In the tests ν_2 was found to vary slightly, but E_1, the instantaneous modulus of elasticity, was very nearly constant ($\simeq 1.65 \times 10^9$ N/m^2 or 2.4×10^5 psi).

It should be emphasized that for higher stress levels the long time strain has a nonlinear relationship with the stress. Kalinnikov[76] observed the creep relation for polyethyleneterephthalate (mylar) to be of the form

$$\varepsilon_c = \varepsilon_{c0} + a\sigma^m t^n \quad ,$$

where a, m, n are material constants. On the other hand, Findley and Khosla[77] have found the creep of polyethylene to follow the equation

$$\varepsilon_c = \varepsilon'_{c0} \sinh(\sigma/\sigma_e) + m' \sinh(\sigma/\sigma_m) t^n \quad ,$$

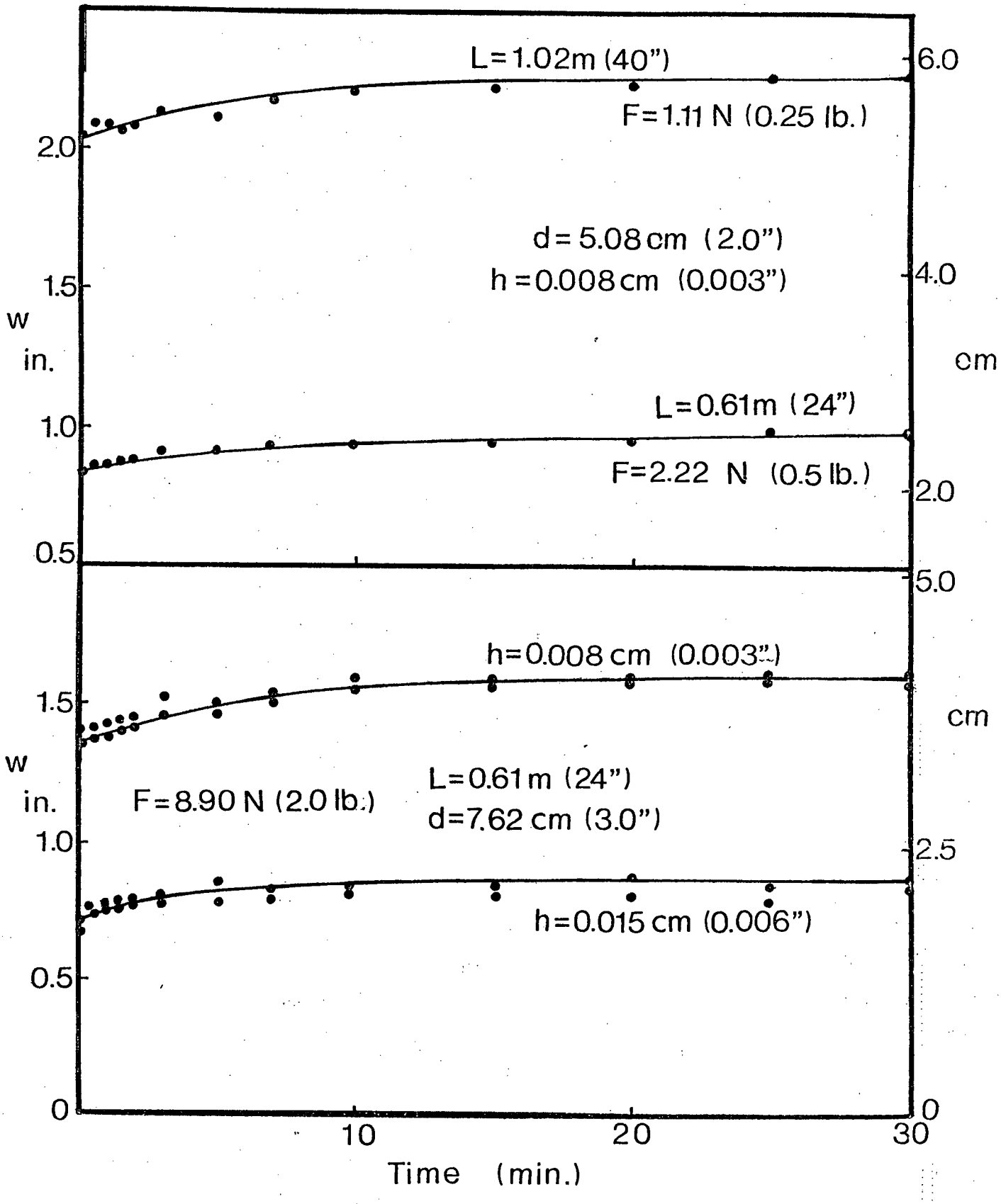

Figure 2-7 Comparison of analytical and experimental results for the static deflection of uniform cylindrical beams

where ε'_{c0}, m', n, σ_e and σ_m are constants. In the study of dynamics of these structures, however, only the short time creep is of significance, since the period of most of the neutrally buoyant beams is very small (around one second).

The effect of internal pressure on the static deflections is shown in Figure 2-8. For the range of pressures considered, the inflation causes little change in the static behaviour of the cantilever beam. This means that the deviations from unity of λ_2^* and λ_3^* in Equations (2.5) are small. In the actual calculation it is found that, since the shear modulus of the material is relatively large, the internal pressure induces geometrical changes of less than 1%. On the other hand, Misra[3] has found that, for polyethylene, the effect may be significant and changes in dimensions can reach as high as 15%.

In the design of these inflated cantilevers the L/d_0 ratio is an important parameter. Figure 2-9 shows the deflection histories for two L/d_0 ratios. Good agreement between theory and experiments confirms the cubic power variation of deflection with L/d_0 ratio predicted by the theoretical analysis.

2.3.2 Tapered Beam

Figure 2-10 shows some of the typical deflection histories and their corresponding analytical predictions. Again the validity the of the theoretical analysis is confirmed by its good agreement with experimental data.

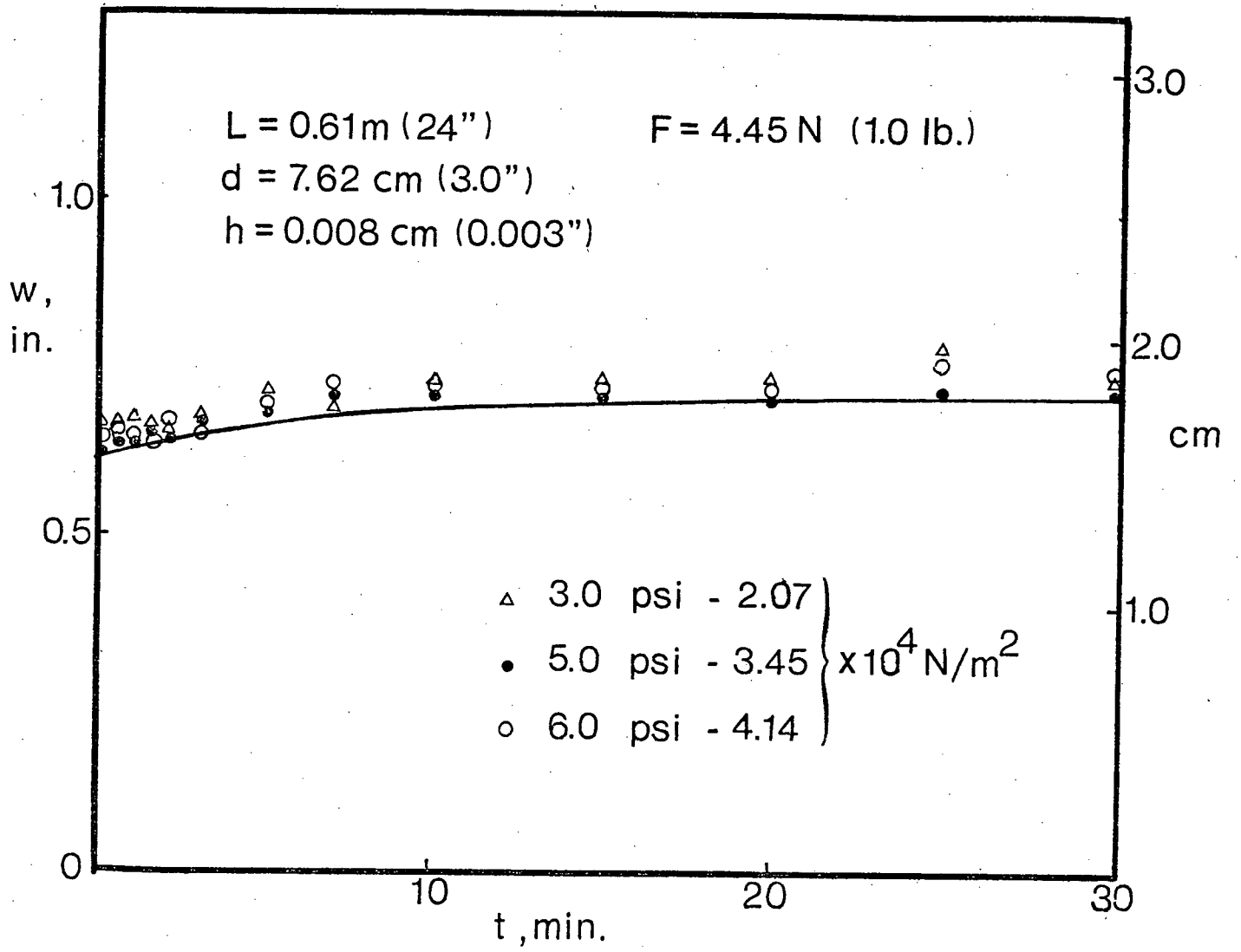

Figure 2-8 Effect of internal pressure on the static deflections of uniform cylindrical beams

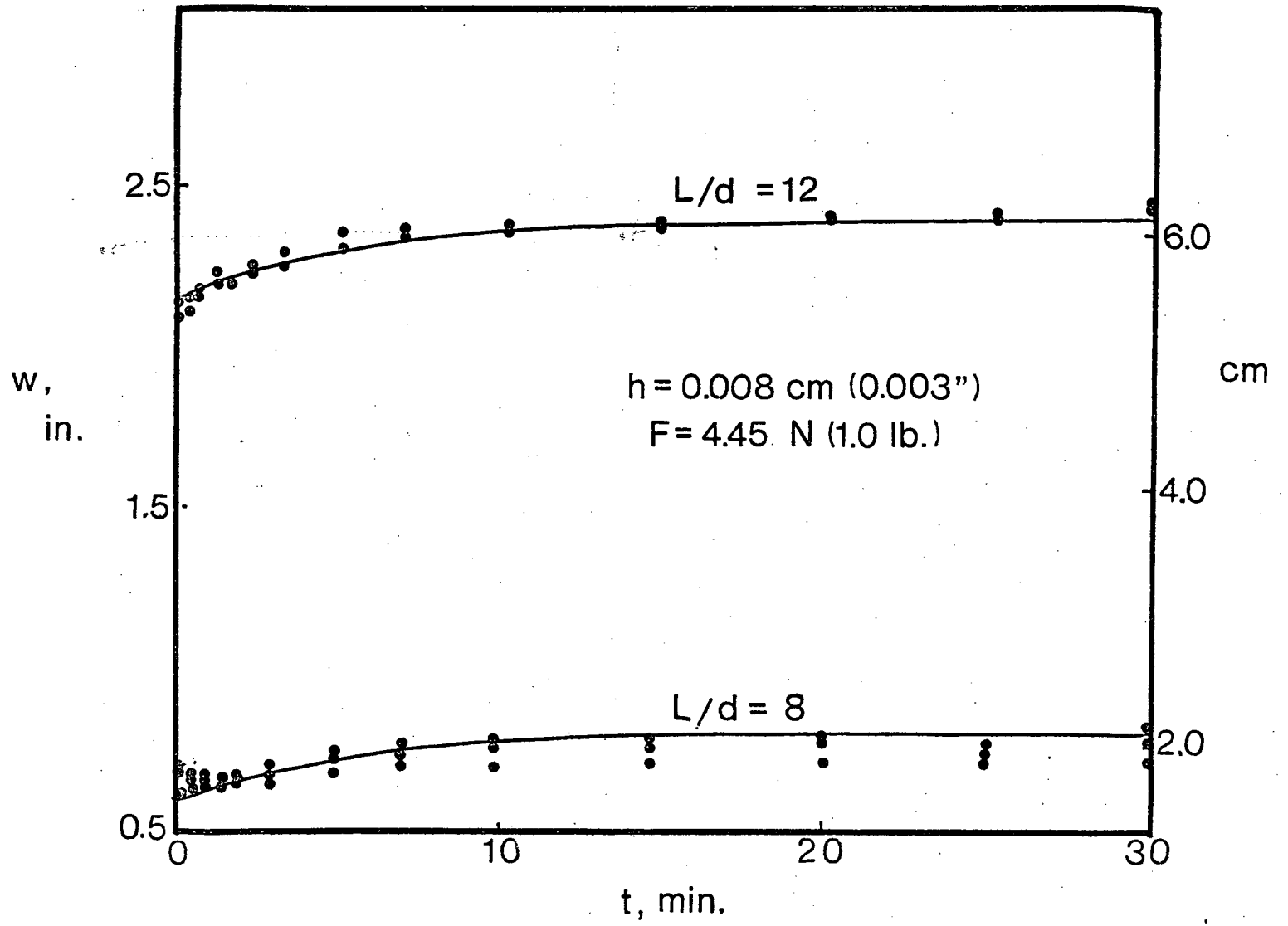

Figure 2-9 Tip deflection histories for two L/d ratios

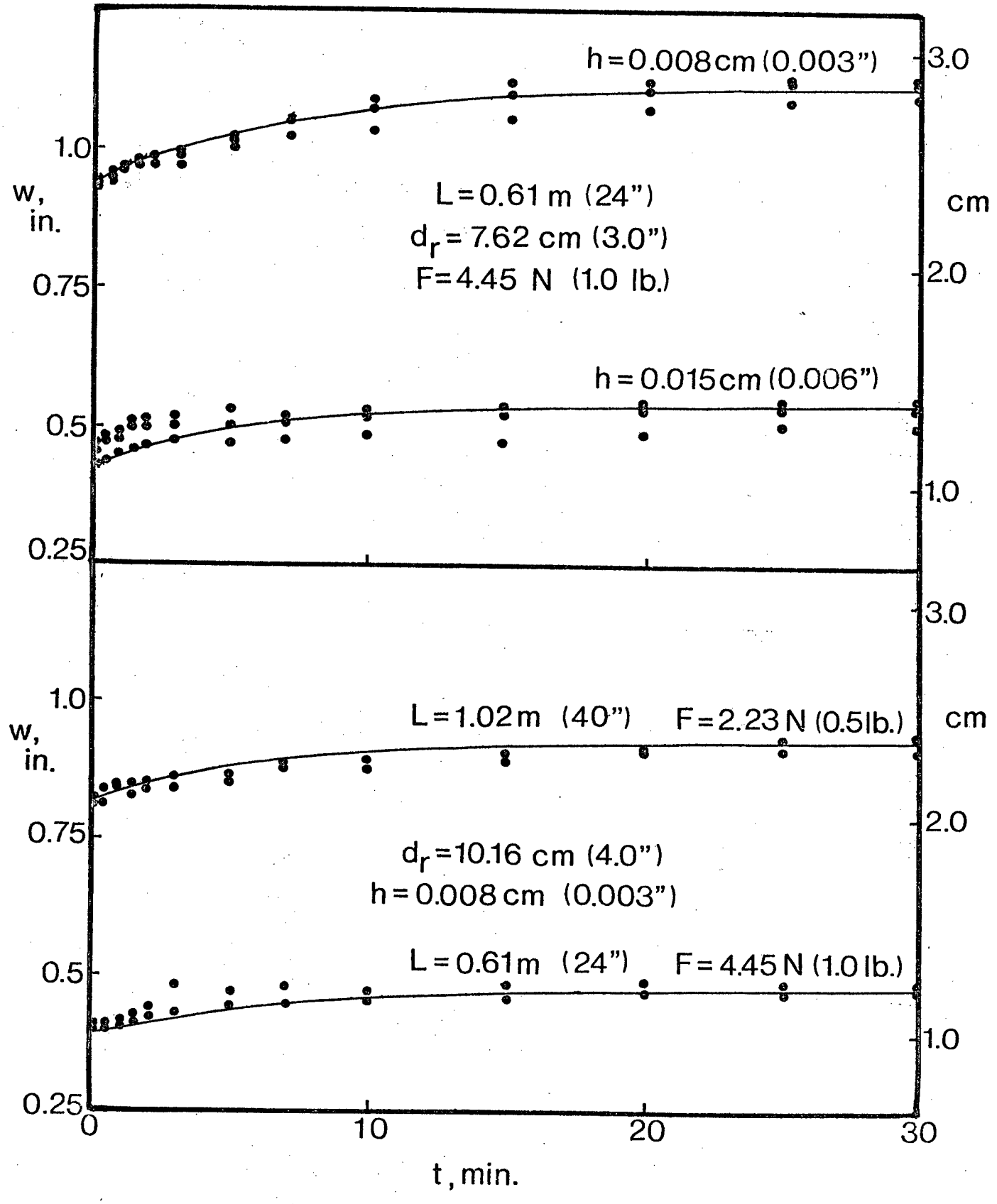

Figure 2-10 Comparison of analytical and experimental results for the static deflections of tapered beams

The deflections of three tapered beams subjected to different internal pressures are plotted in Figure 2-11. The experimental data all fall very close to the zero-inflation theoretical curve, and no significant effects of internal pressure is observed.

The tip deflections at t = 0 (instantaneous) and t = 30 minutes are plotted as functions of L/d_r in Figures 2-12 and 2-13, respectively, for the structural model having a wall thickness of 0.008cm (0.003") and tip load of 4.45N (1.0 lb). The lines represent the analytical results as given by Equation (2.16) while the isolated points indicate the test data. Potential of the analytical approach becomes apparent as it is able to predict with accuracy even large deflections. This suggests that the curvature can be represented by $\frac{d^2w}{dx^2}$ without much error even though the deflections are large.

2.4 Concluding Remarks

From the preceding static analysis several important conclusions can be summarized as follows:

(i) The analysis suggests that the three parameter solid model can be used to yield sufficiently accurate results useful in the design of neutrally buoyant inflated structures made from the viscoelastic sandwiched films specified. Even large deflections can be predicted with accuracy by the simple analysis given.

(ii) Provided the internal pressure is moderate and no wrinkles

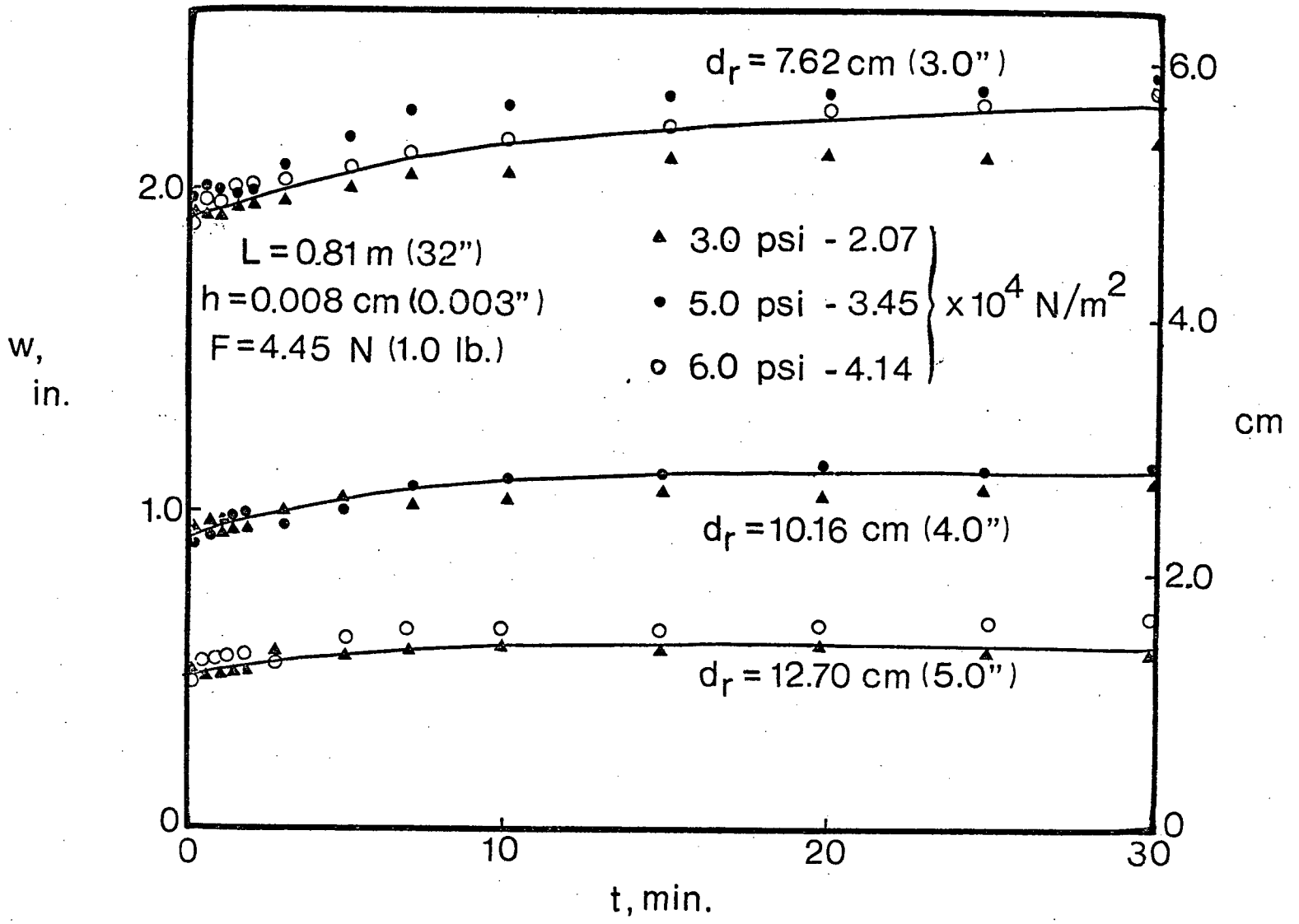

Figure 2-11 Effect of internal pressure on the static deflections of tapered beams

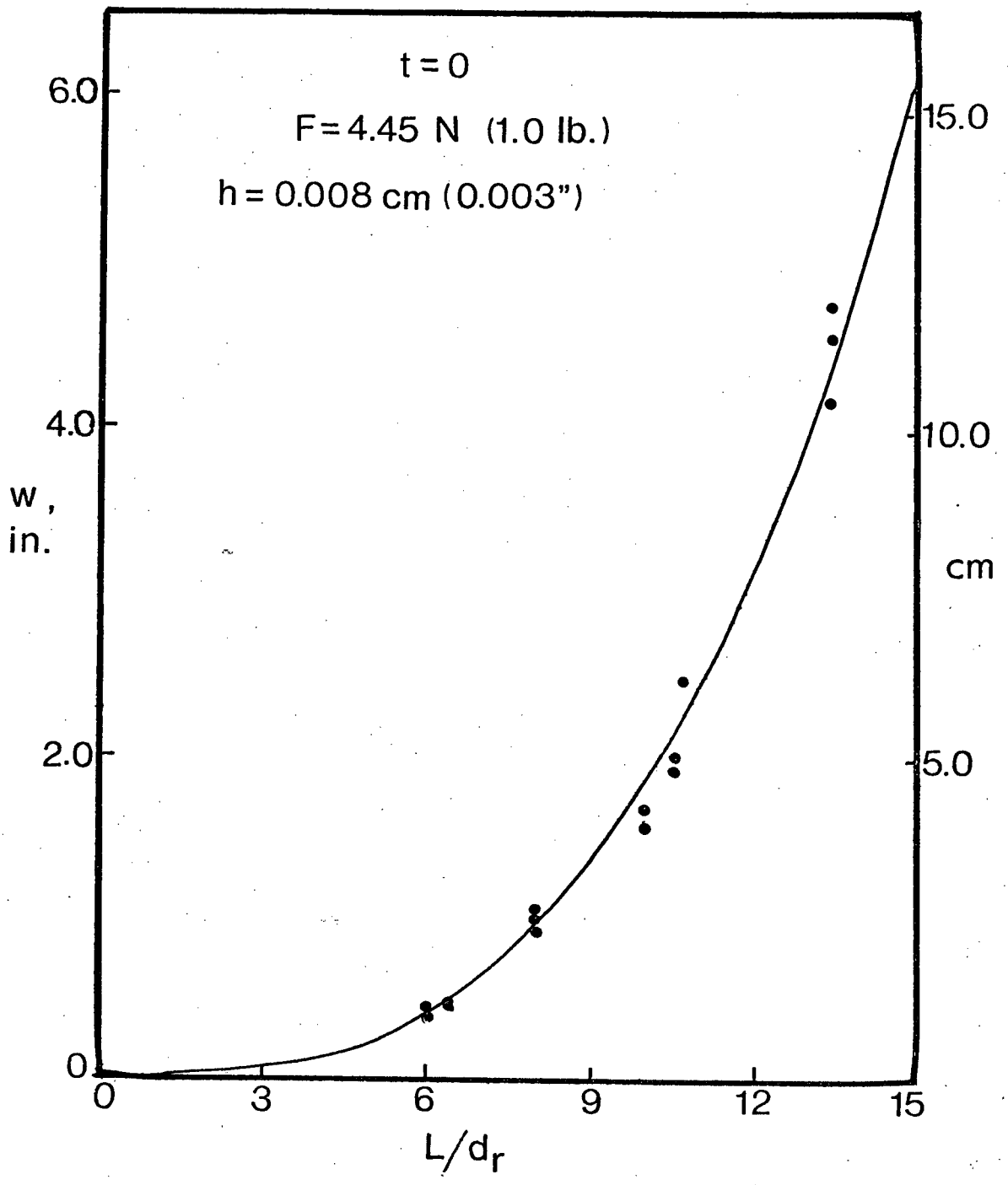

Figure 2-12 Instantaneous tip deflection as a function of L/d_r

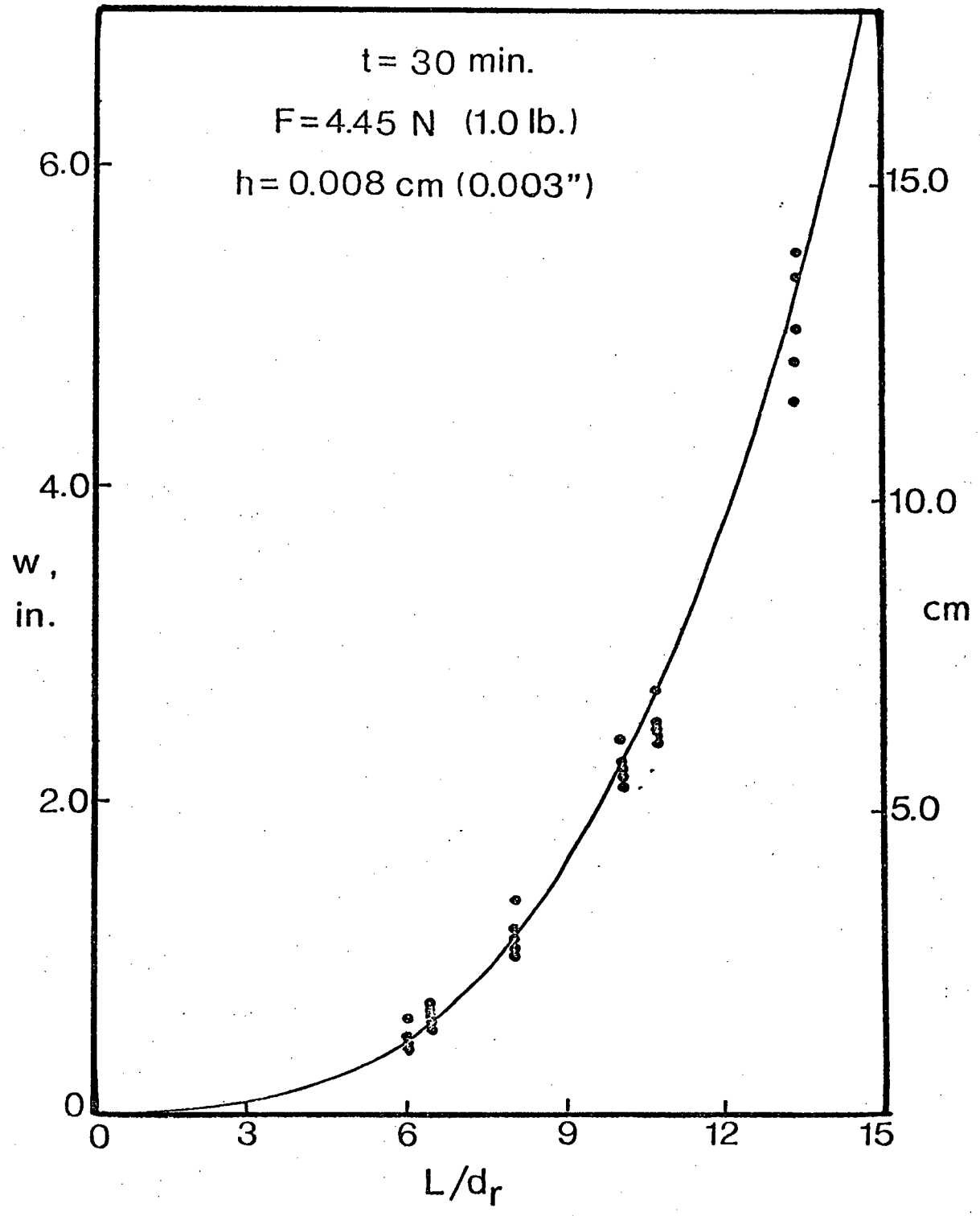

Figure 2-13 Tip deflection at t = 30 min. as a function of L/d_r

occur, inflation has negligible effects on the static bending stiffness of the inflatable beams considered. At high internal pressures, however, changes in both the geometric and the material properties may be significant and the deflection relationship will become nonlinear.

(iii) The instantaneous modulus of elasticity, E_1, for the viscoelastic material considered is found to be nearly constant at 1.65×10^9 N/m^2 (2.4×10^5 psi). Average values for E_2 and ν_2 are experimentally found to be 1.24×10^{10} N/m^2 (1.8×10^6 psi) and 3.72×10^9 N-sec/m^2 (5.4×10^5 psi-sec), respectively. This information on the material properties will be useful in the forthcoming study of the dynamic behaviour of the viscoelastic cantilevers.

3. FREE VIBRATION OF NEUTRALLY BUOYANT INFLATED CANTILEVERS

Static behaviour of the neutrally buoyant inflated viscoelastic cantilevers having been studied, the next logical step would be to analyze dynamic response of the beams vibrating in the ocean environment. The object of this chapter is to investigate free vibration characteristics of uniform circular cylindrical and tapered beams in water.

First, the flexural free vibration of the inflated uniform cylindrical cantilever is considered. Shell equations are used to incorporate the initial stresses due to internal pressure. For relatively long shells vibrating in the beam-bending mode, the governing shell equations are found to be reducible to a single equation very similar to the one for the transverse vibrations of a beam with rotary inertia included. Three different approaches are studied: the membrane, Flügge's, and Herrmann and Armenàkas'. The natural frequencies obtained are compared with the experimental results and those predicted by the Rayleigh-Ritz method in conjunction with the Washizu and membrane shell theories.

The presence of hydrodynamic forces introduces nonlinearities into the governing equation of motion. Effect of this nonlinear drag force on the free response, as given by the reduced Flügge equation, is studied using the perturbation technique.

This is followed by a free vibration analysis of the inflated tapered beam. The elementary beam theory is used and the natural frequencies are found using the mode-approximation procedure. Validity of the approximate method is examined by comparing the results with the experimental data.

As the material under study has relatively small damping, the time dependence of the natural frequencies is of secondary importance in transient response studies presented here. Hence, no attempt is made to incorporate the viscoelastic properties in the investigation, and the material is treated as elastic with Young's modulus E_1.

3.1 Uniform Cylindrical Beam Analysis

3.1.1 Reduced Shell Equation Approach

(a) Formulation

The conventional beam equation, because of its inability to account for stresses induced by the internal pressure, cannot be applied to inflated thin-walled beams. In order to investigate initial stress effects on the dynamic behaviour of the inflated cantilevers one has to resort to thin shell theory.

Shells have all the characteristics of plates but with one difference -- curvature. In other words, plate represents a limiting case of the shell with no curvature. Besides the added complexity

of curvature, shells are more difficult to analyze than plates since their bending cannot, in general, be separated from stretching. Thus, a classical bending theory of shells is governed by a system of eighth order partial differential equations, while the corresponding plate equations are of the fourth order. A further challenge enters the problem through the boundary conditions as well. Four specified conditions, as compared to two in plate theory, are required here.

To complicate matters further, whereas all academicians agree on the form of the classical, fourth order plate equations, such agreement does not exist in shell theory. Numerous different theories have been derived and are in use.

The equations of motion for a thin circular cylindrical shell may be written conveniently in matrix form as

$$\begin{bmatrix} L_{11} & L_{12} & L_{13} \\ L_{21} & L_{22} & L_{23} \\ L_{31} & L_{32} & L_{33} \end{bmatrix} \begin{bmatrix} x \\ y \\ z \end{bmatrix} = \{0\} \quad , \tag{3.1}$$

where x, y, and z are the orthogonal components of displacement in the $\tilde{x}$ (axial), θ (circumferential), and radial directions, respectively (Figure 3-1).

For the most commonly used Flügge's shell theory, the differential operators in Equation (3.1), after neglecting the small terms involving $h^2/(12a^2)$, are[31]

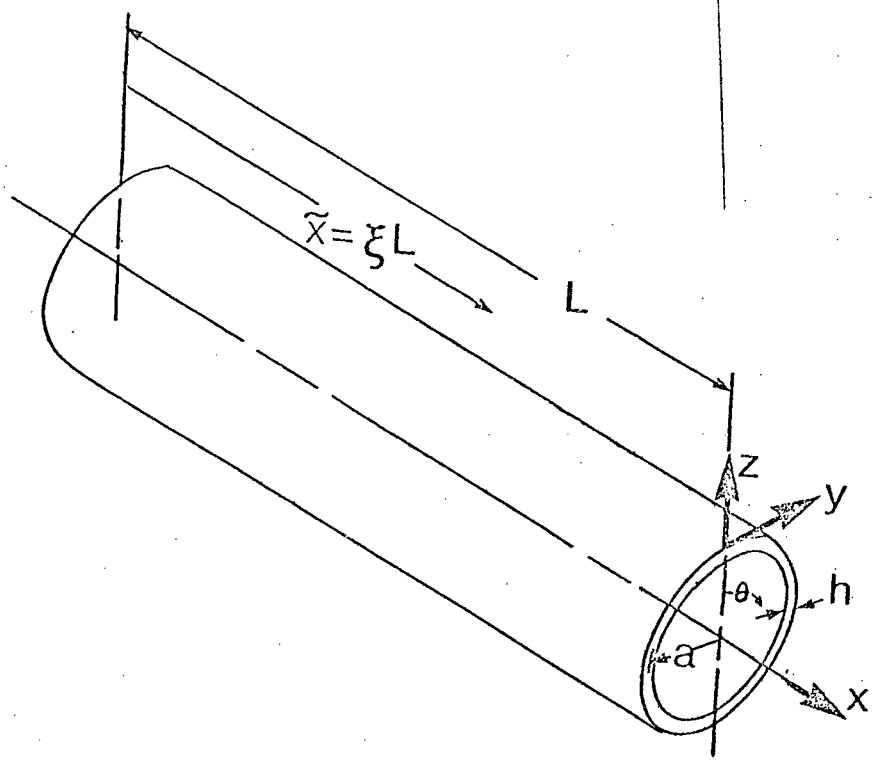

Figure 3-1 Geometry and co-ordinate system for a circular cylindrical shell

$$L_{11} = \left(1+N_x/C\right)\frac{\partial^2}{\partial s^2} + \left(\frac{1-\nu}{2} + \frac{N_\theta}{C}\right)\frac{\partial^2}{\partial \theta^2} - c_1 G\frac{\partial^2}{\partial t^2} \quad ,$$

$$L_{12} = \frac{1+\nu}{2}\frac{\partial^2}{\partial s \partial \theta} \quad ,$$

$$L_{13} = \left(\nu - N_\theta/C\right)\frac{\partial}{\partial s} \quad ,$$

$$L_{21} = \frac{1+\nu}{2}\frac{\partial^2}{\partial s \partial \theta} \quad ,$$

$$L_{22} = \left(\frac{1-\nu}{2} + \frac{N_x}{C}\right)\frac{\partial^2}{\partial s^2} + \left(1+N_\theta/C\right)\frac{\partial^2}{\partial \theta^2} - c_2 G\frac{\partial^2}{\partial t^2} \quad ,$$

$$L_{23} = \left(1+N_\theta/C\right)\frac{\partial}{\partial \theta} \quad ,$$

$$L_{31} = \left(\nu - N_\theta/C\right)\frac{\partial}{\partial s} \quad ,$$

$$L_{32} = (1+N_\theta/C)\frac{\partial}{\partial\theta} \quad ,$$

$$L_{33} = 1 + c_3 G\frac{\partial^2}{\partial t^2} - \frac{N_\theta \partial^2}{C\,\partial\theta^2} - \frac{N_x \partial^2}{C\,\partial s^2} \quad ,$$

where

$$s = \tilde{x}/a \quad , \quad G = \rho a^2(1-\nu^2)/E \quad , \quad C = Eh/(1-\nu^2) \quad ,$$

and c_1, c_2, c_3 are tracers (=0 or 1) introduced to identify the effect of the different inertial forces. c_3 also incorporates the added mass effect of the surrounding water.

The problem of determining the functions x, y, and z satisfying Equation (3.1) can be reduced to solution of a single equation involving one potential function $\Gamma(s, \theta, t)$. Let D be a determinantal operator

$$D = \det |L| \quad , \tag{3.2}$$

it can be shown[30] that each solution of the equation

$$D(\Gamma) = 0 \tag{3.3}$$

corresponds to an integral of the system of homogeneous equations of motion [Equation (3.1)] given by

$$x = \frac{2}{1-\nu} D_{13}(\Gamma) \quad , \tag{3.4a}$$

$$y = \frac{2}{1-\nu} D_{23}(\Gamma) \quad , \tag{3.4b}$$

$$z = \frac{2}{1-\nu} D_{33}(\Gamma) \quad , \tag{3.4c}$$

where D_{i3} denote the corresponding minors of the determinant in Equation (3.2). It should be noted that in the above derivation the differentiation symbols are treated as algebraic quantities. This is applicable only if their coefficients are constants.

Assuming solutions of the form

$$x(s, \theta, t) = \sum_{n=0}^{\infty} x_n(s,t)\cos(n\theta) \quad , \tag{3.5a}$$

$$y(s, \theta, t) = \sum_{n=0}^{\infty} y_n(s,t)\sin(n\theta) \quad , \tag{3.5b}$$

$$z(s, \theta, t) = \sum_{n=0}^{\infty} z_n(s,t)\cos(n\theta) \quad , \tag{3.5c}$$

$$\Gamma(s, \theta, t) = \sum_{n=0}^{\infty} \Gamma_n(s,t)\cos(n\theta) \quad , \tag{3.5d}$$

and substituting into Equations (3.4) yields:

$$x_n(s,t) = \frac{n^2}{1-\nu}\left(1+N_\theta/C\right)\left(\nu-1-2N_\theta/C\right)\Gamma_n' + \left(\frac{2N_\theta N_x}{(1-\nu)C^2} + \frac{N_\theta}{C} - \frac{2\nu N_x}{(1-\nu)C} - \nu\right)\Gamma_n''' + \frac{2c_2 G}{1-\nu}\left(\nu-N_\theta/C\right)\frac{\partial^2 \Gamma_n'}{\partial t^2} \quad , \tag{3.6a}$$

$$y_n(s,t) = -n^3\left(1+N_\theta/C\right)\left(1+\frac{2N_\theta}{(1-\nu)C}\right)\Gamma_n - \frac{2nc_1G}{(1-\nu)}\left(1+N_\theta/C\right)\frac{\partial^2\Gamma_n}{\partial t^2}$$

$$+ \frac{2n}{(1-\nu)}\left(1+\frac{(3+\nu)N_\theta}{2C}+[1+N_\theta/C]\frac{N_x}{C}-\frac{\nu(1+\nu)}{2}\right)\Gamma_n'' \quad , \qquad (3.6b)$$

$$z_n(s,t) = n^4\left(1+N_\theta/C\right)\left(1+\frac{2N_\theta}{(1-\nu)C}\right)\Gamma_n - n^2\left(\frac{2}{1-\nu}[1+N_x/C][1+N_\theta/C]\right.$$

$$\left.+[1+\frac{2N_\theta}{(1-\nu)C}][\frac{1-\nu}{2}+\frac{N_x}{C}]\right)\Gamma_n'' + \left(1+\frac{2N_x}{(1-\nu)C}\right)\left(1+N_x/C\right)\Gamma_n''''$$

$$+n^2\left(c_2G[1+\frac{2N_\theta}{(1-\nu)C}]+\frac{2c_1G}{1-\nu}[1+N_\theta/C]\right)\frac{\partial^2\Gamma_n}{\partial t^2} + \frac{2c_1c_2G^2\partial^4\Gamma_n}{1-\nu}{\partial t^4}$$

$$-\left(c_1G[1+\frac{2N_x}{(1-\nu)C}]+\frac{2c_2G}{1-\nu}[1+N_x/C]\right)\frac{\partial^2\Gamma_n''}{\partial t^2} \quad , \qquad (3.6c)$$

in which the primes denote differentiation with respect to s.

The potential function Γ_n must satisfy Equation (3.3) which appears in explicit form as

$$A_0\Gamma_n + A_1\frac{\partial^2\Gamma_n}{\partial s^2} + A_2\frac{\partial^4\Gamma_n}{\partial s^4} + A_3\frac{\partial^6\Gamma_n}{\partial s^6} + A_4\frac{\partial^2\Gamma_n}{\partial t^2} + A_5\frac{\partial^4\Gamma_n}{\partial s^2\partial t^2}$$

$$+ A_6\frac{\partial^6\Gamma_n}{\partial s^4\partial t^2} + A_7\frac{\partial^4\Gamma_n}{\partial t^4} + A_8\frac{\partial^6\Gamma_n}{\partial s^2\partial t^4} + A_9\frac{\partial^6\Gamma_n}{\partial t^6} = 0 \quad . \qquad (3.7)$$

The following assumptions are now made:

(i) Only the lowest derivatives of Γ with respect to time are important.

(ii) Two adjacent axial nodes are very far apart. This implies that the most significant terms in Equations (3.6) and (3.7)

are those with the lowest derivative of Γ in s, i.e.,

$$\frac{\partial^m \Gamma}{\partial s^m} >> \frac{\partial^{m+1} \Gamma}{\partial s^{m+1}} \quad .$$ [29]

Hence the higher derivatives of Γ with respect to s may be neglected as a first approximation.

For the beam-bending mode of interest here, n = 1, and the initial stresses induced by the internal pressure are

$$N_\theta = pa \quad , \qquad N_x = pa/2 \quad .$$

Defining a dimensionless pressure P = pa/(Eh), and keeping in mind the aforementioned assumptions, Equation (3.7) can be reduced to

$$A_2 \frac{\partial^4 \Gamma_1}{\partial s^4} + A_4 \frac{\partial^2 \Gamma_1}{\partial t^2} + A_5 \frac{\partial^4 \Gamma_1}{\partial s^2 \partial t^2} = 0 \quad , \tag{3.8}$$

where

$$A_2 = \frac{(1-\nu^2)^3}{4} P^3 + \frac{(13+7\nu)(1-\nu^2)^2}{8} P^2 + \frac{(14-2\nu-12\nu^2)(1-\nu^2)}{8} P$$

$$+ \frac{(1-\nu)(1-\nu^2)}{2} \quad ,$$

$$A_4 = G(c_2+c_3)\left[(1-\nu^2)^2 P^2 + \left(\frac{3-\nu}{2}\right)(1-\nu^2)P + \frac{1-\nu}{2}\right] \quad ,$$

$$A_5 = G\Big((c_1+c_3)(1-\nu^2)^2P^2 - [7(1+\nu)c_2+2(3-\nu)c_1+3(3-\nu)c_3](\frac{1-\nu^2}{4})P$$

$$- \frac{(1-\nu)}{2}c_1 - (1-\nu^2)c_2 - (1-\nu)c_3\Big) \quad .$$

Retaining the first-order terms only in this approximation, Equations (3.6) become

$$x_1 = \Big((1+\nu)P[\nu-3-2(1-\nu^2)P]-1\Big)\frac{\partial\Gamma_1}{\partial s} \quad , \tag{3.9a}$$

$$y_1 = -[1+(1-\nu^2)P][1+2(1+\nu)P]\Gamma_1 \quad , \tag{3.9b}$$

$$z_1 = -y_1 \quad , \tag{3.9c}$$

and, by Equations (3.5),

$$x = x_1\cos\theta \quad , \tag{3.10a}$$

$$y = y_1\sin\theta \quad , \tag{3.10b}$$

$$z = z_1\cos\theta = -y_1\cos\theta \quad . \tag{3.10c}$$

Multiplying Equations (3.10b) and (3.10c) by $\sin\theta$ and $\cos\theta$, respectively, and subtracting gives

$$y_1(s,t) = y\sin\theta - z\cos\theta \quad . \tag{3.11a}$$

On the other hand, multiplying them by $\cos\theta$ and $\sin\theta$, respectively, and adding gives

$$0 = z\sin\theta + y\cos\theta \quad . \tag{3.11b}$$

The right-hand side of Equation (3.11a) denotes the vertical while that of (3.11b) the horizontal displacements of the points of the middle surface of the shell (Figure 3-2). Since they do not depend upon θ, the shell behaves like a beam. The cross sections remain rigid in their planes and are displaced vertically by

$$y_1(s,t) = w(s,t) \quad . \tag{3.12}$$

Letting $\xi = \tilde{x}/L$ and using Equation (3.12), Equation (3.8) can be

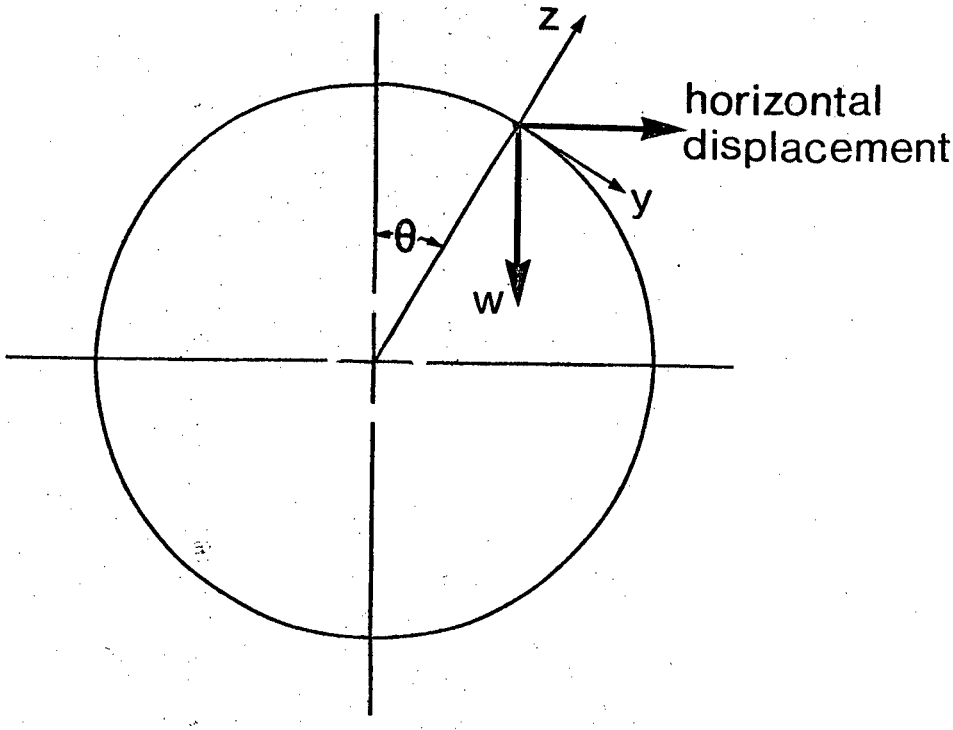

Figure 3-2 Vertical and horizontal displacement components

rewritten as

$$\frac{\partial^2 w}{\partial t^2} + \frac{A_5}{A_4}\left(\frac{a}{L}\right)^2 \frac{\partial^4 w}{\partial \xi^2 \partial t^2} + \frac{A_2}{A_4}\left(\frac{a}{L}\right)^4 \frac{\partial^4 w}{\partial \xi^4} = 0 \quad . \tag{3.13}$$

By Equations (3.9a) and (3.12) the longitudinal displacement is

$$x = \frac{1-(1+\nu)P[\nu-3-2(1-\nu^2)P]}{[1+(1-\nu^2)P][1+2(1+\nu)P]} \frac{\partial w}{\partial s}\cos\theta \quad ,$$

which corresponds to the rotation of the cross section about its horizontal diameter.

Equations (3.9) suggest that the radial and circumferential displacements z and y are of the same order, thus c_2 has to be set to unity. If the rotary inertia is to be taken into account as well, c_1 must also be unity. To incorporate the added inertia of the water both inside and outside the tube, c_3 is adjusted to $1+(1+C_m)\rho_w a/(\rho h)$ (Appendix I). The value of the added mass coefficient C_m, as predicted by the potential theory[78], is 1.0. This was confirmed experimentally by Stelson and Mavis[17] for cylinders with large length to diameter ratios. Hence, in the analysis here the added mass coefficient is taken to be unity.

Note that for a shell vibrating in air with no internal pressure, $c_3 = 1$ and $P = 0$, and Equation (3.13), after some rearranging, reduces to

$$\frac{\partial^2 w}{\partial t^2} + \frac{E}{2\rho a^2}\frac{\partial^4 w}{\partial \xi^4} - \frac{(5+2\nu)}{2}\frac{\partial^4 w}{\partial \xi^2 \partial t^2} = 0 \quad . \tag{3.14}$$

Equation (3.14) is identical to the one derived by Kornecki[29]. It is interesting to compare this with the elementary beam equation for a thin-walled tube including rotary inertia,

$$\frac{\partial^2 w}{\partial t^2} + \frac{E}{2\rho a^2}\frac{\partial^4 w}{\partial \xi^4} - \frac{1}{2}\frac{\partial^4 w}{\partial \xi^2 \partial t^2} = 0 \quad .$$

It is apparent that the reduced shell equation takes into account the Poisson ratio effect which the simple beam theory ignored.

To account for the viscous effect of the surrounding water a hydrodynamic resistance force is added. The hydrodynamic resistance is generally taken as a drag force proportional to the square of the velocity, i.e.,

$$F_d = \frac{1}{2} C_d d \rho_w v_{rel} |v_{rel}| \quad , \tag{3.15}$$

where C_d is the drag coefficient, and v_{rel} the velocity of the shell element relative to the fluid. The value of C_d in the flat portion of the subcritical region is approximately[79] 1.18, and this value is used in the present analysis.

Defining

$$\eta = w/d \quad , \qquad B_3 = \left(\frac{a}{L}\right)^4 \left(\frac{E}{\rho a^2 \left[2+(1+C_m)\left(\frac{\rho_w}{\rho}\right)\left(\frac{a}{h}\right)\right]}\right) \quad ,$$

$$B_1 = \left(\frac{L}{a}\right)^4 \frac{B_3 A_4}{A_2} \quad , \qquad B_2 = \left(\frac{L}{a}\right)^2 \frac{A_5 B_3}{A_2} \quad , \qquad \tau = \sqrt{B_3}\,t \quad , \tag{3.16}$$

Equation (3.13) can be nondimensionalized as

$$\frac{\partial^4 \eta}{\partial \xi^4} + B_2 \frac{\partial^4 \eta}{\partial \xi^2 \partial \tau^2} + B_1 \frac{\partial^2 \eta}{\partial \tau^2} + \alpha \frac{\partial \eta}{\partial \tau} \left| \frac{\partial \eta}{\partial \tau} \right| = 0 \quad , \tag{3.17a}$$

where

$$\alpha = \left(\frac{2}{\pi}\right) C_d \left(\frac{\rho_w}{\rho}\right) \left(\frac{a}{h}\right) / [1 + (1+C_m)(\rho_w/\rho)(a/h)]$$

$$\simeq \frac{2C_d}{\pi(1+C_m)} \quad , \tag{3.17b}$$

since $(1+C_m)(\rho_w/\rho)(a/h) >> 1$.

It may be noted that the damping parameter α is identical to the one formulated by Misra[3] and is independent of the geometrical dimensions of the cylinder if $(a/h) >> 1$. The boundary conditions are given by

$$\eta(0,\tau) = \frac{\partial \eta(0,\tau)}{\partial \xi} = \frac{\partial^2 \eta(1,\tau)}{\partial \xi^2} = \frac{\partial^3 \eta(1,\tau)}{\partial \xi^3} = 0 \quad . \tag{3.17c}$$

This nonlinear partial differential equation does not seem to have any known closed form solution. Hence one is forced to approach the problem through numerical analysis or approximate procedures.

(b) Solution for Zero Drag

For determination of the natural frequency it can be assumed, at least up to the first order approximation, that the period of oscillation is essentially unaffected by the presence of hydrodynamic drag[3]. Dropping the drag term, Equation (3.17a) becomes

$$\frac{\partial^4\eta}{\partial\xi^4} + B_2\frac{\partial^4\eta}{\partial\xi^2\partial\tau^2} + B_1\frac{\partial^2\eta}{\partial\tau^2} = 0 \quad . \tag{3.18}$$

Assuming solution of the form

$$\eta(\xi,\tau) = \beta(\xi)f(\tau) \quad , \tag{3.19}$$

and substituting into Equation (3.18) gives

$$\frac{d^4\beta}{d\xi^4}f + B_2\frac{d^2\beta}{d\xi^2}\frac{d^2f}{d\tau^2} + B_1\beta\frac{d^2f}{d\tau^2} = 0 \quad ,$$

or

$$\frac{\beta''''}{B_2\beta''+B_1\beta} = -\frac{\ddot{f}}{f} = \lambda^4 = \text{constant.} \tag{3.20}$$

This leads to two ordinary differential equations:

$$\frac{d^2f}{d\tau^2} + \lambda^4 f = 0 \quad , \tag{3.21a}$$

$$\frac{d^4\beta}{d\xi^4} - \lambda^4 B_2\frac{d^2\beta}{d\xi^2} - B_1\lambda^4\beta = 0 \quad , \tag{3.21b}$$

with solutions

$$f = f_c\cos(\lambda^2\tau) + f_s\sin(\lambda^2\tau) \quad , \tag{3.22a}$$

$$\beta = C_1\cosh(\lambda'\xi) + C_2\sinh(\lambda'\xi) + C_3\cos(\lambda''\xi) + C_4\sin(\lambda''\xi) \quad . \tag{3.22b}$$

Applying the boundary conditions (3.17c) gives the following equations relating λ, λ', and λ'':

$$B_2^2\lambda^4 + 2\sqrt{B_1}(1+\cosh\lambda'\cos\lambda'') - \sqrt{B_1}B_2\lambda^2\sinh\lambda'\sin\lambda'' = 0 \quad , \tag{3.23a}$$

$$\lambda'^2 - \lambda''^2 = B_2\lambda^4 \quad , \tag{3.23b}$$

$$\lambda'\lambda'' = \sqrt{B_1}\lambda^2 \quad . \tag{3.23c}$$

By solving Equations (3.23) the natural frequencies and the associated mode shapes can be found. The general solution is then given by

$$\eta(\xi,\tau) = \sum_{r=1}^{\infty}\beta_r(\xi)f_r(\tau) \quad , \tag{3.24}$$

where $\beta_r(\xi)$ is the normalized mode shape given by

$$\beta_r(\xi) = K_r[\cosh\lambda_r'\xi - C_5\sinh\lambda_r'\xi - \cos\lambda_r''\xi + C_6\sin\lambda_r''\xi] \quad ,$$

with

$$C_5 = \frac{\lambda_r'^2\cosh\lambda_r' + \lambda_r''^2\cos\lambda_r''}{\lambda_r'^2\sinh\lambda_r' + \lambda_r'\lambda_r''\sin\lambda_r''} \quad ,$$

$$C_6 = \frac{\lambda_r'^2\cosh\lambda_r' + \lambda_r''^2\cos\lambda_r''}{\lambda_r'\lambda_r''\sinh\lambda_r' + \lambda_r''^2\sin\lambda_r''} \quad .$$

Here K_r is chosen to normalize $\beta_r(\xi)$, i.e.,

$$\int_0^1 \beta_r^2(\xi)\,d\xi = 1 \quad .$$

Analysis showed K_r to be

$$K_r = \Big(1 + \frac{(C_6^2 - C_5^2)}{2} + \frac{\sinh\lambda_r'}{2\lambda_r'}[(1+C_5^2)\cosh\lambda_r' - 2C_5\sinh\lambda_r'] + \frac{\sin\lambda_r''}{2\lambda_r''}[(1-C_6^2)\cos\lambda_r'' - 2C_6\sin\lambda_r''] + \frac{2}{\lambda_r'^2+\lambda_r''^2}[(C_5\lambda_r' - C_6\lambda_r'') * \cosh\lambda_r'\cos\lambda_r'' - (\lambda_r'' + C_5C_6\lambda_r')\cosh\lambda_r'\sin\lambda_r'' + (C_5C_6\lambda_r'' - \lambda_r') * \sinh\lambda_r'\cos\lambda_r'' + (C_5\lambda_r'' + C_6\lambda_r')\sinh\lambda_r'\sin\lambda_r'' + C_5\lambda_r' - C_6\lambda_r'']\Big)^{-\frac{1}{2}}. \quad (3.25)$$

The natural frequencies are thus given by

$$\omega_r^2 = \sqrt{B_3}\lambda_r^2 \quad , \quad (3.26)$$

where λ_r is the solution of Equations (3.23), and B_3 is given by

Equation (3.16).

The orthogonality condition for the normalized mode shape $\beta(\xi)$ is found to be (Appendix II)

$$\int_0^1 \beta_m \beta_n d\xi = \frac{B_2}{B_1} \int_0^1 \beta'_m \beta'_n d\xi - \frac{B_2}{B_1(\lambda_m^4 - \lambda_n^4)} [\lambda_m^4 \beta'_m(1)\beta_n(1) - \lambda_n^4 \beta_m(1)\beta'_n(1)] \quad ,$$

$$\text{for } m \neq n \quad . \qquad (3.27)$$

(c) Perturbation Solution

To investigate effect of the hydrodynamic drag on the free response, Equation (3.17a) must be solved. The nonlinear nature of the equation does not permit an exact solution and one is forced to resort to an approximate analysis. In this section the perturbation technique is used to study the response of the inflated cantilever subjected to hydrodynamic drag.

The governing Equation (3.17a) may be rewritten as

$$\frac{\partial^4 \eta}{\partial \xi^4} + B_2 \frac{\partial^4 \eta}{\partial \xi^2 \partial \tau^2} + B_1 \frac{\partial^2 \eta}{\partial \tau^2} \pm \alpha \left(\frac{\partial \eta}{\partial \tau}\right)^2 = 0 \quad , \qquad (3.17a')$$

where the appropriate sign for the drag term is chosen so as to oppose the motion. It is sufficient to solve the above equation either for the positive or negative sign over half a cycle, solution for the other half obtained simply by reversing the sign of α with new initial conditions.

The solution for the negative sign is sought in the form

$$\eta(\xi,\tau) = \eta_0(\xi,\tau) + \alpha\eta_1(\xi,\tau) + \alpha^2\eta_2(\xi,\tau) + \ldots \quad . \tag{3.28}$$

A new time variable $\tilde{t}$ defined by

$$\tilde{t} = \tau[1 + \alpha b_1 + \alpha^2 b_2 + \ldots] \tag{3.29}$$

is introduced where b_1 and b_2 are slowly varying function of ξ, to account for the period of oscillation which may vary along the length. Substituting from Equations (3.28) and (3.29), the governing equation takes the form

$$\frac{\partial^4}{\partial\xi^4}(\eta_0+\alpha\eta_1+\alpha^2\eta_2+\ldots) + \{1+\alpha b_1+\alpha^2 b_2+\ldots\}^2\{B_2\frac{\partial^4}{\partial\xi^2\partial\tilde{t}^2}(\eta_0+\alpha\eta_1$$

$$+\alpha^2\eta_2+\ldots)+B_1\frac{\partial^2}{\partial\tilde{t}^2}(\eta_0+\alpha\eta_1+\alpha^2\eta_2+\ldots)-\alpha[\frac{\partial}{\partial\tilde{t}}(\eta_0+\alpha\eta_1+\alpha^2\eta_2$$

$$+\ldots)]^2\} = 0 \quad .$$

Equating the coefficients of the different powers of α to zero one obtains

$$\alpha^0 \; : \; \frac{\partial^4\eta_0}{\partial\xi^4} + B_2\frac{\partial^4\eta_0}{\partial\xi^2\partial\tilde{t}^2} + B_1\frac{\partial^2\eta_0}{\partial\tilde{t}^2} = 0 \quad , \tag{3.30a}$$

$$\alpha^1 \; : \; \frac{\partial^4\eta_1}{\partial\xi^4} + B_2\frac{\partial^4\eta_1}{\partial\xi^2\partial\tilde{t}^2} + B_1\frac{\partial^2\eta_1}{\partial\tilde{t}^2} = -2b_1(\xi)[B_2\frac{\partial^4\eta_0}{\partial\xi^2\partial\tilde{t}^2} + B_1\frac{\partial^2\eta_0}{\partial\tilde{t}^2}]$$

$$+ \left(\frac{\partial \eta_0}{\partial \tilde{t}}\right)^2 \quad , \tag{3.30b}$$

$$\alpha^2 \; : \; \frac{\partial^4 \eta_2}{\partial \xi^4} + B_2 \frac{\partial^4 \eta_2}{\partial \xi^2 \partial \tilde{t}^2} + B_1 \frac{\partial^2 \eta_2}{\partial \tilde{t}^2} = -[2b_2(\xi) + b_1^2(\xi)]\left[B_2 \frac{\partial^4 \eta_0}{\partial \xi^2 \partial \tilde{t}^2} + B_1 \frac{\partial^2 \eta_0}{\partial \tilde{t}^2}\right]$$

$$-2b_1(\xi)\left[B_2 \frac{\partial^4 \eta_1}{\partial \xi^2 \partial \tilde{t}^2} + B_1 \frac{\partial^4 \eta_1}{\partial \tilde{t}^2}\right] + 2b_1(\xi)\left(\frac{\partial \eta_0}{\partial \tilde{t}}\right)^2 + 2\frac{\partial \eta_0}{\partial \tilde{t}}\frac{\partial \eta_1}{\partial \tilde{t}} \quad , \tag{3.30c}$$

etc.

The objective is to solve this system of equations such that all η_i's conform to the boundary conditions (3.17c) with the prescribed initial conditions satisfied by η_0 alone, and zero initial conditions for other η_i's.

Equation (3.30a) is identical in form to Equation (3.18) whose solution has been shown to be (3.24). However, the rather complex orthogonality condition [Equation (3.27)] for the exact mode function does not permit decoupling of the equations later on in the perturbation analysis. Hence an approximate solution to Equation (3.30a) is sought in the form

$$\eta_0 = \sum_{r=1}^{\infty} \Phi_r(\xi) f_r(\tilde{t}) \quad , \tag{3.31}$$

where $\Phi_r(\xi)$ are the eigenfunctions of a cantilever beam,

$$\Phi_r(\xi) = \cosh(\mu_r\xi) - \cos(\mu_r\xi) - \sigma_r[\sinh(\mu_r\xi) - \sin(\mu_r\xi)] \quad .$$

Here

$$\sigma_r = (\cosh\mu_r + \cos\mu_r)/(\sinh\mu_r + \sin\mu_r) \quad ,$$

and μ_r are the roots of the frequency equation

$$1 + \cosh\mu\cos\mu = 0 \quad .$$

Substitution of Equation (3.31) into Equation (3.30a) gives

$$\sum_{r=1}^{\infty} \left(\frac{d^4\Phi_r}{d\xi^4}f_r + B_2\frac{d^2\Phi_r}{d\xi^2}\frac{d^2f_r}{d\tilde{t}^2} + B_1\Phi_r\frac{d^2f_r}{d\tilde{t}^2}\right) = 0 \quad . \tag{3.32}$$

Noting that

$$\frac{d^4\Phi_r}{d\xi^4} = \mu_r^4\Phi_r \quad , \tag{3.33a}$$

and that $\dfrac{d^2\Phi_r}{d\xi^2}$ can be expressed in terms of $\Phi_r(\xi)$ by the series

$$\frac{d^2\Phi_r}{d\xi^2} = \sum_{i=1}^{\infty} C_{ri}\Phi_i(\xi) \quad , \tag{3.33b}$$

where C_{ri} is given by[80]

$$C_{ri} = \int_0^1 \frac{d^2\Phi_r}{d\xi^2}\Phi_i d\xi = \begin{cases} 4(\mu_r\sigma_r - \mu_i\sigma_i)/[(-1)^{i+r} - (\mu_i/\sigma_r)^2] \ , & i \neq r \\ \mu_r\sigma_r(2-\mu_r\sigma_r) \ , & i = r \ , \end{cases}$$

Equation (3.32) may be rewritten as

$$\sum_{r=1}^{\infty} \left(\mu_r^4 \Phi_r f_r + [B_2 \sum_{i=1}^{\infty} C_{ri}\Phi_i + B_1\Phi_r]\frac{d^2 f_r}{d\tilde{t}^2}\right) = 0 \quad . \tag{3.32a}$$

Multiplying by Φ_j, integrating with respect to ξ over the length, and noting that

$$\int_0^1 \Phi_i \Phi_j d\xi = \delta_{ij} \quad ,$$

where δ_{ij} is the Kronecker delta, Equation (3.32a) becomes

$$\mu_j^4 f_j + [B_2 \sum_{r=1}^{\infty} C_{rj} + B_1]\frac{d^2 f_j}{d\tilde{t}^2} = 0 \quad , \qquad j = 1, 2, \ldots, \infty. \tag{3.34}$$

The solution of this equation is

$$f_j(\tilde{t}) = F_{cj}\cos[\mu_j^2\tilde{t}/(B_1+B_2\sum_{r=1}^{\infty} C_{rj})^{-\frac{1}{2}}] + F_{sj}\sin[\mu_j^2\tilde{t}/(B_1+B_2\sum_{r=1}^{\infty} C_{rj})^{-\frac{1}{2}}] \ . \tag{3.35}$$

Let the initial conditions be

$$\eta(\xi,0) = A_0(\xi) \qquad \text{and} \qquad \frac{\partial \eta}{\partial \tilde{t}}(\xi,0) = 0 \quad , \tag{3.36}$$

the zeroth order solution is then

$$\eta_0(\xi,\tilde{t}) = \sum_{j=1}^{\infty} A_{0j}\Phi_j(\xi)\cos\bar{\mu}_j^2\tilde{t} \quad , \tag{3.37a}$$

where

$$A_{0j} = \int_0^1 A_0(\xi)\Phi_j(\xi)\, d\xi \quad , \tag{3.37b}$$

and

$$\bar{\mu}_j^2 = \mu_j^2/(B_1+B_2\sum_{r=1}^{\infty} C_{rj})^{-\frac{1}{2}} \quad . \tag{3.37c}$$

With this, Equation (3.30b) becomes

$$\frac{\partial^4\eta_1}{\partial\xi^4} + B_2\frac{\partial^4\eta_1}{\partial\xi^2\partial\tilde{t}^2} + B_1\frac{\partial^2\eta_1}{\partial\tilde{t}^2} = q(\xi,\tilde{t}) \quad , \tag{3.38}$$

where

$$q(\xi,\tilde{t}) = 2b_1(\xi)\sum_{j=1}^{\infty} A_{0j}\bar{\mu}_j^4[B_1\Phi_j(\xi)+B_2\frac{d^2\Phi_j(\xi)}{d\xi^2}]\cos\bar{\mu}_j^2\tilde{t}$$

$$+ \frac{1}{2}\sum_{j=1}^{\infty}\sum_{k=1}^{\infty} A_{0j}A_{0k}\bar{\mu}_j^2\bar{\mu}_k^2\Phi_j(\xi)\Phi_k(\xi)[\cos(\bar{\mu}_j^2-\bar{\mu}_k^2)\tilde{t}$$

$$- \cos(\bar{\mu}_j^2+\bar{\mu}_k^2)\tilde{t}] \quad .$$

A solution to Equation (3.38) can be taken in the form

$$\eta_1(\xi,\tilde{t}) = \sum_{m=1}^{\infty} \Phi_m(\xi) f_m(\tilde{t}) \quad . \tag{3.39}$$

Substituting Equation (3.39) into Equation (3.38), multiplying by $\Phi_n(\xi)$, integrating with respect to ξ over the length and using the orthogonality condition leads to

$$\mu_n^4 f_n(\tilde{t}) + [B_1+B_2 \sum_{m=1}^{\infty} C_{mn}] \frac{d^2 f_n(\tilde{t})}{d\tilde{t}^2} = \bar{Q}_n(\tilde{t}) \quad , \quad n = 1, 2, \ldots, \infty. \tag{3.40}$$

where

$$\bar{Q}_n(\tilde{t}) = \int_0^1 q(\xi,\tilde{t}) \Phi_n(\xi) d\xi \quad .$$

Equation (3.40) can be rewritten as

$$\frac{d^2 f_n}{d\tilde{t}^2} + \bar{\mu}_n^4 f_n = Q_n(\tilde{t}) \quad , \qquad n = 1, 2, \ldots, \infty.$$

where

$$Q_n(\tilde{t}) = \bar{Q}_n(\tilde{t}) / [B_1+B_2 \sum_{m=1}^{\infty} C_{mn}] = [1/(B_1+B_2 \sum_{m=1}^{\infty} C_{mn})] *$$

$$\left(2 \sum_{j=1}^{\infty} A_{0j} \bar{\mu}_j^4 \int_0^1 b_1(\xi) \Phi_n(\xi) [B_1+B_2 \frac{d^2 \Phi_j}{d\xi^2}] d\xi \cos \bar{\mu}_j^2 \tilde{t} \right.$$

$$\left. + \frac{1}{2} \sum_{j=1}^{\infty} \sum_{k=1}^{\infty} \beta_{jkn} \bar{\mu}_j^2 \bar{\mu}_k^2 A_{0j} A_{0k} [\cos(\bar{\mu}_j^2 - \bar{\mu}_k^2)\tilde{t} - \cos(\bar{\mu}_j^2 + \bar{\mu}_k^2)\tilde{t}] \right) \quad , \tag{3.40a}$$

and

$$\beta_{jkn} = \int_0^1 \Phi_j(\xi)\Phi_k(\xi)\Phi_n(\xi)d\xi \quad . \tag{3.40b}$$

As the term involving $b_1(\xi)$ in Equation (3.40a) gives rise to secular quantities, it must vanish for all j,

$$b_1(\xi) = 0 \quad , \tag{3.41}$$

i.e. the natural frequencies are independent of the nonlinear hydrodynamic drag up to the first order. This confirms the approximation made in the previous section that the period of oscillation is unaffected by the presence of the hydrodynamic drag.

The solution to Equation (3.40) can now be written as

$$f_n(\tilde{t}) = C_{1n}\cos\bar{\mu}_n^2\tilde{t} + D_{1n}\sin\bar{\mu}_n^2\tilde{t} + \tfrac{1}{2}[1/(B_1+B_2\sum_{m=1}^{\infty}C_{mn})] *$$

$$\sum_{j=1}^{\infty}\sum_{k=1}^{\infty}\beta_{jkn}\bar{\mu}_j^2\bar{\mu}_k^2A_{0j}A_{0k}\left(\cos(\bar{\mu}_j^2-\bar{\mu}_k^2)\tilde{t}/[\bar{\mu}_n^4-(\bar{\mu}_j^2-\bar{\mu}_k^2)^2]\right.$$

$$\left. - \cos(\bar{\mu}_j^2+\bar{\mu}_k^2)\tilde{t}/[\bar{\mu}_n^4-(\bar{\mu}_j^2+\bar{\mu}_k^2)^2]\right) \quad . \tag{3.42}$$

Applying the zero initial conditions gives

$$C_{1n} = -\tfrac{1}{2}[1/(B_1+B_2\sum_{m=1}^{\infty}C_{mn})]\sum_{j=1}^{\infty}\sum_{k=1}^{\infty}\beta_{jkn}\bar{\mu}_j^2\bar{\mu}_k^2A_{0j}A_{0k} *$$

$$\left(\frac{1}{\bar{\mu}_n^4-(\bar{\mu}_j^2-\bar{\mu}_k^2)^2} - \frac{1}{\bar{\mu}_n^4-(\bar{\mu}_j^2+\bar{\mu}_k^2)^2}\right) \quad , \tag{3.43a}$$

$$D_{1n} = 0 \quad . \tag{3.43b}$$

Substitution of Equation (3.43) into (3.42) yields

$$\eta_1(\xi,\tilde{t}) = -\frac{1}{2}\sum_{j=1}^{\infty}\sum_{k=1}^{\infty}\sum_{n=1}^{\infty}\left(\frac{\beta_{jkn}\bar{\mu}_j^2\bar{\mu}_k^2 A_{0j}A_{0k}\Phi_n(\xi)}{B_1+B_2\sum_{m=1}^{\infty}C_{mn}}\right) * \left([\cos\bar{\mu}_n^2\tilde{t}-\cos(\bar{\mu}_j^2-\bar{\mu}_k^2)\tilde{t}]/[\bar{\mu}_n^4-(\bar{\mu}_j^2-\bar{\mu}_k^2)^2]\right.$$

$$\left. - [\cos\bar{\mu}_n^2\tilde{t}-\cos(\bar{\mu}_j^2+\bar{\mu}_k^2)\tilde{t}]/[\bar{\mu}_n^4-(\bar{\mu}_j^2+\bar{\mu}_k^2)^2]\right) \quad . \tag{3.44}$$

Thus the solution, up to the first order of approximation, is

$$\eta(\xi,\tilde{t}) = \eta_0(\xi,\tilde{t}) + \alpha\eta_1(\xi,\tilde{t}) \quad . \tag{3.45}$$

3.1.2 Rayleigh-Ritz Method

Consider a uniform cylindrical shell in equilibrium acted upon by static initial stress σ_x^i, σ_θ^i, and $\sigma_{x\theta}^i$. During vibration the internal stresses in the shell consist of the initial stresses and the additional vibratory stresses σ_x, σ_θ, and $\sigma_{x\theta}$. Assuming there is no interaction between the prestress displacements and the vibratory stresses, the internal strain energy of the shell, taking the prestressed equilibrium state as the reference level, can be written as[31]

$$U = \frac{1}{2}\int_{Vol.}(\sigma_x e_x + \sigma_\theta e_\theta + \sigma_{x\theta}\gamma_{x\theta})d(Vol.)$$

$$+\int_{Vol.}(\sigma^i_x e_x + \sigma^i_\theta e_\theta + \sigma^i_{x\theta}\gamma_{x\theta})d(Vol.) \qquad (3.46)$$

$$= U_1 + U_2 \quad .$$

The vibratory stresses σ_x, σ_θ, and $\sigma_{x\theta}$ are related to the vibratory strains by Hooke's Law

$$\sigma_x = \frac{E}{1-\nu^2}(e_x + \nu e_\theta) \quad , \qquad (3.47a)$$

$$\sigma_\theta = \frac{E}{1-\nu^2}(e_\theta + \nu e_x) \quad , \qquad (3.47b)$$

$$\sigma_{x\theta} = \frac{E}{2(1+\nu)}\gamma_{x\theta} \quad . \qquad (3.47c)$$

Substituting Equations (3.47) together with the strain-displacement relations of a given shell theory into (3.46) and integrating over the thickness yields the strain energy. Because the initial stresses may be large it is necessary to use the second-order, nonlinear strain-displacement equations in the U_2 of Equation (3.46) while using only the linear relations in U_1. This maintains the proper homogeneity in the orders of magnitude of the terms in the integrands[31].

U_1 is made up of two parts, one due to stretching (membrane) and the other due to the addition of bending stiffness, i.e.,

$$U_1 = U_{membrane} + U_{bending} \quad . \tag{3.48}$$

The membrane component is given by[81]

$$U_{membrane} = \frac{Eh}{2(1-\nu^2)} \iint \Big(a\left(\frac{\partial x}{\partial \tilde{x}}\right)^2 + \frac{1}{a}\left(\frac{\partial y}{\partial \theta}+z\right)^2 + 2\nu\frac{\partial x}{\partial \tilde{x}}\left(\frac{\partial y}{\partial \theta}+z\right)$$

$$+ \frac{(1-\nu)}{2a}\left(\frac{\partial x}{\partial \theta}+a\frac{\partial y}{\partial \tilde{x}}\right)^2 \Big) d\tilde{x}d\theta \quad , \tag{3.48a}$$

while $U_{bending}$ contains small terms proportional to $(h/a)^3$ that are negligible for modes with small number of circumferential waves[82]. It should be noted that all the existing shell theories lead to the identical expression for $U_{membrane}$, the differences occur in the $U_{bending}$.

For pressurized tubes the initial stresses are given by

$$\sigma_x^i = \frac{\sigma_\theta^i}{2} = \frac{pa}{2h} = \frac{N_x}{h} \quad , \qquad \sigma_{x\theta}^i = 0 \quad . \tag{3.49}$$

The strain e of an element at a distance $\tilde{z}$ from the middle surface consists of the stretching of the middle surface and that due to rotation of the element. Accordingly,

$$e_x = \varepsilon_x + \tilde{z}\kappa_x \quad , \tag{3.50a}$$

$$e_\theta = \varepsilon_\theta + \tilde{z}\kappa_\theta \quad , \tag{3.50b}$$

where ε_x, ε_θ denote the middle surface strains and κ_x, κ_θ the changes

in curvature. Note that ε's and κ's are not functions of $\tilde{z}$.

Equations (3.50) may also be derived from strain-displacement relations of the three-dimensional theory of elasticity. In order to satisfy the Kirchhoff hypothesis, which states that the normals to the undeformed middle surface remain straight and normal to the deformed middle surface and suffer no extension, the diaplacements are restricted to linear relationships. Using the linear relations and neglecting the $(\tilde{z}/a)$ terms in comparison with unity the strain-displacement relations simplify to Equations (3.50).

The second order strain-displacement relations according to Washizu's shell theory[83] are

$$\varepsilon_x = \frac{\partial x}{\partial \tilde{x}} + \frac{1}{2}[(\frac{\partial x}{\partial \tilde{x}})^2 + (\frac{\partial y}{\partial \tilde{x}})^2 + (\frac{\partial z}{\partial \tilde{x}})^2] \quad , \tag{3.51a}$$

$$\varepsilon_\theta = \frac{1}{a}\frac{\partial y}{\partial \theta} + \frac{z}{a} + \frac{1}{2a^2}(\frac{\partial z}{\partial \theta})^2 - \frac{y}{a^2}\frac{\partial z}{\partial \theta} \quad . \tag{3.51b}$$

Since the initial stresses are assumed to be due to membrane action, i.e., uniform through the thickness, it is sufficient to retain only linear terms in the expressions relating curvature changes to displacements[84]. There is general agreement among the shell theories for expressions of the middle surface curvatures κ_x and κ_θ, usually taken as

$$\kappa_x = -\frac{\partial^2 z}{\partial \tilde{x}^2} \quad , \tag{3.52a}$$

$$\kappa_\theta = \frac{1}{a^2}\frac{\partial y}{\partial \theta} - \frac{1}{a^2}\frac{\partial^2 z}{\partial \theta^2} \quad . \tag{3.52b}$$

Substitution of Equations (3.49) to (3.52) into U_2 and integration through the thickness gives

$$\begin{aligned} U_2 = \iint \Big(& N_x \frac{\partial x}{\partial \tilde{x}} + \frac{N_x}{2}\left(\frac{\partial x}{\partial \tilde{x}}\right)^2 + \frac{N_x}{2}\left(\frac{\partial y}{\partial \tilde{x}}\right)^2 + \frac{N_x}{2}\left(\frac{\partial z}{\partial \tilde{x}}\right)^2 - \frac{N_x h}{4}\frac{\partial^2 z}{\partial \tilde{x}^2} \\ & + \frac{N_{\theta\partial} y}{a \partial \theta} + N_\theta \frac{z}{a} + \frac{N_\theta}{2a^2}\left(\frac{\partial x}{\partial \theta}\right)^2 + \frac{N_\theta}{2a^2}\left[\frac{\partial y}{\partial \theta} + z\right]^2 + \frac{N_\theta}{2a^2}\left[y - \frac{\partial z}{\partial \theta}\right]^2 \\ & + \frac{N_\theta h \partial y}{4a^2 \partial \theta} - \frac{N_\theta h \partial^2 z}{4a^2 \partial \theta^2} - \frac{N_\theta h \partial y}{4a^2 \partial \theta} - \frac{N_\theta h}{4a^2} z - \frac{N_\theta h}{8a^3}\left(\frac{\partial x}{\partial \theta}\right)^2 \\ & - \frac{N_\theta h}{8a^3}\left[\frac{\partial y}{\partial \theta} + z\right]^2 - \frac{N_\theta h}{8a^3}\left[y - \frac{\partial z}{\partial \theta}\right]^2 \Big) a d\tilde{x} d\theta \quad . \end{aligned} \tag{3.53}$$

The kinetic energy of the inflated shell accounting for the added inertia is

$$\begin{aligned} T &= \frac{1}{2}\rho h \iint \left[\left(\frac{\partial x}{\partial t}\right)^2 + \left(\frac{\partial y}{\partial t}\right)^2 + \left(\frac{\partial z}{\partial t}\right)^2\right] a d\theta d\tilde{x} \\ &\quad + \frac{1}{2}(1+C_m)\rho_w \iiint \left[\frac{\partial y}{\partial t}\sin\theta + \frac{\partial z}{\partial t}\cos\theta\right]^2 r d\theta d\tilde{x} dr \\ &= \frac{1}{2}\rho h \iint \left[\left(\frac{\partial x}{\partial t}\right)^2 + \left(\frac{\partial y}{\partial t}\right)^2 + \left(\frac{\partial z}{\partial t}\right)^2 + \frac{(1+C_m)\rho_w a}{2 \rho h}\left(\frac{\partial y}{\partial t}\sin\theta \right.\right. \\ &\quad \left.\left. + \frac{\partial z}{\partial t}\cos\theta\right)^2\right] a d\theta d\tilde{x} \quad . \end{aligned} \tag{3.54}$$

The assumed displacements in the beam bending mode are

$$x = [a_1\Phi_r'(\xi) + a_2\Psi_r'(\xi)]\cos\theta\cos\omega t \quad , \tag{3.55a}$$

$$y = [a_3\Phi_r(\xi) + a_4\Psi_r(\xi)]\sin\theta\cos\omega t \quad , \tag{3.55b}$$

$$z = [a_5\Phi_r(\xi) + a_6\Psi_r(\xi)]\cos\theta\cos\omega t \quad , \tag{3.55c}$$

where $\Phi_r(\xi)$ are the characteristic beam functions for cantilevers and

$$\Psi_r(\xi) = \cosh\upsilon_r\xi - \cos\upsilon_r\xi - \bar{\sigma}_r(\sinh\upsilon_r\xi - \sin\upsilon_r\xi)$$

are the characteristic functions for a clamped-pinned beam. Here

$$\bar{\sigma}_r = \cot\upsilon_r L \quad ,$$

and υ_r are the roots of the frequency equation

$$\tan\upsilon L - \tanh\upsilon L = 0 \quad .$$

The modal forms used in Equations (3.55) are quite realistic as in practice behaviour of an inflated shell suggests boundary conditions between the two sets mentioned above[82].

According to the Rayleigh-Ritz Method

$$\frac{\partial}{\partial a_i}(U-T) = 0 \quad . \tag{3.56}$$

Substituting the assumed modes (3.55) into the energy expressions, integrating over the period, and applying the Rayleigh-Ritz procedure one obtains a sixth degree frequency equation, which can be rearranged to form an eigenvalue problem of the type

$$[M](a) = \Omega^2[N](a) \quad , \tag{3.57a}$$

where Ω^2 is the dimensionless frequency given by

$$\Omega^2 = \frac{\rho a^2(1-\nu^2)\omega^2}{E} \quad . \tag{3.57b}$$

The order of the matrices will be 3n in general, where n is the number of mode shapes in the assumed solution.

Premultiplying Equation (3.57a) by $[N]^{-1}$ gives

$$[N]^{-1}[M](a) = \Omega^2(a)$$

or

$$[Q](a) = \Omega^2(a) \quad , \tag{3.57c}$$

where

$$[Q] = [N]^{-1}[M] \quad .$$

The system of Equations (3.57c) can now be solved by an iteration procedure (e.g. UBC DREIGN) to obtain the frequencies and mode shapes. The elements of the matrices [M] and [N] are given in Appendix III for Washizu's shell theory.

3.2 Tapered Beam Analysis

For a tapered beam one has to resort to the conical shell theory to account for initial stresses induced by inflation pressure. The conical shell theory is a simple generalization of the uniform cylindrical shell theory. Uniform cylindrical shells are a special case of conical shells with zero vertex angle. Due to varying radius along the length, the inflation prestresses are functions of x, the axial co-ordinate. Hence the potential reduction technique employed in the previous section for the uniform cylindrical shells cannot be applied in the present case. The exact solution of the conical shell equations themselves is far from simple. In general, approximate and numerical techniques have been used in the inflated conical shell studies to date. As pressure effects on the natural frequencies of the conical shells are expected to be small for the beam-bending mode of interest here, a first simplification would be to neglect the internal pressure effects and study the tapered cantilever using the elementary beam theory.

Equilibrium of the forces acting on a section of a tapered beam (Figure 3-3) oscillating in water leads to

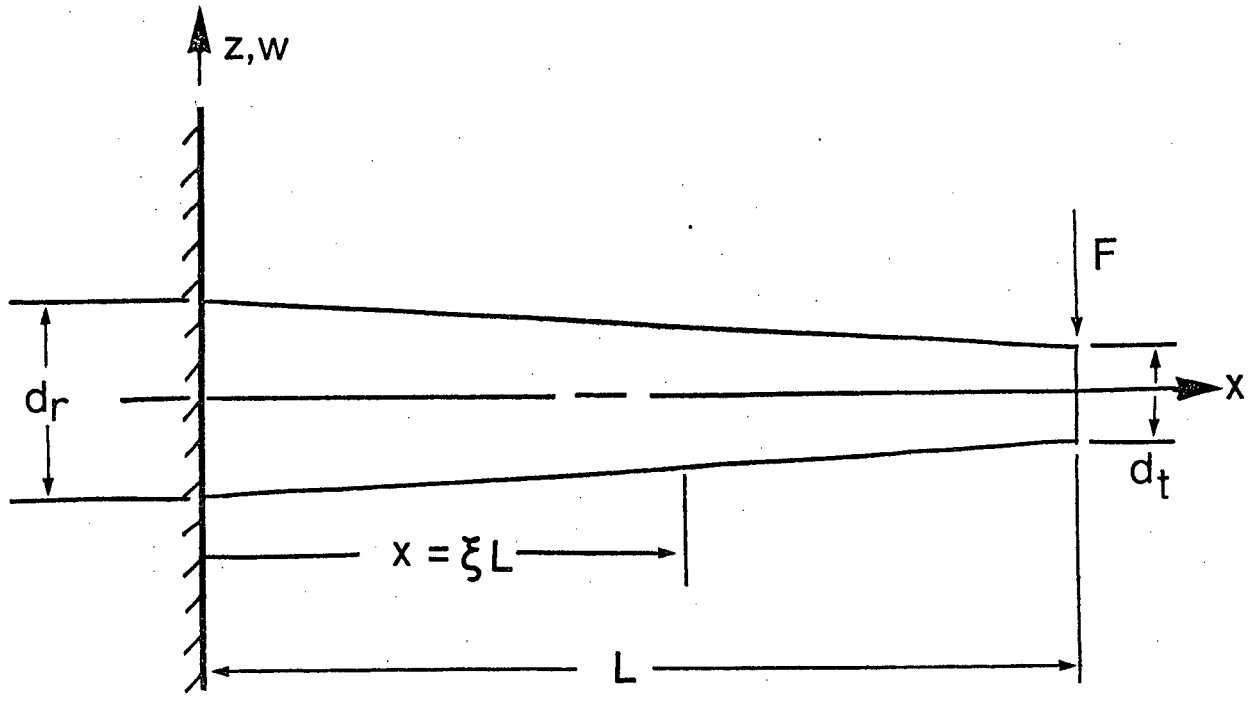

Figure 3-3 Geometry of motion of a tapered cantilever

$$\frac{\partial^2}{\partial x^2}\left[EI(x)\frac{\partial^2 w}{\partial x^2}\right] + \rho_w A_w(x)\frac{\partial^2 w}{\partial t^2} + F_H = 0 \quad , \tag{3.58a}$$

where F_H is the total hydrodynamic force on the element. It may be noted that the second term representing the inertia force of the section is primarily due to the water inside the cantilever since the mass of the wall material is very small. The resistance F_H is taken to be of the Morison type[15], i.e., made up of a drag force proportional to the square of the velocity and an added inertia force caused by the acceleration of the surrounding water,

$$F_H = \frac{1}{2}C_d d(x)\rho_w v_{rel}|v_{rel}| + C_m A_w(x)\rho_w \frac{dv_{rel}}{dt} \quad , \tag{3.58b}$$

where C_d and C_m are the drag and added mass coefficients, respectively, and v_{rel} the velocity of the cantilever relative to the fluid. This assumes that the drag and the inertia effects are free of appreciable mutual interference. In the study the values of C_d and C_m are assumed to be constant and equal to 1.18 and 1.0, respectively, as in the uniform cylindrical beam analysis.

From quations (3.58a) and (3.58b) one obtains

$$\frac{\partial^2}{\partial x^2}[EI(x)\frac{\partial^2 w}{\partial x^2}] + (1+C_m)\rho_w A_w(x)\frac{\partial^2 w}{\partial t^2} + \frac{1}{2}C_d d(x)\rho_w \frac{\partial w}{\partial t}\left|\frac{\partial w}{\partial t}\right| = 0 \quad . \tag{3.58c}$$

Defining

$$\eta = w/d_r \quad , \qquad \xi = x/L \quad , \qquad k = (d_r - d_t)/d_r \quad ,$$

and noting that

$$I(x) = I_r(1-k\xi)^3 \quad , \qquad A_w(x) = A_{w_r}(1-k\xi)^2 \quad ,$$

$$d(x) = d_r(1-k\xi) \quad , \tag{3.59}$$

Equation (3.58c) can be rewritten as

$$\frac{EI_r}{L^4}\frac{\partial^2}{\partial \xi^2}[(1-k\xi)^3\frac{\partial^2 \eta}{\partial \xi^2}] + (1+C_m)\rho_w A_{w_r}(1-k\xi)^2\frac{\partial^2 \eta}{\partial t^2}$$

$$+ \frac{1}{2}C_d\rho_w d_r^2(1-k\xi)\frac{\partial \eta}{\partial t}\left|\frac{\partial \eta}{\partial t}\right| = 0 \quad . \tag{3.60}$$

For the purpose of finding natural frequencies, Equation (3.60) may be simplified considerably if it is assumed that the nonlinear drag term has only a second order effect and may be neglected as a first approximation. Discarding the nonlinear term, Equation (3.60) can be rewritten as

$$(1-k\xi)^2\frac{\partial^4\eta}{\partial\xi^4} - 6k(1-k\xi)\frac{\partial^3\eta}{\partial\xi^3} + 6k^2\frac{\partial^2\eta}{\partial\xi^2} + \frac{(1+C_m)\rho_w A_{w_r} L^4}{EI_r}(1-k\xi)\frac{\partial^2\eta}{\partial t^2}$$

$$= 0 \quad . \tag{3.61}$$

In absence of any known closed form solution an approximate procedure has to be used. The solution is assumed to be of the form

$$\eta(\xi,t) = \sum_{i=1}^{\infty}\Phi_i(\xi)f_i(t) \quad , \tag{3.62}$$

where, as before, Φ_i are the characteristic beam functions for a cantilever.

Substituting (3.62) into Equation (3.61), multiplying by $\Phi_r(\xi)$ and integrating over the length gives

$$\sum_{i=1}^{\infty}\int_0^1\Big[(1-k\xi)^2\frac{d^4\xi_i}{d\xi^4}\Phi_r f_i - 6k(1-k\,)\frac{d^3\Phi_i}{d\xi^3}\Phi_r f_i + 6k^2\frac{d^2\Phi_i}{d\xi^2}\Phi_r f_i$$

$$+ \frac{(1+C_m)\rho_w A_{w_r} L^4}{EI_r}(1-k\xi)\Phi_i\Phi_r\frac{d^2f_i}{dt^2}\Big)d\xi = 0 \quad . \tag{3.63a}$$

For natural vibrations, f_i vary harmonically with the same circular frequency ω. Thus

$$\frac{d^2 f_i}{dt^2} = - \omega_i^2 f_i \quad .$$

Noting that

$$\frac{d^4 \Phi_i}{d\xi^4} = \mu_i^4 \Phi_i \quad ,$$

Equation (3.63a) becomes

$$\sum_{i=1}^{\infty} \int_0^1 \Big[-6k(1-k\xi)\frac{d^3\Phi_i}{d\xi^3}\Phi_r + 6k^2\frac{d^2\Phi_i}{d\xi^2}\Phi_r + (1-k\xi)\Big[\mu_i^4(1-k\xi) - \frac{(1+C_m)\rho_w A_{w_r} L^4 \omega_i^2}{EI_r}\Big]\Phi_i\Phi_r\Big] f_i d\xi = 0 \quad , \quad r = 1, 2, \ldots, i. \tag{3.63b}$$

The above set containing an infinite number of frequency equations gives rise to the eigenvalue problem of the form

$$[S](f) = \lambda^2 [V](f) \quad , \tag{3.64a}$$

or

$$[Z](f) = \lambda^2 (f) \quad , \tag{3.64b}$$

where [S], [V], and [Z] are square matrices of order i, with

$$[Z] = [V]^{-1}[S] \quad ,$$

and λ^2 is the dimensionless frequency given by

$$\lambda_i^2 = \frac{(1+C_m)\rho_w A_w r^4 \omega_i^2}{EI_r} \quad .$$

A detailed calculation procedure and the elements of the matrices [S] and [V] are given in Appendix IV for i = 1, 2, and 3, respectively.

3.3 Results and Discussion

To assess validity of the analytical procedures, it was thought appropriate to experimentally determine natural frequency over the range of system parameters of interest in practice. The tests were carried out in the hydraulic tank, (Figure 2-4), described in Chapter 2. A series of cantilevers of varying radius, length, taper, film thickness and internal pressure were tested. Natural frequencies were monitored through two waterproof strain gauges attached to the top and bottom side of an inflated beam near its root (clamped end). Free vibrations were triggered through initial displacement and release, and the cyclic strain recorded on the oscilloscope indicated the natural frequency. A typical trace on the oscilloscope screen is shown in Figure 2-4. In general, the tests for a given setting were repeated at least five times and the average was used. The

tests can be repeated with deviations less than 2%.

3.3.1 Uniform Cylindrical Cantilever

Table 3.1 compares the experimentally measured frequencies of five inflated cantilevers with various theoretical predictions. Experimental results show a slight increase in frequency with pressure. Although the increase is quite small and almost negligible for all practical purposes, it is significant to recognize that this trend is correctly predicted by the solutions to Flügge's reduced equation (3.13). The difference between the exact frequency [Equation (3.26)] and that obtained by the mode-approximation [Equation (3.37c)] is negligible for all cases considered. Both solutions are capable of predicting the natural frequencies with excellent accuracy. Besides Flügge's theory, the reduction procedure was also applied to the membrane and Herrmann-Armenàkas theories (Appendix V). The results obtained from these reduced equations are included in the table for comparison. Both the methods tend to overstress the pressure effects, with the Herrmann-Armenàkas theory erroneously predicting a decrease in frequency with internal pressures. In a few cases the frequencies drop to zero and turn imaginary, rendering the validity of the reduced Herrmann-Armenàkas equation questionable. The reduced membrane equation predicts a much larger increase in frequency with internal pressure than that observed. On the other hand, the much simpler elementary beam theory, despite its inability to predict the pressure effects on natural frequencies, gives results of reasonable accuracy.

TUBE SIZES	Pressure N/m^2 (psi)	Experimental Data	Beam Theory	Reduced Equations				Rayleigh-Ritz		
				Membrane	Herr.-Armen.	Flugge		Washizu		Membrane
						I	II	1-term	2-term	2-term
L = 1.02m (40") d = 5.08cm (2.0") h=0.008cm (.003")	0		0.69	0.69	0.69	0.69	0.69	1.05	1.02	1.02
	2.07×10^4 (3.0)	0.70		1.05	0.20	0.69	0.69	2.40	2.22	1.47
	3.45×10^4 (5.0)	0.70		1.23	Im.	0.69	0.69	2.97	2.65	1.69
	4.14×10^4 (6.0)	0.70		1.31	Im.	0.69	0.69	3.22	2.89	1.78
L = 0.91m (36") d = 7.62cm (3.0") h=0.008cm (.003")	0		1.04	1.04	1.04	1.05	1.04	1.58	1.54	1.54
	2.07×10^4 (3.0)	1.06		1.36	0.74	1.05	1.04	2.86	2.71	1.94
	3.45×10^4 (5.0)	1.07		1.54	0.45	1.05	1.05	3.45	3.19	2.16
	4.14×10^4 (6.0)	1.08		1.62	0.16	1.06	1.05	3.71	3.39	2.26
L = 0.61m (24") d = 5.08cm (2.0") h=0.008cm (.003")	0		1.91	1.91	1.91	1.92	1.91	2.90	2.82	2.82
	2.07×10^4 (3.0)	2.01		2.32	1.56	1.93	1.91	4.61	4.44	3.34
	3.45×10^4 (5.0)	2.01		2.56	1.28	1.93	1.92	5.45	5.14	3.64
	4.14×10^4 (6.0)	2.02		2.67	1.12	1.93	1.92	5.82	5.44	3.77
L = 0.61m (24") d = 7.62cm (3.0") h=0.008cm (.003")	0		2.34	2.34	2.34	2.38	2.34	3.52	3.41	3.41
	2.07×10^4 (3.0)	2.38		2.70	2.07	2.39	2.35	4.99	4.82	3.85
	3.45×10^4 (5.0)	2.39		2.91	1.87	2.39	2.36	5.76	5.48	4.10
	4.14×10^4 (6.0)	2.39		3.01	1.77	2.39	2.36	6.11	5.76	4.22
L = 0.61m (24") d = 7.62cm (3.0") h=0.015cm (.006")	0		3.31	3.31	3.31	3.36	3.31	4.97	4.81	4.81
	2.07×10^4 (3.0)	3.36		3.57	3.12	3.37	3.32	6.10	5.93	5.13
	3.45×10^4 (5.0)	3.37		3.73	3.00	3.37	3.32	6.75	6.53	5.33
	4.14×10^4 (6.0)	3.37		3.81	2.93	3.37	3.32	7.05	6.78	5.43

I - Exact solution [Equation (3.26)]

II - Mode-approximation solution [Equation (3.37c)]

Table 3.1 Comparison between Analytically and Experimentally Obtained Frequencies for Uniform Beams (Hz)

Also shown in Table 3.1 are the theoretical predictions based on the Rayleigh-Ritz method applied to the Washizu and the membrane shell theories. The derivation of the energy expressions for the membrane theory is presented in Appendix VI. For the Washizu theory results for one- and two-term approximations are shown for comparison. Their agreement with experimental results is poor, and the large difference between the one- and two-term approximations indicates a slow convergence of the natural frequencies. The fact that the convergence of results can be very slow has been observed by other investigators such as Sewall and Naumann[44], and Resnick and Dugundji[45]. Sewall and Naumann compared analytical frequencies with experimental results for clamped-free shells without prestress. They used seven terms in the assumed mode shapes to obtain convergence of the Ritz procedure. Resnick and Dugundji, using an energy approach, found that the theoretical and experimental data agreed only for modes with more than five circumferential waves. Thus a large number of terms will be required to converge to the right value, but the amount of algebra involved is great since the order of the governing matrices increases rapidly with the number of terms used in the approximation (order of matrices equals three times the number of terms used).

3.3.2 Tapered Cantilever

Variation of the fundamental and second mode eigenvalues ($\sqrt{\lambda_i}$) with the taper ratio k is shown in Figure 3-4 for the cases of one-, two-, and three-term approximations. For the fundamental mode the three-term approximation gives eigenvalues that lie in between the ones predicted by the one- and two-term approximations. If more terms are taken in the evaluation, results will probably converge to intermediate values bounded by the two- and three-term approximations. For the second mode, the eigenvalue remains relatively unchanged up to a taper ratio of about 0.5. For larger tapers the two-term approximation fails to give accurate predictions. On the other hand, the one-term approximation, employing the second-mode cantilever beam function, provides estimates deviating less than 2.5% from their corresponding three-term approximation values. Nevertheless, the deviations among the three approximations shown are negligible for small tapers ($k \leq 0.5$).

Table 3.2 shows the experimental results and the associated theoretical predictions. The agreement is very good and the simple beam theory used is capable of accurate predictions. It is obvious from the experimental results that the increase in frequency due to internal pressure may be considered negligible from practical design considerations.

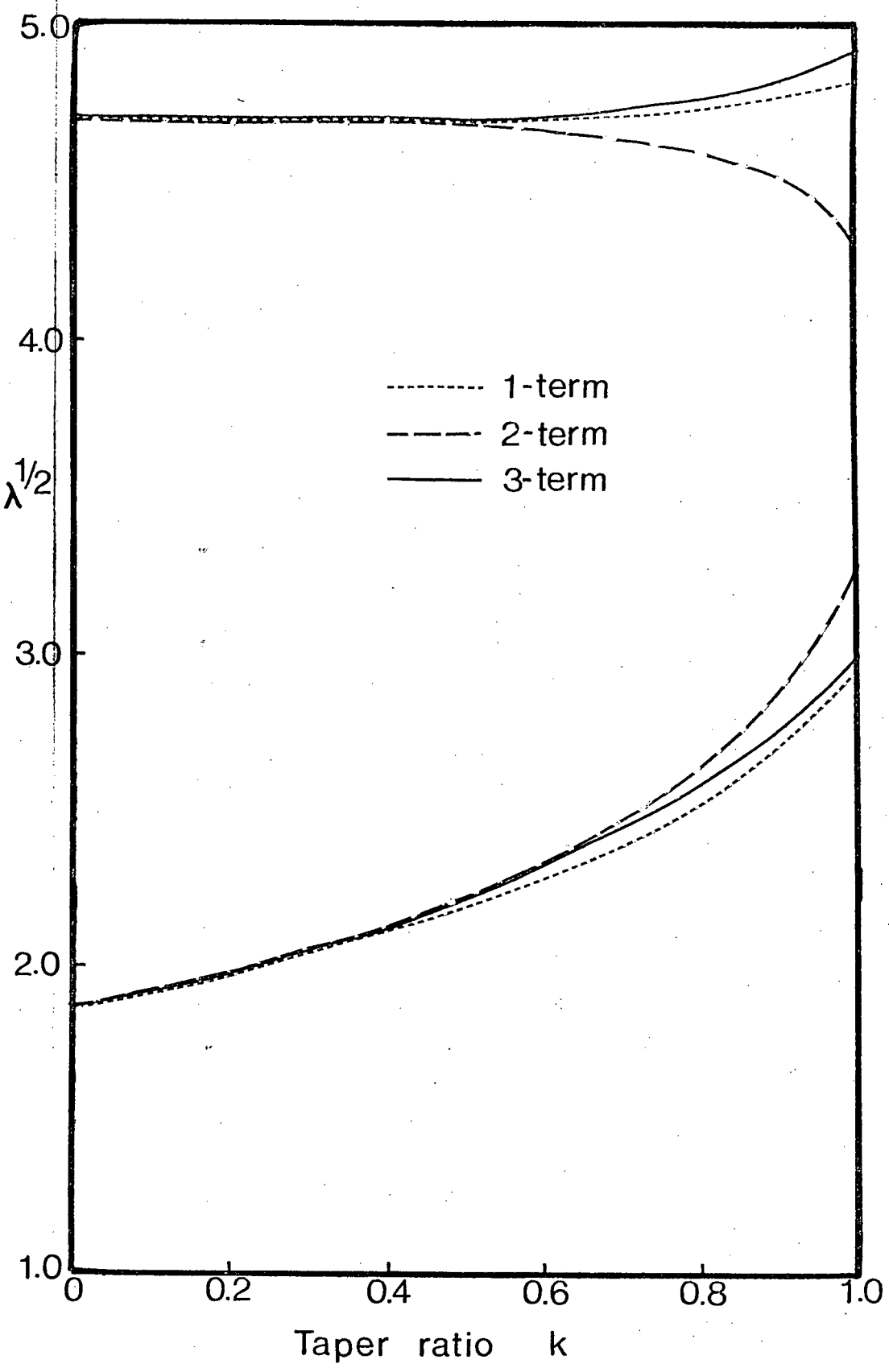

Figure 3-4 Variation of eigenvalues with taper ratio

	PRESSURE N/m^2 (psi)	TUBE LENGTH 0.61m (24") Beam Theory	0.61m (24") Expt. Data	0.81m (32") Beam Theory	0.81m (32") Expt. Data	1.02m (40") Beam Theory	1.02m (40") Expt. Data
d_r=7.62cm (3.0") d_t=3.81cm (1.5") h=0.008cm (.003")	0	3.27		1.84		1.18	
	2.07×10^4 (3.0)		3.22		1.84		1.21
	3.45×10^4 (5.0)		3.25		1.84		1.22
	4.14×10^4 (6.0)		3.25		1.85		1.22
d_r=10.16cm (4.0") d_t=5.08cm (2.0") h=0.008cm (.003")	0	3.74		2.13		1.36	
	2.07×10^4 (3.0)		3.74		2.13		1.30
	3.45×10^4 (5.0)		3.76		2.14		1.32
	4.14×10^4 (6.0)		3.77		2.15		1.33
d_r=12.70cm (5.0") d_t=6.35cm (2.5") h=0.008cm (.003")	0	4.22		2.38		1.52	
	2.07×10^4 (3.0)		4.23		2.39		1.53
	3.45×10^4 (5.0)		4.24		2.40		1.53
	4.14×10^4 (6.0)		4.24		2.40		1.54
d_r=7.62cm (3.0") d_t=3.81cm (1.5") h=0.015cm (0.006")	0	4.63		2.60		1.67	
	2.07×10^4 (3.0)		4.64		2.49		1.64
	3.45×10^4 (5.0)		4.65		2.52		1.65
	4.14×10^4 (6.0)		4.66		2.53		1.65

Table 3.2 Comparison Between Analytically and Experimentally Obtained Frequencies (Hz) for Tapered Beams (Hz)

3.4 Concluding Remarks

The significant conclusions based on the free vibration analysis can be summarized as follows:

(i) For the uniform cylindrical inflated cantilevers vibrating in the beam-bending mode, the governing three-dimensional shell equations do not permit simple solutions. Although an exact procedure is available, it has been sparingly applied because of the great amount of work required. Numerical and approximate techniques have mostly been used in the shell vibration studies to date. For the present study, it is found that the shell equations can be reduced to a single equation similar in form to the one for the transverse vibrations of a beam with rotary inertia included. Flügge's shell equation in reduced form is capable of predicting the vibrational behaviour of uniform cylindrical beams subjected to internal pressure. Accurate predictions are possible even with the approximate solution of the equation discussed here. However, the reduction technique should be applied with care, since various shell theories give results which may be significantly different. The reduced equations for the membrane and Herrmann-Armenàkas theories fail to give reasonable results. It should also be noted that for certain shell theories the equations are nonsymmetric (e.g., the Timoshenko-Voss equations used by Fung et al.[37]) and the

potential function Γ will not be simply related to the lateral displacement w. In these cases the reduction process will not give meaningful results.

(ii) The elementary beam theory gives predictions of reasonable accuracy for both the uniform cylindrical and the tapered beams although the theory does not incorporate internal pressure effects. Fortunately the effect of pressure, at least in the range investigated here ($< 4.14 \times 10^4 N/m^2$ or 6.0 psi) appears to be insignificant. Even with the internal pressure of $4.14 \times 10^4 N/m^2$ or 6.0psi ($P = 0.02$), the increase in frequency would amount to less than 2%.

(iii) The Rayleigh-Ritz method does not give accurate results in the present investigation. The convergence of the results is slow and the relatively great amount of work required to achieve acceptable accuracy cannot be justified.

(iv) The hydrodynamic drag damping causes only an amplitude decay and does not affect the resonant frequencies of the cantilevers up to the first order approximation.

(v) For the tapered beam the fundamental frequency increases with the amount of taper. On the other hand, the second natural frequency stays relatively constant up to a taper ratio of about 0.5. For beams with taper ratios less than

0.5, there is no apparent advantage in employing more than one term in the assumed mode solution (3.62).

4. FORCED VIBRATION OF NEUTRALLY BUOYANT VISCOELASTIC INFLATED CANTILEVERS

The previous chapter investigated free response of the inflated cantilevers. It was noted that with increasing pressure, the increase in resonant frequencies is so small that the pressure effects may be neglected. The object of this chapter is to study the steady state response of the viscoelastic cantilever to wave excitation.

A preliminary study on the coupled motion of the submarine detection system was made by Misra[3], who concluded that displacements of the cantilever tips, where the hydrophones are located, may be reduced by using an elastic cable with small stiffness and a heavy central head. With a soft cable the transmission to the array of the buoy movements due to the surface waves will be relatively small. Of course, in general, such a submerged platform is subjected to a variety of disturbances including those due to surface and internal waves, and ocean currents. The configuration of the submarine detection system of interest here suggests that wave excitation felt by the buoy and transmitted by the cable are ultimately experienced by the central head. Hence in the present investigation, the disturbance is taken to be a generalized known displacement objective being the resulting response of the inflated cantilever.

To incorporate viscoelastic nature of the beam material, equivalent dissipative terms are included in the governing equation. This can be achieved quite readily by replacing the modulus of elasticity by the complex Young's modulus[3,85]. For a three parameter solid the complex Young's modulus can be represented as[75]

$$E^*(\omega) = E_1(E_2+i\nu_2\omega)/(E_1+E_2+i\nu_2\omega) \quad . \tag{4.1a}$$

Equation (4.1a) may be rewritten as a sum of real and imaginary parts, i.e.,

$$E^*(\omega) = E_1(\delta+i\omega\bar{\gamma}) = E_1(\delta+\bar{\gamma}\frac{\partial}{\partial t}) \quad , \tag{4.1b}$$

where

$$\delta = 1 - E_1(E_1+E_2)/[(E_1+E_2)^2+\nu_2^2\omega^2] \quad , \tag{4.1c}$$

and $\bar{\gamma}$ is the loss factor given by

$$\bar{\gamma} = E_1\nu_2/[(E_1+E_2)^2+\nu_2^2\omega^2] \quad . \tag{4.1d}$$

4.1 Uniform Cylindrical Beam

For forced vibration, the root (clamped end) of the cantilever is assumed to be displaced periodically by

$$\eta_r = \sum_{m=1}^{\infty} (\eta^*_{c,m} \cos m\omega\tau + \eta^*_{s,m} \sin m\omega\tau) \quad , \tag{4.2}$$

where τ is related to the real time t by (3.16) with the Young's modulus E replaced by the instantaneous modulus E_1. It should be noted that Equation (4.2) is a Fourier series and is capable of representing any periodic excitation. In the analysis, however, only the first two terms are included as spectral analysis of a typical ocean wave shows a steep reduction in energy content at higher harmonics (Figure 4-1). Recognizing that the maximum energy content

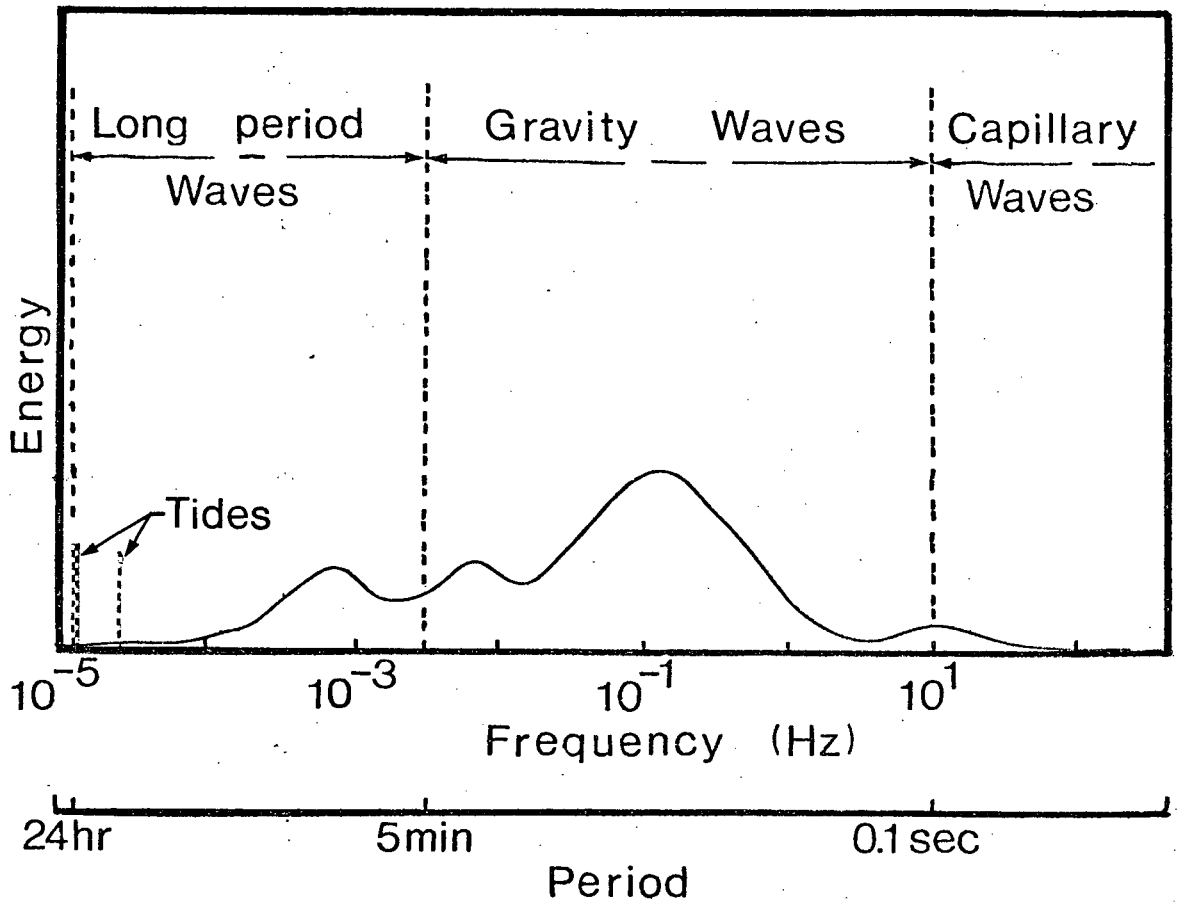

Figure 4-1 Schematic representation of the energy contained in the surface waves of the oceans -- (Reference 86)

of the surface waves is at around 0.1 Hz while the natural frequency of the inflated beam is in the range of 0.7 to 4 Hz (table 3.1, p. 79) the effect of higher harmonics is expected to be negligible.

The absolute lateral displacement of the beam is

$$\eta(\xi,\tau) = \eta_r + \bar{\eta}(\xi,\tau) \quad , \tag{4.3a}$$

where $\bar{\eta}(\xi,\tau)$ is the displacement of the cantilever relative to the root. In general the relative displacement can be represented by

$$\bar{\eta}(\xi,\tau) = \sum_{n=1}^{\infty} [\eta_{c,n}(\xi)\cos n\omega\tau + \eta_{s,n}(\xi)\sin n\omega\tau] \quad . \tag{4.3b}$$

Substituting Equations (4.1) and (4.3) into the nondimensionalized governing equation of motion (3.17a) leads to

$$\sum_{n=1}^{\infty}\sum_{m=1}^{\infty} \{[\delta+\gamma\frac{\partial}{\partial\tau}][\frac{d^4\eta_{c,n}}{d\xi^4}\cos n\omega\tau + \frac{d^4\eta_{s,n}}{d\xi^4}\sin n\omega\tau] - n^2\omega^2 B_2 *$$

$$[\frac{d^2\eta_{c,n}}{d\xi^2}\cos n\omega\tau + \frac{d^2\eta_{s,n}}{d\xi^2}\sin n\omega\tau] - \omega^2 B_1[m^2(\eta^*_{c,m}\cos m\omega\tau$$

$$+\eta^*_{c,m}\sin m\omega\tau)+n^2(\eta_{c,n}\cos n\omega\tau+\eta_{s,n}\sin n\omega\tau)] + \omega^2\alpha[m(\eta^*_{s,m}\cos m\omega\tau$$

$$-\eta^*_{c,m}\sin m\omega\tau)+n(\eta_{s,n}\cos n\omega\tau-\eta_{c,n}\sin n\omega\tau)]|m(\eta^*_{s,m}\cos m\omega\tau$$

$$-\eta^*_{c,m}\sin m\omega\tau)+n(\eta_{s,n}\cos n\omega\tau-\eta_{c,n}\sin n\omega\tau)|\} = 0 \quad , \tag{4.4}$$

where

$$\gamma = \sqrt{B_3}\bar{\gamma} \quad .$$

Taking two terms (n=2) in the assumed solution (4.3b) the nonlinear drag term in Equation (4.4) can be rewritten as

$$\pm\omega^2\alpha[A^2\sin^2(\omega\tau-\phi_1)+2AB\sin(\omega\tau-\phi_1)\sin(2\omega\tau-\phi_2)+B^2\sin^2(2\omega\tau-\phi_2)] \quad ,$$

where

$$A^2 = [(\eta^*_{c,1}+\eta_{c,1})^2 + (\eta^*_{s,1}+\eta_{s,1})^2] \quad ,$$

$$B^2 = 4[(\eta^*_{c,2}+\eta_{c,2})^2 + (\eta^*_{s,2}+\eta_{s,2})^2] \quad ,$$

$$\phi_1 = \arctan\left(\frac{\eta^*_{s,1}+\eta_{s,1}}{\eta^*_{c,1}+\eta_{c,1}}\right) \quad ,$$

$$\phi_2 = \arctan\left(\frac{\eta^*_{s,2}+\eta_{s,2}}{\eta^*_{c,2}+\eta_{c,2}}\right) \quad .$$

Multiplying Equation (4.4) by $\cos\omega\tau$, $\cos2\omega\tau$, $\sin\omega\tau$, and $\sin2\omega\tau$, respectively, and integrating with respect to $\omega\tau$ over the period gives four independent equations. It should be noted that the hydrodynamic drag force represented by the last term in Equation (4.4) is in phase with the velocity and changes direction twice during a cycle. Hence

the correct sign should be chosen accordingly. However, the positive and negative intervals of this term is dependent on the amplitudes A and B. Here, as a first approximation, it is assumed that A>>B such that the direction of the force is governed by the term involving A^2. This is justified as the second harmonic response will be in general much smaller than the fundamental one. A better estimate may be obtained by examining the first-approximation solutions of A and B and adjust the sign accordingly to give more accurate results.

Assuming the sign of the drag term to be governed by $\omega^2\alpha A^2\sin^2(\omega\tau-\phi_1)$ and carrying out the integration results in the following four equations:

$$\delta\frac{d^4\eta_{c,1}}{d\xi^4} + \gamma\omega\frac{d^4\eta_{s,1}}{d\xi^4} - \omega^2B_2\frac{d^2\eta_{c,1}}{d\xi^2} - \omega^2B_1(\eta^*_{c,1}+\eta_{c,1}) + \frac{\alpha\omega^2}{\pi}\{\frac{8}{3}A^2\sin\phi_1+B^2[2\sin\phi_1-\frac{1}{3}\sin(3\phi_1-2\phi_2)-\frac{1}{5}\sin(5\phi_1-2\phi_2)]\} = 0 \quad , \tag{4.5a}$$

$$\delta\frac{d^4\eta_{c,2}}{d\xi^4} + 2\gamma\omega\frac{d^4\eta_{s,2}}{d\xi^4} - 4\omega^2B_2\frac{d^2\eta_{c,2}}{d\xi^2} - 4\omega^2B_1(\eta^*_{c,2}+\eta_{c,2}) + \frac{2}{\pi}AB\alpha\omega^2[2\sin\phi_2+\frac{1}{3}\sin(2\phi_1+\phi_2)-\frac{1}{5}\sin(4\phi_1-\phi_2)] = 0 \quad , \tag{4.5b}$$

$$\delta\frac{d^4\eta_{s,1}}{d\xi^4} - \gamma\omega\frac{d^4\eta_{c,1}}{d\xi^4} - \omega^2B_2\frac{d^2\eta_{s,1}}{d\xi^2} - \omega^2B_1(\eta^*_{s,1}+\eta_{s,1}) - \frac{\alpha\omega^2}{\pi}\{\frac{8}{3}A^2\cos\phi_1+B^2[2\cos\phi_1+\frac{1}{3}\cos(3\phi_1-2\phi_2)-\frac{1}{5}\cos(5\phi_1-2\phi_2)]\} = 0 \quad , \tag{4.5c}$$

$$\delta\frac{d^4\eta_{s,2}}{d\xi^4} - 2\gamma\omega\frac{d^4\eta_{c.2}}{d\xi^4} - 4\omega^2 B_2\frac{d^2\eta_{s,2}}{d\xi^2} - 4\omega^2 B_1(\eta^*_{s,2}+\eta_{s,2})$$

$$- \frac{4}{\pi}AB\alpha\omega^2[\cos\phi_2+\frac{1}{15}\cos(4\phi_1-\phi_2)] = 0 \quad . \tag{4.5d}$$

The quantities $\eta_{c,n}$, $\eta_{s,n}$, $\eta^*_{c,n}$, and $\eta^*_{s,n}$ can be represented as

$$\eta_{c,n}(\xi) = \sum_{j=1}^{\infty}\bar{C}_{nj}\Phi_j(\xi) \quad , \tag{4.6a}$$

$$\eta_{s,n}(\xi) = \sum_{j=1}^{\infty}\bar{S}_{nj}\Phi_j(\xi) \quad , \tag{4.6b}$$

$$\eta^*_{c,n} = \sum_{j=1}^{\infty}C^*_{nj}\Phi_j(\xi) \quad , \tag{4.6c}$$

$$\eta^*_{s,n} = \sum_{j=1}^{\infty}S^*_{nj}\Phi_j(\xi) \quad . \tag{4.6d}$$

Substituting these into Equations (4.5), multiplying by Φ_1 and Φ_2, respectively, and integrating with respect to ξ over the length, one obtains eight simultaneous algebraic equations:

$$[\mu_1^4\delta-\omega^2(B_2C_{11}+B_1)]\bar{C}_{11} - \omega^2B_2C_{21}\bar{C}_{12} + \mu_1^4\gamma\omega\bar{S}_{11} - \omega^2B_1C^*_{11}$$

$$+ \frac{\alpha\omega^2}{\pi}I_1 = 0 \quad , \tag{4.7a}$$

$$[\mu_1^4\delta-4\omega^2(B_2C_{11}+B_1)]\bar{C}_{21} - 4\omega^2B_2C_{21}\bar{C}_{22} + 2\mu_1^4\gamma\omega\bar{S}_{21} - 4\omega^2B_1C^*_{21}$$

$$+ 2\frac{\alpha\omega^2}{\pi}I_2 = 0 \quad , \tag{4.7b}$$

$$\mu_1^4\gamma\omega\bar{C}_{11} - [\mu_1^4\delta-\omega^2(B_2C_{11}+B_1)]\bar{S}_{11} + \omega^2B_2C_{21}\bar{S}_{12}$$

$$+ \omega^2B_1S^*_{11} + \frac{\alpha\omega^2}{\pi}I_3 = 0 \quad , \tag{4.7c}$$

$$2\mu_1^4\gamma\omega\bar{C}_{21} - [\mu_1^4\delta-4\omega^2(B_2C_{11}+B_1)]\bar{S}_{21} + 4\omega^2B_2C_{21}\bar{S}_{22}$$

$$+ 4\omega^2B_1S^*_{21} + 4\frac{\alpha\omega^2}{\pi}I_4 = 0 \quad , \tag{4.7d}$$

$$\omega^2B_2C_{12}\bar{C}_{11} - [\mu_2^4\delta-\omega^2(B_2C_{22}+B_1)]\bar{C}_{12} - \mu_2^4\gamma\omega\bar{S}_{12}$$

$$+ \omega^2B_1C^*_{12} - \frac{\alpha\omega^2}{\pi}I_5 = 0 \quad , \tag{4.7e}$$

$$4\omega^2B_2C_{12}\bar{C}_{21} - [\mu_2^4\delta-4\omega^2(B_2C_{22}+B_1)]\bar{C}_{22} - 2\mu_2^4\gamma\omega\bar{S}_{22}$$

$$+ 4\omega^2B_1C^*_{22} - 2\frac{\alpha\omega^2}{\pi}I_6 = 0 \quad , \tag{4.7f}$$

$$\mu_2^4\gamma\omega\bar{C}_{12} + \omega^2B_2C_{12}\bar{S}_{11} - [\mu_2^4\delta-\omega^2(B_2C_{22}+B_1)]\bar{S}_{12}$$

$$+ \omega^2B_1S^*_{12} + \frac{\alpha\omega^2}{\pi}I_7 = 0 \quad , \tag{4.7g}$$

$$2\mu_2^4\gamma\omega\bar{C}_{22} + 4\omega^2B_2C_{12}\bar{S}_{21} - [\mu_2^4\delta-4\omega^2(B_2C_{22}+B_1)]\bar{S}_{22}$$

$$+ 4\omega^2B_1S^*_{22} + 4\frac{\alpha\omega^2}{\pi}I_8 = 0 \quad , \tag{4.7h}$$

where

$$I_1 = \int_0^1 \Phi_1\{\frac{8}{3}A^2\sin\Phi_1 + B^2[2\sin\Phi_1 - \frac{1}{3}\sin(3\Phi_1-2\Phi_2) - \frac{1}{5}\sin(5\Phi_1-2\Phi_2)]\}d\xi \quad , \tag{4.8a}$$

$$I_2 = \int_0^1 AB\Phi_1[2\sin\Phi_2 + \frac{1}{3}\sin(2\Phi_1+\Phi_2) - \frac{1}{5}\sin(4\Phi_1-\Phi_2)]d\xi \quad , \tag{4.8b}$$

$$I_3 = \int_0^1 \{\frac{8}{3}A^2\cos\Phi_1 + B^2[2\cos\Phi_1 + \frac{1}{3}\cos(3\Phi_1-2\Phi_2) - \frac{1}{5}\cos(5\Phi_1-2\Phi_2)]\}\Phi_1 d\xi \quad , \tag{4.8c}$$

$$I_4 = \int_0^1 AB[\cos\Phi_2 + \frac{1}{15}\cos(4\Phi_1-\Phi_2)]\Phi_1 d\xi \quad , \tag{4.8d}$$

$$I_5 = \int_0^1 \{\frac{8}{3}A^2\sin\Phi_1 + B^2[2\sin\Phi_1 - \frac{1}{3}\sin(3\Phi_1-2\Phi_2) - \frac{1}{5}\sin(5\Phi_1-2\Phi_2)]\}\Phi_2 d\xi \quad , \tag{4.8e}$$

$$I_6 = \int_0^1 [2\sin\Phi_2 + \frac{1}{3}\sin(2\Phi_1+\Phi_2) - \frac{1}{5}\sin(4\Phi_1-\Phi_2)]AB\Phi_2 d\xi \quad , \tag{4.8f}$$

$$I_7 = \int_0^1 \{\frac{8}{3}A^2\cos^2\Phi_1 + B^2[2\cos\Phi_1 + \frac{1}{3}\cos(3\Phi_1-2\Phi_2) - \frac{1}{5}\cos(5\Phi_1-2\Phi_2)]\}\Phi_2 d\xi \quad , \tag{4.8g}$$

$$I_8 = \int_0^1 [\cos\Phi_2 + \frac{1}{15}\cos(4\Phi_1-\Phi_2)]AB\Phi_2 d\xi \quad . \tag{4.8h}$$

The set of Equations (4.7) has to be solved simultaneously to obtain the response amplitudes. Here it was accomplished numerically.

4.2 Tapered Beam

The governing equation based on the elementary beam theory was given previously in Section 3.2,

$$\frac{EI_r}{L^4}\frac{\partial^2}{\partial\xi^2}\left[(1-k\xi)^3\frac{\partial^2\eta}{\partial\xi^2}\right] + (1+C_m)\rho_w A_{w_r}(1-k\xi)^2\frac{\partial^2\eta}{\partial t^2}$$

$$+ \frac{1}{2}C_d\rho_w d_r^2(1-k\xi)\frac{\partial\eta}{\partial t}\left|\frac{\partial\eta}{\partial t}\right| = 0 \quad .$$

Accounting for the viscoelastic dissipation the equation may be nondimensionalized as

$$\left[\delta+\gamma\frac{\partial}{\partial\tau}\right]\left[(1-k\xi)^2\frac{\partial^4\eta}{\partial\xi^4} - 6k(1-k\xi)\frac{\partial^3\eta}{\partial\xi^3} + 6k^2\frac{\partial^2\eta}{\partial\xi^2}\right] + (1-k\xi)\frac{\partial^2\eta}{\partial\tau^2}$$

$$+ \alpha\frac{\partial\eta}{\partial\tau}\left|\frac{\partial\eta}{\partial\tau}\right| = 0 \quad .$$

With a periodic root excitation given by (4.2) and an assumed solution similar to that for the uniform cylindrical beam eight simultaneous equations are obtained after following the anlytical procedure similar to that for the uniform case:

$$\{\mu_1^4\delta - \omega^2 + [(\omega^2-2\mu_1^4\delta)\chi_3 - 6\delta\chi_1]k + [\mu_1^4\chi_4 + 6(\chi_2+C_{11})]\delta k^2\}\bar{C}_{11}$$

$$+ \{[\omega^2\chi_7 - \delta(2\mu_2^4\chi_7+6\chi_5)]k + [\mu_2^4\chi_8 + 6(\chi_6+C_{21})]\delta k^2\}\bar{C}_{12}$$

$$+ \{\mu_1^4\gamma\omega - [2\mu_1^4\chi_3 + 6\chi_1]\gamma\omega k + [\mu_1^4\chi_4 + 6(C_{11}+\chi_2)]\gamma\omega k^2\}\bar{S}_{11}$$

$$- \gamma\omega\{[2\mu_2^4\chi_7 + 6\chi_5]k - [\mu_2^4\chi_8 + 6(\chi_6+C_{21})]\}\bar{S}_{12}$$

$$- \omega^2\{C_{11}^* - [\chi_3 C_{11}^* + \chi_7 C_{12}^*]k - \frac{\alpha}{\pi}I_1\} = 0 \quad , \qquad (4.9a)$$

$$\{\mu_1^4\delta - 4\omega^2 + [2\chi_3(2\omega^2-\mu_1^4\delta) - 6\delta\chi_1]k + [\mu_1^4\chi_4 + 6(\chi_2+C_{11})]\delta k^2\}\bar{C}_{21}$$

$$+ \{[2\chi_7(2\omega^2-\mu_2^4\delta) - 6\delta\chi_5]k + [\mu_2^4\chi_8 + 6(\chi_6+C_{21})]\delta k^2\}\bar{C}_{22}$$

$$+ \{2\mu_1^4 - 4[\mu_1^4\chi_3 - 3\chi_1]k + 2[\mu_1^4\chi_4 + 6(\chi_2+C_{11})]k^2\}\gamma\omega\bar{S}_{21}$$

$$- \{4[\mu_2^4\chi_7 + 3\chi_5] - 2[\mu_2^4\chi_8 + 6(\chi_6+C_{21})]\}\gamma\omega\bar{S}_{22}$$

$$- 4\omega^2\{C_{21}^* - [\chi_3 C_{21}^* + \chi_7 C_{22}^*]k + 2\frac{\alpha\omega^2}{\pi}I_2\} = 0 \quad , \qquad (4.9b)$$

$$\{\mu_1^4 - 2[\mu_1^4\chi_3 + 3\chi_1]k + [\mu_1^4\chi_4 + 6(\chi_2+C_{11})]\}\gamma\omega\bar{C}_{11}$$

$$- \{2[\mu_2^4\chi_7 + 3\chi_5] - [\mu_2^4\chi_8 + 6(\chi_6+C_{21})]\}\gamma\omega\bar{C}_{12}$$

$$- \{\mu_1^4\delta - \omega^2 - [(2\mu_1^4\delta-\omega^2)\chi_3 + 6\delta\chi_1]k + [\mu_1^4\chi_4 + 6(\chi_2+C_{11})]\delta k^2\}\bar{S}_{11}$$

$$+ \{[(2\mu_2^4\delta-\omega^2)\chi_7 + 6\delta\chi_5]k - [\mu_2^4\chi_8 + 6(\chi_6+C_{21})]\delta k^2\}\bar{S}_{12}$$

$$+ \omega^2\{S_{11}^* - [\chi_3 S_{11}^* + S_{12}^*\chi_7]k + \frac{\alpha}{\pi}I_3\} = 0 \quad , \qquad (4.9c)$$

$$\{2\mu_1^4 - 4[\mu_1^4\chi_3 + 3\chi_1]k + 2[\mu_1^4\chi_4 + 6(\chi_2+C_{11})]k^2\}\gamma\omega\bar{C}_{21}$$

$$- \{4[\mu_2^4\chi_7 + 3\chi_5]k - 2[\mu_2^4\chi_8 + 6(\chi_6+C_{21})]k^2\}\gamma\omega\bar{C}_{22}$$

$$- \{\mu_1^4\delta - 4\omega^2 - 2[(\mu_1^4\delta-2\omega^2)\chi_3 + 6\delta\chi_1]k + [\mu_1^4\chi_4 + 6(\chi_2+C_{11})]\delta k^2\}\bar{S}_{21}$$

$$+ \{2[(\mu_2^4\delta-2\omega^2)\chi_7 + 3\delta\chi_5]k - [\mu_2^4\chi_8 + 6(\chi_6+C_{21})]\delta k^2\}\bar{S}_{22}$$

$$+ 4\omega^2\{S_{21}^* - [S_{21}^*\chi_3 + S_{22}^*\chi_7]k + \frac{\alpha}{\pi}I_4\} = 0 \quad , \qquad (4.9d)$$

$$\{[(\omega^2-2\mu_1^4\delta)\chi_7 - 6\delta\chi_9]k + [\mu_1^4\chi_8 + 6(\chi_{10}+C_{12})]\delta k^2\}\bar{C}_{11}$$

$$+ \{\mu_2^4\delta - \omega^2 + [(\omega^2-2\mu_2^4\delta)\chi_{13} - 6\delta\chi_{11}]k + [\mu_2^4\chi_{14} + 6(\chi_{12}+C_{22})]\delta k^2\}\bar{C}_{12}$$

$$- \{2[\mu_1^4\chi_7 + 3\chi_9]k - [\mu_1^4\chi_8 + 6(\chi_{10}+C_{12})]\}\gamma\omega\bar{S}_{11}$$

$$+ \{\mu_2^4 - 2[\mu_2^4\chi_{13} + 3\chi_{11}]k + [\mu_2^4\chi_{14} + 6(\chi_{12}+C_{22})]\}\gamma\omega\bar{S}_{12}$$

$$- \omega^2\{C_{12}^* - [C_{11}^*\chi_7 + C_{12}^*\chi_{13}]k - \frac{\alpha}{\pi}I_5\} = 0 \quad , \qquad (4.9e)$$

$$\{2[(2\omega^2-\mu_1^4\delta)\chi_7 - 3\delta\chi_9]k + [\mu_1^4\chi_8 + 6(\chi_{10}+C_{12})]\delta k^2\}\bar{C}_{21}$$

$$+ \{\mu_2^4\delta - 4\omega^2 - 2[(\mu_2^4\delta-2\omega^2)\chi_{13} + 3\delta\chi_{11}]k + [\mu_2^4\chi_{14} +$$

$$6(\chi_{12}+C_{22})]\delta k^2\}\bar{C}_{22} - \{4[\mu_1^4\chi_7 + 3\chi_9]k - 2[\mu_1^4\chi_8 + 6(\chi_{10}+C_{12})] *$$

$$k^2\}\gamma\omega\bar{S}_{21} + 2\mu_2^4 - 4[\mu_2^4\chi_{13} + 3\chi_{11}]k + 2[\mu_2^4\chi_{14} + 6(\chi_{12}+C_{22})] *$$

$$k^2\}\gamma\omega\bar{S}_{22} - 4\omega^2\{C_{22}^* - [C_{21}^*\chi_7 + C_{22}^*\chi_{13}]k - \frac{\alpha}{2\pi}I_6\} = 0 \quad , \tag{4.9f}$$

$$\{2[\mu_1^4\chi_7 + 3\chi_9]k - [\mu_1^4\chi_8 + 6(\chi_{10}+C_{12})]k^2\}\gamma\omega\bar{C}_{11} - \{\mu_2^4 -$$

$$2[\mu_2^4\chi_{13} + 3\chi_{11}]k + [\mu_2^4\chi_{14} + 6(\chi_{12}+C_{22})]k^2\}\gamma\omega\bar{C}_{12} +$$

$$\{[(\omega^2-2\mu_1^4\delta)\chi_7 - 6\delta\chi_9]k + [\mu_1^4\chi_8 + 6(\chi_{10}+C_{12})]\delta k^2\}\bar{S}_{11}$$

$$+ \{\mu_2^4\delta - \omega^2 - [(2\mu_2^4\delta-\omega^2)\chi_{13} + 6\delta\chi_{11}]k + [\mu_2^4\chi_{14} + 6(\chi_{12}+C_{22})] *$$

$$\delta k^2\}\bar{S}_{12} - \omega^2\{S_{12}^* - [S_{11}^*\chi_7 + S_{12}^*\chi_{13}]k + \frac{\alpha}{\pi}I_7\} = 0 \quad , \tag{4.9g}$$

$$\{4[\mu_1^4\chi_7 + 3\chi_9]k - 2[\mu_1^4\chi_8 + 6(\chi_{10}+C_{12})]k^2\}\gamma\omega\bar{C}_{21} - \{2\mu_2^4$$

$$- 4[\mu_2^4\chi_{13} + 3\chi_{11}]k + 2[\mu_2^4\chi_{14} + 6(\chi_{12}+C_{22})]k^2\}\gamma\omega\bar{C}_{22}$$

$$+ \{2[(2\omega^2-\mu_2^4\delta)\chi_7 - 3\delta\chi_9]k + [\mu_1^4\chi_8 + 6(\chi_{10}+C_{12})]\delta k^2\}\bar{S}_{21}$$

$$+ \{\mu_2^4\delta - 4\omega^2 + 2[(2\omega^2-\mu_2^4\delta)\chi_{13} - 3\delta\chi_{11}]k + [\mu_2^4\chi_{14} +$$

$$6(\chi_{12}+C_{22})]\delta k^2\}\bar{S}_{22} - 4\omega^2\{S_{22}^* - [S_{21}^*\chi_7 + S_{22}^*\chi_{13}]k$$

$$+ \frac{\alpha}{\pi}I_8\} = 0 \quad , \tag{4.9h}$$

where

$$\chi_1 = \int_0^1 \Phi_1\Phi_1'''d\xi \quad , \quad \chi_2 = \int_0^1 \xi\Phi_1\Phi_1'''d\xi \quad ,$$

$$\chi_3 = \int_0^1 \xi\Phi_1^2 d\xi \quad , \quad \chi_4 = \int_0^1 \xi^2\Phi_1^2 d\xi \quad ,$$

$$\chi_5 = \int_0^1 \Phi_1\Phi_2'''d\xi \quad , \quad \chi_6 = \int_0^1 \xi\Phi_1\Phi_2'''d\xi \quad ,$$

$$\chi_7 = \int_0^1 \xi\Phi_1\Phi_2 d\xi \quad , \quad \chi_8 = \int_0^1 \xi^2\Phi_1\Phi_2 d\xi \quad ,$$

$$\chi_9 = \int_0^1 \Phi_1'''\Phi_2 d\xi \quad , \quad \chi_{10} = \int_0^1 \xi\Phi_1'''\Phi_2 d\xi \quad ,$$

$$\chi_{11} = \int_0^1 \Phi_2\Phi_2'''d\xi \quad , \quad \chi_{12} = \int_0^1 \xi\Phi_2\Phi_2'''d\xi \quad ,$$

$$\chi_{13} = \int_0^1 \xi\Phi_2^2 d\xi \quad , \quad \chi_{14} = \int_0^1 \xi^2\Phi_2^2 d\xi \quad .$$

As in the case of the uniform cylindrical beams, Equations (4.9) were solved numerically using a simultaneous-equation computer subroutine

(e.g. UBC NDINVT).

4.3 Results and Discussion

In order to evaluate the response, the relative magnitudes in the chosen harmonics and the modes are rewritten in two different forms as

$$\bar{\eta} = H_1 \sin(\omega\tau+\psi_1) + H_2 \sin(2\omega\tau+\psi_2) \quad , \tag{4.10a}$$

and

$$\bar{\eta} = [R_{11}\sin(\omega\tau+\Delta_1) + R_{12}\sin(2\omega\tau+\Delta_2)]\Phi_1 + [R_{21}\sin(\omega\tau+\Delta_3) + R_{22}\sin(2\omega\tau+\Delta_4)]\Phi_2 \quad . \tag{4.10b}$$

Here H_1 and H_2 correspond to amplitude responses in first and second harmonics of the forcing frequency, respectively, while R_{ij} refers to amplitude response in the i^{th} mode due to j^{th} harmonic.

Figures 4-2 and 4-3 show the response amplitudes at three different points along the beams of various degrees of taper subjected to excitations at the root. It should be noted that ω is dimensionless and proportional to the frequency ratio ω_f/ω_n (ω_f = forcing frequency, ω_n = natural frequency). ω and ω_f are related by

$$\omega = \omega_f/\sqrt{B_3} \quad ,$$

where B_3 is defined in (3.16). For a particular beam $\sqrt{B_3}$ can be calculated and ω may be found if the forcing frequency is known. Figure 4-2 shows the response to a one-term harmonic excitation. There is no second-harmonic response (i.e. $H_2=0$) in this case. With an increase in taper ratio, the peak tends to occur at a larger ω but has a smaller magnitude. The first and second mode contributions, R_{11} and R_{21}, are also shown as functions of ω. These are constant along the length of the beam. For an increase in taper ratio, the R_{11} response peaks at a larger ω with a smaller amplitude. On the other hand, the R_{21} amplitude is larger for a higher taper ratio. The internal pressure effects for the range of interest here are less than 1% and can certainly be considered negligible. Figure 4-3 shows the responses for an excitation including a second harmonic of a representative amplitude. Here the second-harmonic response is apparent. The response H_1 is identical to that in Figure 4-2 for simple harmonic excitation. The fundamental response components, R_{11} and R_{21}, are also very much similar except for minor magnitude differences. The superharmonic response components, R_{12} and R_{22}, are due to the presence of the second harmonic exciting term. It is apparent that the response amplitude decreases with an increase in taper ratio. It should be noted that the amplitude components R_{11}, R_{12}, R_{21}, and R_{22} are independent of the locations along the beam and are thus identical for all values of ξ.

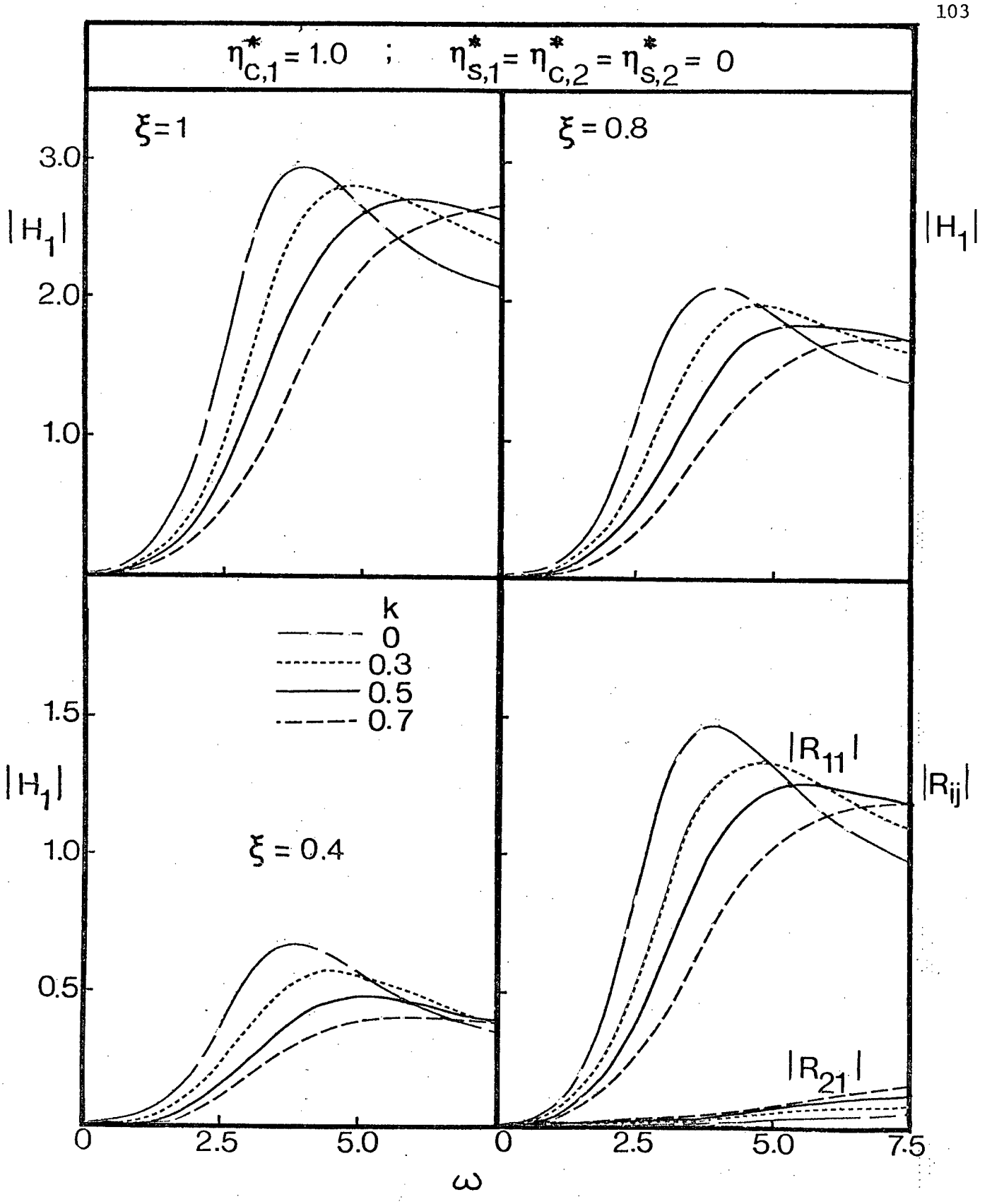

Figure 4-2 Response of viscoelastic cantilevers to simple harmonic root excitation

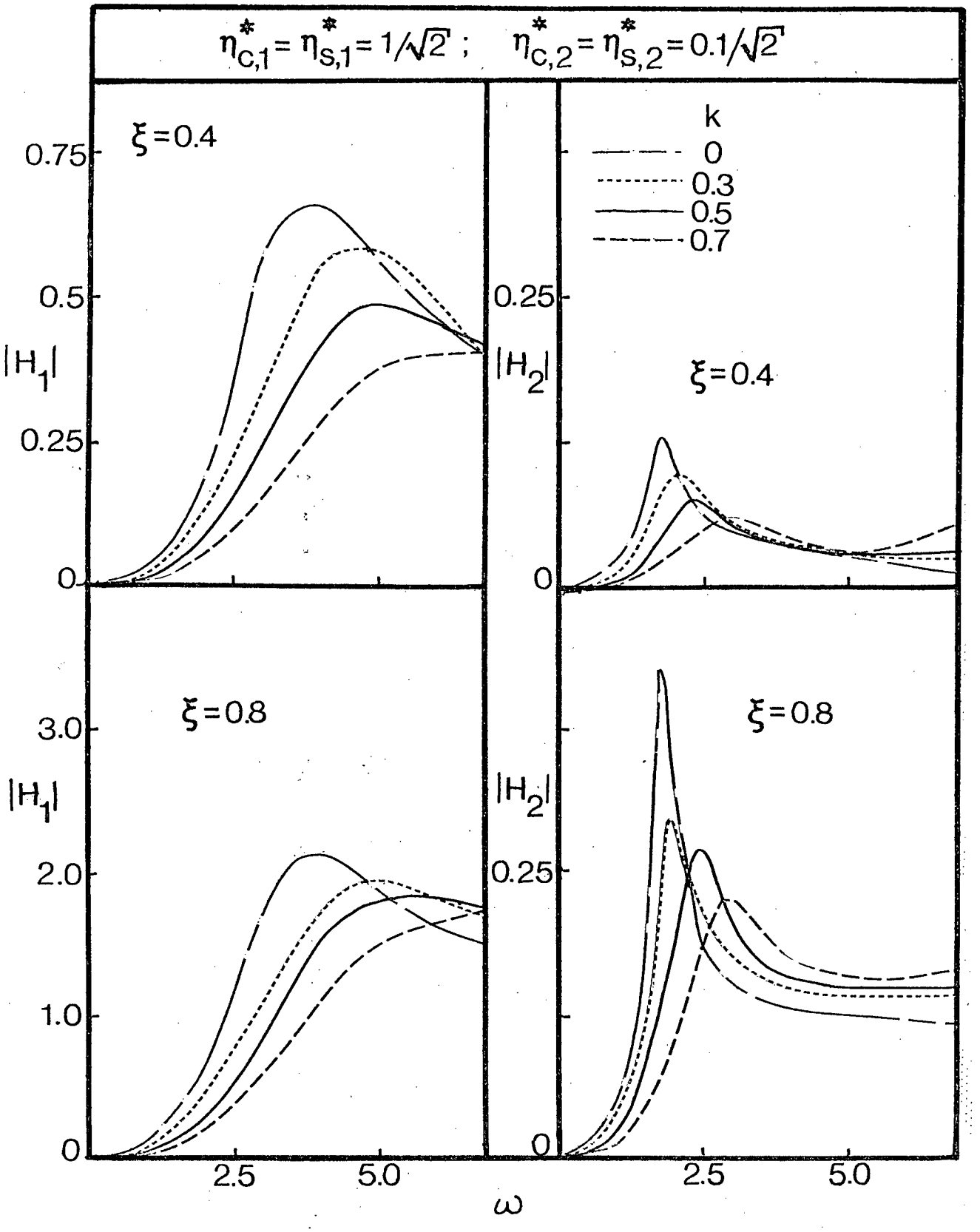

Figure 4-3 Response of viscoelastic cantilevers to excitation with a small second-harmonic component:
(a) ξ = 0.4, 0.8

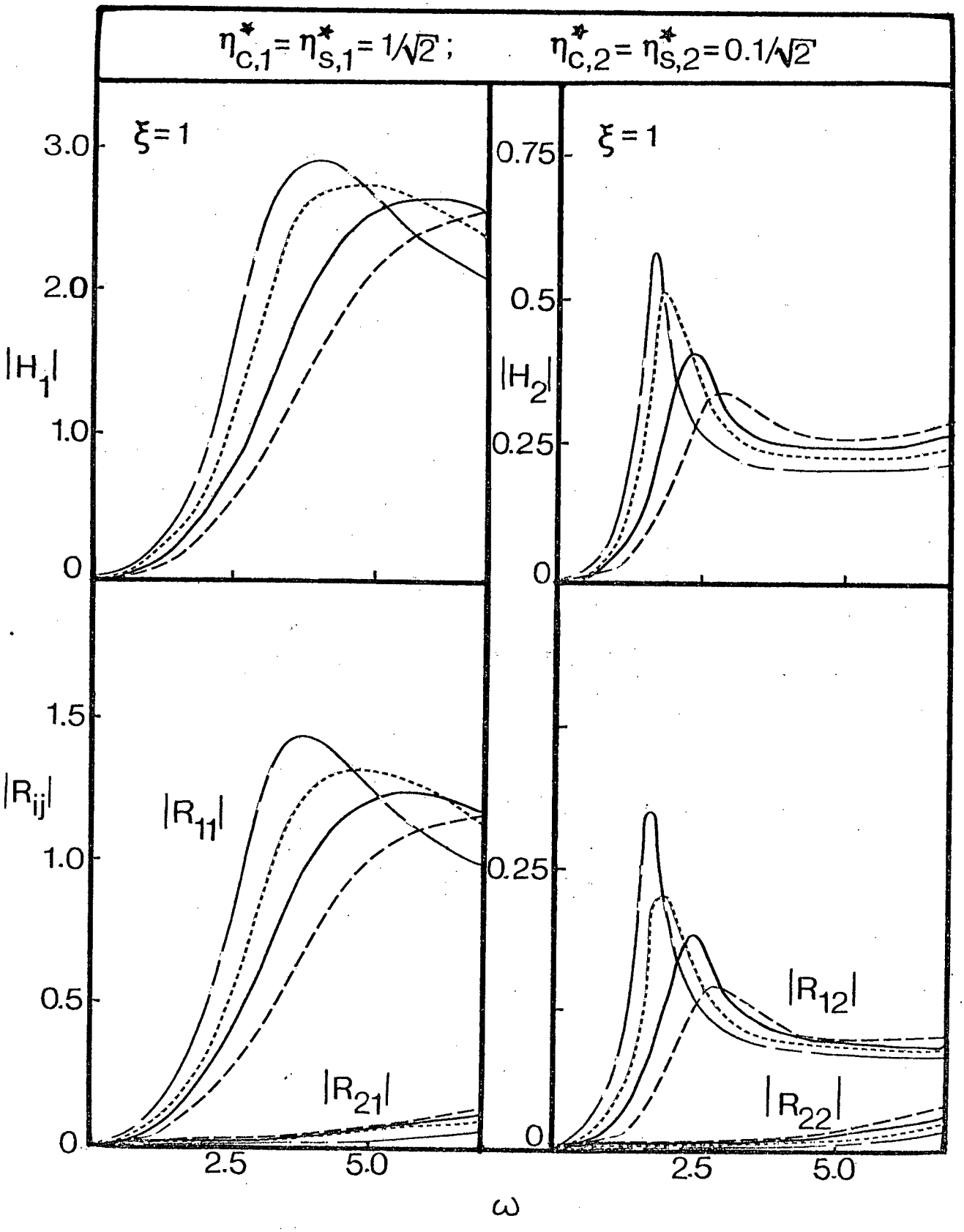

Figure 4-3 Response of viscoelastic cantilevers to excitation with a small second-harmonic component:
(b) $\xi = 1$

Before closing a comment concerning the effect of low temperature on response of the system would be appropriate. This is quite relevant because of the interest in its performance in the arctic region. Although material properties of polymers vary with temperature, the glass transition temperature is expected to be very low (below -50°C for polyethylene[87]), hence the material is likely to behave as viscoelastic under almost all practical conditions. However, at low temperatures, the stiffness of the material increases while the creep rate decreases. Hence for certain applications, e.g., submarine detection in the Arctic, the material properties will be different from the aforementioned ones (Section 2.4, p. 36), which are measured at a temperature of around 10°C. A typical stiffness-temperature plot for polyethylene is presented in Figure 4-4. It is apparent that with a

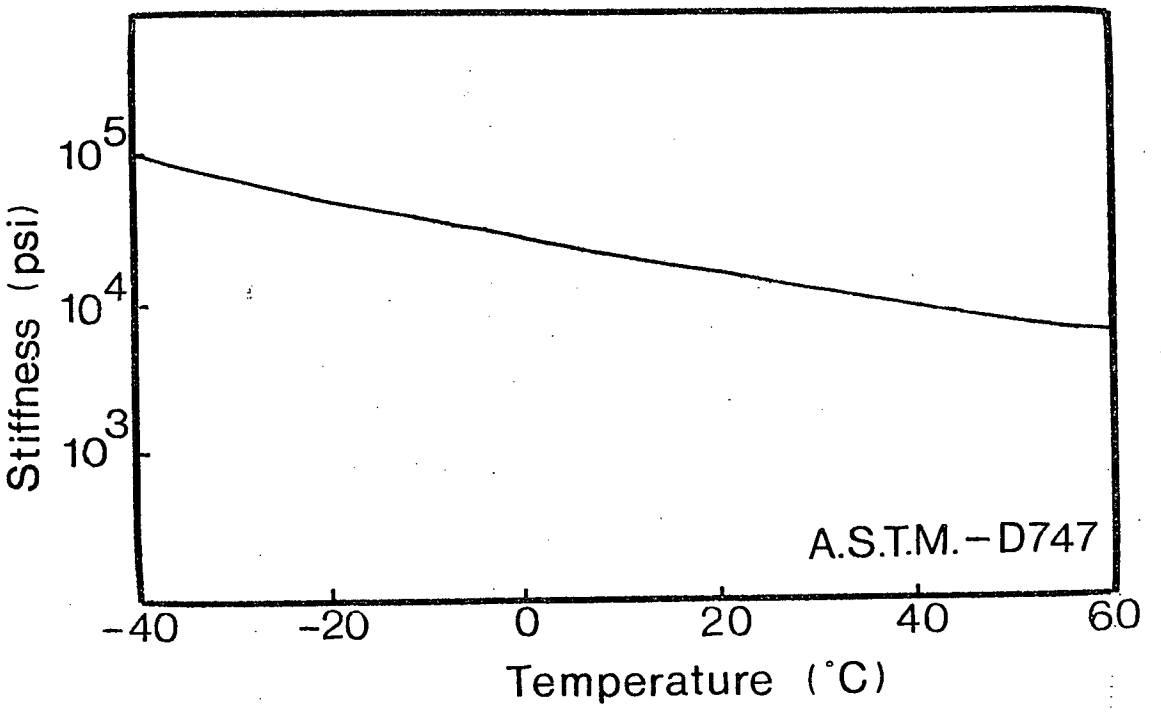

Figure 4-4 Effect of temperature on the stiffness of polyethylene

decrease in temperature from 10°C to 0°C the rise in stiffness can be by around 20%. This would be reflected in the corresponding reduction in the frequency ratio (ω_f/ω_n) and hence a reduction in the response amplitude. Thus the system performance is expected to improve in the low temperature environment. However, this does not necessarily imply better performance in the arctic region as now the character of the forcing function is expected to be substantially different due to floating-colliding ice masses. Literature survey reveals considerable effort in progress to assess this. Unfortunately, no precise information is yet available.

4.4 Concluding Remarks

The above analysis of the viscoelastic cantilevers subjected to periodic root excitation leads to the following conclusions:

(i) Within the range of internal pressures studied the inflation has negligible effects on the forced response of the viscoelastic cantilevers in water.

(ii) The analysis enables the prediction of the response of the viscoelastic cantilevers to periodic excitations that are expressible in terms of the fundamental forcing frequency and its second harmonic.

(iii) For the case of the simple harmonic excitation, the nonlinear hydrodynamic drag introduces no superharmonic components into the response.

(iv) At low exciting frequencies typical in the ocean an increase in taper ratio will reduce the displacements of the leg tips. However, for frequencies above the fundamental resonance, a high taper ratio will increase the tip displacement amplitudes.

(v) Dynamical response of the uniform cylindrical and tapered viscoelastic beams to root excitation accounting for the hydrodynamic drag should prove useful in the design of an underwater submarine detection system.

5. CLOSING COMMENTS

5.1 Summary of Conclusions

As stated at the outset, the objective of this investigation has been to gain an understanding of the statics and dynamics of the neutrally buoyant inflated viscoelastic structural members constituting a submarine detection system. The emphasis has been on the determination of trends rather than presenting massive data. The important conclusions based on the study can be summarized as follows:

(i) The specified materials of the inflatable members are viscoelastic and can be described with good accuracy by the three parameter solid model.

(ii) The elementary beam theory, with the three parameter solid model, is capable of predicting accurately the static behaviour of both the uniform cylindrical and the tapered cantilevers.

(iii) The free response of the uniform cylindrical beams may be studied using the reduced shell equation derived in this dissertation. The shell theory includes the initial stress effects due to inflation, and the reducing technique described combines the three shell equations into one that gives results of adequate accuracy for the beam-bending mode of interest here. The elementary beam theory is adequate in

predicting the dynamical behaviour of the inflated tapered beams. Experimental data obtained confirms the validity of the analysis. The results should be useful in the subsequent study of the submarine detection system.

(iv) For the range of inflation of interest here, the internal pressure has a negligible effect on the dynamical behaviour of the neutrally buoyant inflated cantilevers. The pressure, however, should be adequate to prevent wrinkling of the cantilevers at all times.

(v) The forced response of the cantilever to root excitation should prove useful in the design of the system. The analysis enables an estimate of the beam response to displacement excitations expressible by the first two terms of the Fourier series.

5.2 Recommendation for Future Work

There are numerous possibilities for extension of the present investigation. Some of the important areas of interest are indicated below:

(i) An intensive experimental program to determine the apparent mass coefficient, one of the uncertain parameters in the study, should prove very useful.

(ii) Prototype tests in the ocean would undoubtedly provide valuable insight. The possibility of excessive flexural

displacements for legs with very large L/d ratios may necessitate a more refined large-amplitude theory as the slope effects may become significant.

(iii) The current study could first be extended to the coupled motion of three similar flexible inflated cantilevers placed around a central head to form an array. The possibility of dynamic instability should be investigated. This could be followed by the consideration of the entire submarine detection system consisting of the array joined to a floating buoy by a cable. The dynamics of the drifting assembly and its stability will pose a challenging problem.

(iv) A detailed experimental study of the material behaviour at low temperatures will enable its application to regions of extreme cold, e.g., submarine detection in the Arctic. The dynamical analysis of the buoy-cable-array assembly in the arctic environment should prove to be of practical significance.

BIBLIOGRAPHY

1. Leonard, U.W., "State-of-the-Art in Inflatable Shell Research," Journal of the Engineering Mechanics, Vol. 100-EM1, February 1974, pp. 17-25.

2. Brauer, K.O., "Present and Future Applications of Expandable Structures for Spacecraft and Space Experiments," Presented at the XXIInd International Astronautical Congress, Brussels, September 1971.

3. Misra, A.K., "Dynamics of Neutrally Buoyant Inflatable Structures Used in Submarine Detection," Ph.D. Thesis, University of British Columbia, Vancouver, B.C., Canada, September 1974.

4. Leonard, R.W., Brooks, G.W., and McComb, H.G. (Jr), "Structural Considerations of Inflatable Re-entry Vehicles," NASA TN D-457, September 1960.

5. Stein, M., and Hedgepeth, M.M., "Analysis of Partly Wrinkled Membranes," NASA TN D-813, July 1961.

6. Comer, R.L., and Levy, S., "Deflections of an Inflated Circular Cylindrical Cantilever Beam," AIAA Journal, Vol. 1, No. 7, July 1963, pp. 1652-1655.

7. Topping, A.D., "Shear Deflections and Buckling Characteristics of Inflated Members," Journal of Aircraft, Vol. 1, No. 5, September-October 1964, pp. 289-292.

8. Corneliussen, A.H., and Shield, R.T., "Finite Deformations of Elastic Membranes with Application to the Stability of an Inflated and Extended Tube," Archives of Rational Mechanical Analysis, Vol. 7, 1961, pp. 273-304.

9. Huang, Tseng, "A Study of an Inflated Cylindrical Shell," U.S. National Congress of Applied Mechanics, Vol. 5, 1966, pp. 205-219.

10. Douglas, W.J., "Bending Stiffness of an Inflated Cylindrical Cantilever Beam," AIAA Journal, Vol. 7, July 1969, pp. 1248-1253.

11. Narasimhan, K.Y., "Effect of Internal Pressure on the Influence Coefficients of Cylindrical Shells of Finite Length," Rept. AE279S, June 1970, Department of Aeronautical Engineering, Indian Institute of Science, India.

12. Nachbar, W., "Discontinuity Stresses in Pressurized Thin Shells of Revolution," LMSD-48483, March 1957, Lockheed Missiles & Space Division, Sunnyvale, California.

13. Koga, T., "Bending Rigidity of an Inflated Circular Cylindrical Membrane of Rubbery Materials," AIAA Journal, Vol. 10, No. 11, November 1972, pp. 1485-1489.

14. Wiegel, R.L., Oceanographical Engineering, Prentice-Hall, Englewood Cliffs, N.J., 1964, pp. 11-21.

15. Morison, J.R., O'Brien, M.P., Johnson, J.W., and Schaaf, S.A., "The Forces Exerted by Surface Waves on Piles," Journal of Petroleum Technology, AIMME, Vol. 2, No. 5, May 1950, pp. 149-154.

16. Keulegan, G.H., and Carpenter, L.H., "Forces on Cylinders and Plates in an Oscillating Fluid," Journal of Research of the National Bureau of Standards, Vol. 60, No. 5, May 1958, pp. 423-440.

17. Stelson, T.E., and Mavis, T., "Virtual Mass and Acceleration in Fluids," Transactions, ASCE, Vol. 122, 1957, pp. 518-525.

18. Jen, Yuan, "Laboratory Study of Inertia Forces on a Pile," Journal of the Waterways and Harbors, Vol. 95-WW1, February 1968, pp. 59-76.

19. Laird, A.D.K., Johnson, C.A., and Walker, R.W., "Water Forces on Accelerated Cylinders," Journal of Waterways and Harbors, Vol. 85-WW1, March 1959, pp. 99-119.

20. Toebes, G.H., and Ramamurthy, A.S., "Fluidelastic Forces on Circular Cylinders," Journal of Engineering Mechanics, Vol. 93-EM6, December 1967, pp. 1-20.

21. Protos, A., Goldschmidt, V.W., and Toebes, G.H., "Hydroelastic Forces on Bluff Cylinders," Journal of Basic Engineering, Vol. 90, 1968, pp. 378-386.

22. Laird, A.D.K., Johnson, C.A., and Walker, R.W., "Water Eddy Forces on Oscillating Cylinders," Transactions, ASCE, Vol. 127, 1962, pp. 335-346.

23. Landweber, L., "Vibration in an Incompressible Fluid," IIHR Report, Contract Nonr. 3271 (01)(X), May 1963.

24. Landweber, L., "Vibration of a Flexible Cylinder in a Fluid," Journal of Ship Research, Vol. 11, No. 3, September 1967, pp. 143-150.

25. Warnock, R.G., "Added Masses of Vibrating Elastic Bodies," IIHR Report, Contract Nonr. 3271 (01)(X), February 1964.

26. Douglas, W.J., "Natural Vibrations of Finitely Deformable Structures," AIAA Journal, Vol. 5, No. 12, December 1967, pp. 2248-2253.

27. Simmonds, J.G., "Modifications of the Timoshenko Beam Equations Necessary for Thin-Walled Circular Tubes," International Journal of Mechanical Sciences, Vol. 9, 1967, pp. 237-244.

28. Forsberg, K., "Axisymmetric and Beam-Type Vibrations of Thin Cylindrical Shells," AIAA Journal, Vol. 7, No. 2, February 1969, pp. 221-227.

29. Kornecki, A., "A Note on Beam-Type Vibrations of Circular Cylindrical Shells," Journal of Sound and Vibration, Vol. 14, No. 1, 1971, pp. 1-6.

30. Goldenveizer, A.L., Theory of Thin Elastic Shells, London: Pergamon Press, New York, 1961, p. 230.

31. Leissa, A.W., Vibration of Shells, NASA SP-288, Washington, D.C., 1973.

32. Reissner, E., "Notes on Vibrations of Thin, Pressurized Cylindrical Shells," Report AM 5-4, The Ramo-Wooldridge Corp., Redondo Beach, California, November 1955.

33. Vlasov, V.Z., "General Theory of Shells and Its Applications in Engineering," NASA TT F-99, April 1964.

34. Greenspon, J.E., "Effect of External or Internal Static Pressure on the Natural Frequencies of Unstiffened, Cross Stiffened, and Sandwich Cylindrical Shells," Contract No. Nonr-2733(00) (FBM), Proj. No. NR 185-300, Tech. Rept. No. 11, Office of Naval Research, November 1964.

35. Bleich, H.H., and Baron, M.L., "Free and Forced Vibrations of an Infinitely Long Cylindrical Shell in an Infinite Acoustic Medium," Journal of Applied Mechanics, Vol. 21, No. 2, June 1954, pp. 167-177.

36. DiGiovanni, P.R., and Dugundji, J., "Vibrations of Freely-Supported Orthotropic Cylindrical Shells Under Internal Pressure," AFOSR Sci. Rept. 65-0640, ASRL TR 112-4 (AD 617 269), February 1965.

37. Fung, Y.C., Sechler, E.E., and Kaplan, A., "On the Vibration of Thin Cylindrical Shells Under Internal Pressure," Journal of Aeronautical Science, Vol. 24, No. 9, September 1957, pp. 650-661.

38. Herrmann, G., and Shaw, J., "Vibration of Thin Shells Under Initial Stress," Journal of Engineering Mechanics, Vol. 91-EM5, October 1965, pp. 37-59.

39. Reissner, E., "Non-Linear Effects in Vibrations of Cylindrical Shells," Report AM 5-6, The Ramo-Wooldridge Corp., Redondo Beach, California, August 1955.

40. Seggelke, P., "Vibration Behaviour of Axial-Symmetrically Loaded Thin-Walled Circular Cylinders Under Different Boundary Conditions," Report 64-43, Deutsche Luft-und Raumfahrt, 1964.

41. Mixson, J.S., and Herr, R.W., "An Investigation of the Vibration Characteristics of Pressurized Thin-Walled Circular Cylinders Partly Filled With Liquid," NASA TR R-145, 1962.

42. Miserentino, R., and Vosteen, L.F., "Vibration Tests of Pressurized Thin-Walled Cylindrical Shells," NASA TN D-3066, October 1965.

43. Nikulin, M.V., "Natural Oscillations of Smooth and Structurally Anisotropic Cylindrical Shells in the Presence of Static Loads," Strength and Dynamics of Aircraft Engines, Izdatel'stvo Mashinostroenie, Moscow, 1965, pp. 52-128. (in Russian).

44. Sewall, J.L., and Naumann, E.C., "An Experimental and Analytical Vibration Study of Thin Cylindrical Shells With and Without Longitudinal Stiffeners," NASA TN D-4705, September 1968.

45. Resnick, B.S., and Dugundji, J., "Effects of Orthotropicity, Boundary Conditions, and Eccentricity on the Vibrations of Cylindrical Shells," AFOSR Science Report AFOSR 66-2821, ASRL TR 134-2 (AD648 077), November 1966.

46. Sharma, C.B., and Johns, D.J., "Vibration Characteristics of a Clamped-Free and Clamped-Ring-Stiffened Circular Cylindrical Shell," Journal of Sound and Vibration, Vol. 14, No. 4, 1971, pp. 459-474.

47. Sharma, C.B., and Johns, D.J., "Natural Frequencies of Clamped-Free Circular Cylindrical Shells," Journal of Sound and Vibration, Vol. 21, No. 3, 1972, pp. 317-327.

48. Sharma, C.B., and Johns, D.J., "Free Vibrations of Cantilever Circular Cylindrical Shells -- A Comparative Study," Journal of Sound and Vibration, Vol. 25, No. 3, 1972, pp. 433-449.

49. Arya, A.S., Thakkar, S.K., and Goyal, A.C., "Vibration Analysis of Thin Cylindrical Containers," Journal of the Engineering Mechanics, Vol. 97-EM2, April 1971, pp. 317-331.

50. Baron, M.L., and Skalak, R., "Free Vibrations of Fluid-Filled Cylindrical Shells," Journal of the Engineering Mechanics, Vol. 88-EM3, June 1962, pp. 17-43.

51. Jain, R.K., "Vibration of Fluid-Filled, Orthotropic Cylindrical Shells," Journal of Sound and Vibration, Vol. 37, No. 3, 1974, pp. 379-388.

52. Stillman, W.E., "Free Vibration of Cylinders Containing Liquid," Journal of Sound and Vibration, Vol. 30, No. 4, 1973, pp. 509-524.

53. Greenspon, J.E., "Vibrations of Thick and Thin Cylindrical Shells Surrounded by Water," The Journal of the Acoustical Society of America, Vol. 33, No. 10, October 1961, pp. 1321-1328.

54. Warburton, G.B., "Vibration of a Cylindrical Shell in an Acoustic Medium," Journal of Mechanical Engineering Science, Vol. 3, No. 1, March 1961, pp. 69-79.

55. Bleich, H.H., and Baron, M.L., "Free and Forced Vibrations of an Infinitely Long Cylindrical Shell in an Infinite Acoustic Medium," Journal of Applied Mechanics, Vol. 21, No. 2, June 1954, pp. 167-177.

56. Herrmann, G., and Russel, J.E., "Forced Motions of Shell and Plates Surrounded by an Acoustic Fluid," Proceedings of the Symposium on the Theory of Shells, University of Houston, Houston, Texas, 1967, pp. 311-342.

57. Berger, B.S., "Dynamic Response of an Infinite Cylindrical Shell in an Acoustic Medium," Journal of Applied Mechanics, Vol. 91, pp. 342-345.

58. Conway, H.D., Becker, E.C.H., and Dubil, J.F., "Vibration Frequencies of Tapered Bars and Circular Plates," Journal of Applied Mechanics, Vol. 31, No. 2, June 1964, pp. 329-331.

59. Housner, G.W., and Keightley, W.O., "Vibrations of Linearly Tapered Cantilever Beams," Journal of the Engineering Mechanics, Vol. 88-EM2, April 1962, pp. 95-123.

60. Gaines, J.H., and Volterra, E., "Transverse Vibrations of Cantilever Bars of Variable Cross Section," The Journal of the Acoustical Society of America, Vol. 39, No. 4, 1966, pp. 674-679.

61. Cranch, E.T., and Adler, A.A., "Bending Vibrations of Variable Section Beams," Journal of Applied Mechanics, Vol. 23, 1956, pp. 103-108.

62. Siddall, J.N., and Isakson, G., "Approsimate Analytical Methods for Determining Natural Modes and Frequencies of Vibration," M.I.T. Report ONR Proj. NR-035-259, January 1951, pp. 141-146.

63. Pinney, E., "Vibration Modes of Tapered Beams," American Math. Monthly, Vol. 54, 1947, pp. 391-394.

64. Weingarten, V.I., "The Effect of Internal or External Pressure on the Free Vibrations of Conical Shells," International Journal of Mechanical Sciences, Vol. 8, 1966, pp. 115-124.

65. Goldberg, J.E., Bogdanoff, J.L., and Alspaugh, D.W., "On the Calculation of the Modes and Frequencies of Vibration of Pressurized Conical Shells," Proceedings of AIAA 5th Annual Structures and Materials Conference, 1964, pp. 243-249.

66. Goldberg, J.E., Bogdanoff, J.L., and Alspaugh, D.W., "Modes and Frequencies of Pressurized Conical Shells," Journal of Aircraft, Vol. 1, No. 6, 1964, pp. 372-374.

67. Lee, H.C., "Forced Lateral Vibration of a Uniform Cantilever Beam With Internal and External Damping," Journal of Applied Mechanics, Vol. 27, September 1960, pp. 551-556.

68. Leissa, A.W., and Hwee, M.O., "Forced Vibrations of Timoshenko Beams with Viscous Damping," Developments in Mechanics, John Wiley & Sons, Inc., N.Y., Vol. 3, Part 2, 1965, pp. 71-81.

69. Baker, W.E., Woolam, W.E., and Young, D., "Air and Internal Damping of Thin Cantilever Beams," International Journal of Mechanical Sciences, Vol. 9, 1967, pp. 743-766.

70. Paidoussis, M.P., and des Trois Maisons, P.E., "Free Vibration of a Heavy, Damped Cantilever in a Plane Inclined to the Vertical," M.E.R.L. Report No. 69-6, Department of Mechanical Engineering, McGill University, Montreal, Quebec, August 1969.

71. Fu, C.C., "Beam Vibrations with Nonlinear Damping," Developments in Mechanics, John Wiley & Sons, Inc., N.Y., Vol. 3, Part 2, 1965, pp. 131-139.

72. Pisarenko, G.S., Oscillations of Elastic Systems with Scattering of Energy in the Material, Acad. Sci. Ukr. SSR., 1955 (Russian).

73. Choo, Y., and Casarella, M.J., "A Survey of Analytical Methods for Dynamic Simulation of Cable-Body Systems," Journal of Hydronautics, Vol. 7, No. 4, October 1973, pp. 137-144.

74. Eames, M.C., and Drummond, T.G., "Hydronautics in Canada," Canadian Aeronautics and Space Journal, Vol. 17, No. 9, November 1971, pp. 381-389.

75. Flügge, W., Viscoelasticity, Blaisdell Publishing Company, Waltham, Massachusetts, 1967, pp. 32-50.

76. Kalinnikov, A.E., "Creep and Aftereffect of PET Films Under Conditions of Uniaxial Stress," Mekhanika Polimerov, Vol. 1, No. 2, 1965, pp. 59-63.

77. Findley, W.N., and Khosla, G., "An Equation for Tension Creep of Three Unfilled Thermoplastics," Society of Plastic Engineers Journal, Vol. 12, No. 12, December 1956, pp. 20-25.

78. Lamb, H., Hydrodynamics, Cambridge University Press, London, 6th Edition, 1932, p. 644.

79. Hoerner, S.F., Fluid Dynamic Drag, Published by the Author, Midland Park, N.J., 1965, pp. 3-8.

80. Gregory, R.W., and Paidoussis, M.P., "Unstable Oscillation of Tubular Cantilevers Conveying Fluid," Proceedings of the Royal Society, London, Vol. 293(A), 1966, pp. 512-542.

81. Bleich, H.H., and DiMaggio, F., "A Strain-Energy Expression for Thin Cylindrical Shells," Journal of Applied Mechanics, Vol. 20, No. 3, 1953, pp. 448-449.

82. Sharma, C.B., "Calculation of Natural Frequencies of Fixed-Free Circular Cylindrical Shells," Journal of Sound and Vibration, Vol. 35, No. 1, 1974, pp. 55-76.

83. Washizu, K., Variational Methods in Elasticity and Plasticity, Pergamon Press, New York, 1968.

84. Sampath, S.G., "Vibrations of Circular Cylindrical Shells Under Space-Varying Initial Stresses and Body Forces," Ph.D. Dissertation, Ohio State University, Ohio, 1970.

85. Snowdon, J.C., Vibration and Shock in Damped Mechanical Systems, John Wiley and Sons Inc., New York, 1968.

86. Kinsman, B., Wind Waves - Their Generation and Propagation on the Ocean, Prentice-Hall, Inc., Englewood Cliffs, New Jersey, 1965, p. 23.

87. Raff, R.A.V., and Allison, J.B., Polyethylene, Interscience Publishers, Inc., New York, 1956.

APPENDIX I

DERIVATION OF WATER INERTIA TERM IN SHELL EQUATIONS

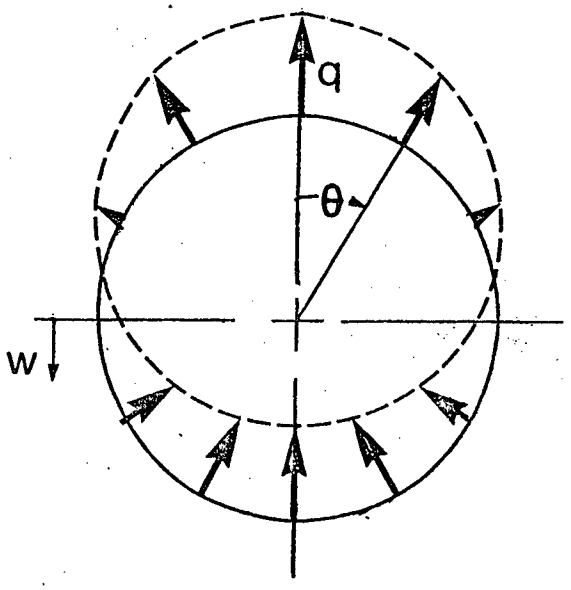

Figure I-1 Geometry of lateral displacement of a shell section

Let q be the normal pressure acting on shell due to inertia of water inside. q is defined positive outwards.

From geometry,

$$m_w \frac{\partial^2 w}{\partial t^2} = m_w \frac{\partial^2 y}{\partial t^2}\sin\theta - m_w \frac{\partial^2 z}{\partial t^2}\cos\theta \quad . \tag{I.1}$$

A force balance in the vertical direction gives

$$\int_0^{2\pi} qa\cos\theta d\theta = \int m_w \frac{\partial^2 w}{\partial t^2} = \rho_w \int_0^{2\pi}\int_0^a [\frac{\partial^2 y}{\partial t^2}\sin\theta - \frac{\partial^2 z}{\partial t^2}\cos\theta]adrd\theta \quad .$$

(I.2)

Assuming

$$q = q_0\psi(x)\cos\theta\cos\omega t \quad ,$$

and

$$y = Y\psi(x)\sin\theta\cos\omega t \quad , \qquad z = Z\psi(x)\cos\theta\cos\omega t \quad ,$$

Equation (I.2) becomes

$$\int_0^{2\pi} q_0\psi(x)\cos^2\theta\cos\omega t a d\theta = -\frac{\rho_w\omega^2 a^2\psi(x)}{2}\int_0^{2\pi}\int_0^a (Y\sin^2\theta - Z\cos^2\theta)\cos\omega t d\theta \quad . \tag{I.3}$$

For the beam-bending mode, Y =-Z, and Equation (I.3) becomes

$$q_0 = \rho_w a\omega^2 Z \quad .$$

Thus

$$-qa = -\rho_w a^2\omega^2 Z\psi(x)\cos\theta\cos\omega t = \rho_w a^2\frac{\partial^2 z}{\partial t^2} \quad . \tag{I.4}$$

In the shell equations the force term is $-q\frac{a^2(1-\nu^2)}{Eh}$, and is equivalent to

$$\frac{\rho_w a^3(1-\nu^2)}{Eh}\frac{\partial^2 z}{\partial t^2} \quad ,$$

or

$$G\frac{\rho_w a}{\rho h}\frac{\partial^2 z}{\partial t^2} \quad .$$

To account for the inertia of the water surrounding the beam, an added inertia coefficient, C_m, is introduced. The term to be added to the shell equations is then

$$(1+C_m)G\frac{\rho_w a}{\rho h}\frac{\partial^2 z}{\partial t^2} \quad .$$

APPENDIX II

ORTHOGONALITY CONDITION FOR EQUATION (3.22b)

Equation (3.21b) may be rewritten, for modes m and n, as

$$\beta_m'''' = \lambda_m^4(B_2\beta_m'' + B_1\beta_m) \quad , \tag{II.1a}$$

$$\beta_n'''' = \lambda_n^4(B_2\beta_n'' + B_1\beta_n) \quad . \tag{II.1b}$$

Multiplying Equations (II.1a) and (II.1b) by β_n and β_m, respectively, subtracting and integrating over the length, one obtains

$$\int_0^1 (\beta_m''''\beta_n - \beta_m\beta_n'''')d\xi = \int_0^1 [\lambda_m^4(B_2\beta_m''\beta_n + B_1\beta_m\beta_n) - \lambda_n^4(B_2\beta_m\beta_n'' + B_1\beta_m\beta_n)]d\xi \quad . \tag{II.2}$$

Integrating by parts, Equation (II.2) becomes

$$0 = B_2[\lambda_m^4\beta_m'\beta_n - \lambda_n^4\beta_m\beta_n']_0^1 + (\lambda_m^4 - \lambda_n^4)B_1 \int_0^1 \beta_m\beta_n d\xi - B_2(\lambda_m^4 - \lambda_n^4) \int_0^1 \beta_m'\beta_n' d\xi \quad . \tag{II.3}$$

Applying the cantilever boundary condition, Equation (II.3) can be rearranged to give

$$\int_0^1 \beta_m \beta_n d\xi - \frac{B_2}{B_1} \int_0^1 \beta_m' \beta_n' d\xi + \frac{B_2[\lambda_m^4 \beta_m'(1)\beta_n(1) - \lambda_n^4 \beta_m(1)\beta_n'(1)]}{B_1(\lambda_m^4 - \lambda_n^4)}$$

$$= 0 \quad , \quad \text{for } m \neq n \quad . \tag{II.4}$$

This is the condition of orthogonality of the eigenfunctions $\beta(\xi)$.

APPENDIX III

RAYLEIGH-RITZ MATRIX ELEMENTS FOR WASHIZU'S SHELL THEORY

The eigenvalue problem given by Equation (3.57a) is

$$[M](a) = \Omega^2[N](a) \quad .$$

The elements of [M] and [N] are:

$$m_{11} = (1-\nu)\int_0^1 \Phi'^2 d\xi + 2(\frac{a}{L})^2 \int_0^1 \Phi''^2 d\xi + (1-\nu^2)P *$$

$$[(2-\frac{h}{2a}+\frac{h^2}{6a^2})\int_0^1 \Phi'^2 d\xi + (\frac{a}{L})^2 \int_0^1 \Phi''^2 d\xi] \quad ;$$

$$m_{12} = (1-\nu)\int_0^1 \Phi'\Psi' d\xi + 2(\frac{a}{L})^2 \int_0^1 \Phi''\Psi'' d\xi + (1-\nu^2)P *$$

$$[(2-\frac{h}{2a}+\frac{h^2}{6a^2})\int_0^1 \Phi'\Psi' d\xi + (\frac{a}{L})^2 \int_0^1 \Phi''\Psi'' d\xi] \quad ;$$

$$m_{13} = (\frac{a}{L})[2\nu\int_0^1 \Phi''\Phi d\xi - (1-\nu)\int_0^1 \Phi'^2 d\xi] \quad ;$$

$$m_{14} = (\frac{a}{L})[2\nu\int_0^1 \Phi''\Psi d\xi - (1-\nu)\int_0^1 \Phi'\Psi' d\xi] \quad ;$$

$$m_{15} = 2\nu(\frac{a}{L})\int_0^1 \Phi''\Phi d\xi \quad ;$$

$$m_{16} = 2\nu(\frac{a}{L})\int_0^1 \Phi''\Psi d\xi \quad ;$$

$$m_{21} = (1-\nu)\int_0^1 \Phi'\Psi'd\xi + 2(\frac{a}{L})^2\int_0^1 \Phi''\Psi''d\xi + (1-\nu^2)P *$$

$$[(2-\frac{h}{2a}+\frac{h^2}{6a^2})\int_0^1 \Phi'\Psi'd\xi + (\frac{a}{L})^2\int_0^1 \Phi''\Psi''d\xi] \quad ;$$

$$m_{22} = (1-\nu)\int_0^1 \Psi'^2d\xi + 2(\frac{a}{L})^2\int_0^1 \Psi''^2d\xi + (1-\nu^2)P *$$

$$[(2-\frac{h}{2a}+\frac{h^2}{6a^2})\int_0^1 \Psi'^2d\xi + (\frac{a}{L})^2\int_0^1 \Psi''^2d\xi] \quad ;$$

$$m_{23} = (\frac{a}{L})[2\nu\int_0^1 \Phi\Psi''d\xi - (1-\nu)\int_0^1 \Phi'\Psi'd\xi] \quad ;$$

$$m_{24} = (\frac{a}{L})[2\nu\int_0^1 \Psi\Psi''d\xi - (1-\nu)\int_0^1 \Psi'^2d\xi] \quad ;$$

$$m_{25} = 2\nu(\frac{a}{L})\int_0^1 \Phi\Psi''d\xi \quad ;$$

$$m_{26} = 2\nu(\frac{a}{L})\int_0^1 \Psi\Psi''d\xi \quad ;$$

$$m_{31} = (\frac{a}{L})[2\nu\int_0^1 \Phi\Phi''d\xi - (1-\nu)\int_0^1 \Phi'^2d\xi] \quad ;$$

$$m_{32} = (\frac{a}{L})[2\nu\int_0^1 \Phi\Psi''d\xi - (1-\nu)\int_0^1 \Phi'\Psi'd\xi] \quad ;$$

$$m_{33} = 2 + (1-\nu)(\frac{a}{L})^2\int_0^1 \Phi'^2d\xi + (1-\nu^2)P[4-\frac{h}{a}+\frac{h^2}{3a^2}+(\frac{a}{L})^2\int_0^1 \Phi'^2d\xi] \quad ;$$

$$m_{34} = 2\int_0^1 \Phi\Psi d\xi + (1-\nu)(\frac{a}{L})^2\int_0^1 \Phi'\Psi'd\xi + (1-\nu^2)P *$$

$$[(4-\frac{h}{a}+\frac{h^2}{3a^2})\int_0^1 \Phi\Psi d\xi + (\frac{a}{L})^2\int_0^1 \Phi'\Psi'd\xi] \quad ;$$

$$m_{35} = 2 + (1-\nu^2)P[4 - \frac{h}{a} + \frac{h^2}{3a^2}] \quad ;$$

$$m_{36} = 2\int_0^1 \Phi\Psi d\xi + (1-\nu^2)P(4 - \frac{h}{a} + \frac{h^2}{3a^2})\int_0^1 \Phi\Psi d\xi \quad ;$$

$$m_{41} = (\frac{a}{L})[2\nu\int_0^1 \Phi''\Psi d\xi - (1-\nu)\int_0^1 \Phi'\Psi' d\xi] \quad ;$$

$$m_{42} = (\frac{a}{L})[2\nu\int_0^1 \Psi\Psi'' d\xi - (1-\nu)\int_0^1 \Psi'^2 d\xi] \quad ;$$

$$m_{43} = 2\int_0^1 \Phi\Psi d\xi + (1-\nu)(\frac{a}{L})^2\int_0^1 \Phi'\Psi' d\xi + (1-\nu^2)P *$$

$$[(4 - \frac{h}{a} + \frac{h^2}{3a^2})\int_0^1 \Phi\Psi d\xi + (\frac{a}{L})^2\int_0^1 \Phi'\Psi' d\xi] \quad ;$$

$$m_{44} = 2 + (1-\nu)(\frac{a}{L})^2\int_0^1 \Psi'^2 d\xi + (1-\nu^2)P[4 - \frac{h}{a} + \frac{h^2}{3a^2}$$

$$+ (\frac{a}{L})^2\int_0^1 \Psi'^2 d\xi] \quad ;$$

$$m_{45} = 2\int_0^1 \Phi\Psi d\xi + (1-\nu^2)P(4 - \frac{h}{a} + \frac{h^2}{3a^2})\int_0^1 \Phi\Psi d\xi \quad ;$$

$$m_{46} = 2 + (1-\nu^2)P(4 - \frac{h}{a} + \frac{h^2}{3a^2}) \quad ;$$

$$m_{51} = 2\nu(\frac{a}{L})\int_0^1 \Phi\Phi'' d\xi \quad ;$$

$$m_{52} = 2\nu(\frac{a}{L})\int_0^1 \Phi\Psi'' d\xi \quad ;$$

$$m_{53} = 2 + (1-\nu^2)(4 - \frac{h}{a} + \frac{h^2}{3a^2})P \quad ;$$

$$m_{54} = 2\int_0^1 \Phi\Psi d\xi + (1-\nu^2)P(4 - \frac{h}{a} + \frac{h^2}{3a^2})\int_0^1 \Phi\Psi d\xi \quad ;$$

$$m_{55} = 2 + (1-\nu^2)P[4 - \frac{h}{a} + \frac{h^2}{3a^2} + (\frac{a}{L})^2\int_0^1 \Phi'^2 d\xi] \quad ;$$

$$m_{56} = 2\int_0^1 \Phi\Psi d\xi + (1-\nu^2)P[(4 - \frac{h}{a} + \frac{h^2}{3a^2})\int_0^1 \Phi\Psi d\xi + (\frac{a}{L})^2\int_0^1 \Phi'\Psi' d\xi] \quad ;$$

$$m_{61} = 2\nu(\frac{a}{L})\int_0^1 \Phi''\Psi d\xi \quad ;$$

$$m_{62} = 2\nu(\frac{a}{L})\int_0^1 \Psi''\Psi d\xi \quad ;$$

$$m_{63} = 2\int_0^1 \Phi\Psi d\xi + (1-\nu^2)P(4 - \frac{h}{a} + \frac{h^2}{3a^2})\int_0^1 \Phi\Psi d\xi \quad ;$$

$$m_{64} = 2 + (1-\nu^2)(4 - \frac{h}{a} + \frac{h^2}{3a^2})P$$

$$m_{65} = 2\int_0^1 \Phi\Psi d\xi + (1-\nu^2)P[(4 - \frac{h}{a} + \frac{h^2}{3a^2})\int_0^1 \Phi\Psi d\xi + (\frac{a}{L})^2\int_0^1 \Phi'\Psi' d\xi] \quad ;$$

$$m_{66} = 2 + (1-\nu^2)P[4 - \frac{h}{a} + \frac{h^2}{3a^2} + (\frac{a}{L})^2\int_0^1 \Psi'^2 d\xi] \quad ;$$

$$n_{11} = 2\int_0^1 \Phi'^2 d\xi \quad ;$$

$$n_{12} = 2\int_0^1 \Phi'\Psi' d\xi \quad ;$$

$$n_{13} = n_{14} = n_{15} = n_{16} = 0 \quad ;$$

$$n_{21} = 2\int_0^1 \Phi'\Psi' d\xi \quad ;$$

$$n_{22} = 2\int_0^1 \Psi'^2 d\xi \quad ;$$

$$n_{23} = n_{24} = n_{25} = n_{26} = n_{31} = n_{32} = 0 \quad ;$$

$$n_{33} = 2 + \frac{3(1+C_m)\rho_w a}{4\rho h} \quad ;$$

$$n_{34} = [2 + \frac{3(1+C_m)\rho_w a}{4\rho h}]\int_0^1 \Phi\Psi d\xi \quad ;$$

$$n_{35} = \frac{(1+C_m)\rho_w a}{4\rho h} \quad ;$$

$$n_{36} = \frac{(1+C_m)\rho_w a}{4\rho h}\int_0^1 \Phi\Psi d\xi \quad ;$$

$$n_{41} = n_{42} = 0 \quad ;$$

$$n_{43} = [2 + \frac{3(1+C_m)\rho_w a}{4\rho h}]\int_0^1 \Phi\Psi d\xi \quad ;$$

$$n_{44} = 2 + \frac{3(1+C_m)\rho_w a}{4\rho h} \quad ;$$

$$n_{45} = \frac{(1+C_m)\rho_w a}{4\rho h}\int_0^1 \Phi\Psi d\xi \quad ;$$

$$n_{46} = \frac{(1+C_m)\rho_w a}{4\rho h} \quad ;$$

$$n_{51} = n_{52} = 0 \quad ;$$

$$n_{53} = \frac{(1+C_m)\rho_w a}{4\rho h} \quad ;$$

$$n_{54} = \frac{(1+C_m)\rho_w a}{4\rho h_0}\int^1 \Phi\Psi d\xi \quad ;$$

$$n_{55} = 2 + \frac{3(1+C_m)\rho_w a}{4\rho h} \quad ;$$

$$n_{56} = [2 + \frac{3(1+C_m)\rho_w a}{4\rho h}]\int_0^1 \Phi\Psi d\xi \quad ;$$

$$n_{61} = n_{62} = 0 \quad ;$$

$$n_{63} = \frac{(1+C_m)\rho_w a}{4\rho h_0}\int^1 \Phi\Psi d\xi \quad ;$$

$$n_{64} = \frac{(1+C_m)\rho_w a}{4\rho h} \quad ;$$

$$n_{65} = [2 + \frac{3(1+C_m)\rho_w a}{4\rho h}]\int_0^1 \Phi\Psi d\xi \quad ;$$

$$n_{66} = 2 + \frac{3(1+C_m)\rho_w a}{4\rho h} \quad .$$

APPENDIX IV

FREQUENCY EQUATION FOR TAPERED BEAMS USING 1-, 2-, AND 3-TERM APPROXIMATIONS

i=1:

For one-term approximation Equation (3.59b) becomes

$$\int_0^1 \{-6k(1-k\xi)\frac{d^3\Phi_1}{d\xi^3}\Phi_1 + 6k^2\Phi_1\frac{d^2\Phi_1}{d\xi^2} + (1-k\xi)[\mu_1^4(1-k\xi) - \lambda^2]\Phi_1^2\}d\xi = 0 \quad . \tag{IV.1}$$

The solution can be written as

$$\lambda_m = \mu_m\{\frac{1}{1-kI_{1m}}[1 + k(12\frac{\sigma_m^2}{\mu_m^2} - 2I_{1m}) + k^2(I_{2m} - \frac{12\sigma_m}{\mu_m^3} + \frac{9C_{mm}}{\mu_m^4}\}^{1/4} \quad , \tag{IV.2}$$

where

$$I_{1m} = \int_0^1 \xi\Phi_m^2 d\xi \quad ,$$

$$I_{2m} = \int_0^1 \xi^2\Phi_m^2 d\xi \quad ,$$

and C_{mm} is given by Equation (3.33c).

i=2:

Two equations are obtained from Equation (3.59b) for the two-term approximation:

$$\int_0^1 \{\left(-6k(1-k\xi)\Phi_1\frac{d^3\Phi_1}{d\xi^3} + 6k^2\Phi_1\frac{d^2\Phi_1}{d\xi^2} + (1-k\xi)[\mu_1^4(1-k\xi) - \lambda^2]\Phi_1^2\right)f_1$$

$$+ \left(-6k(1-k\xi)\Phi_1\frac{d^3\Phi_2}{d\xi^3} + 6k^2\Phi_1\frac{d^2\Phi_2}{d\xi^2} + (1-k\xi)[\mu_2^4(1-k\xi)\right.$$

$$\left. - \lambda^2]\Phi_1\Phi_2\right)f_2\}d\xi = 0 \quad , \tag{IV.3a}$$

$$\int_0^1 \{\left(-6k(1-k\xi)\frac{d^3\Phi_1}{d\xi^3}\Phi_2 + 6k^2\frac{d^2\Phi_1}{d\xi^2}\Phi_2 + (1-k\xi)[\mu_1^4(1-k\xi) - \lambda^2]\Phi_1\Phi_2\right)f_1$$

$$+ \left(-6k(1-k\xi)\Phi_2\frac{d^3\Phi_2}{d\xi^3} + 6k^2\Phi_2\frac{d^2\Phi_2}{d\xi^2} + (1-k\xi)[\mu_2^4(1-k\xi)\right.$$

$$\left. - \lambda^2]\Phi_2^2\right)f_2\}d\xi = 0 \quad . \tag{IV.3b}$$

Equations (IV.3) may be put in the form of (3.64a), i.e.,

$$[S](f) = \lambda^2[V](f) \quad ,$$

where

$$s_{11} = \mu_1^4 - [6\chi_1 + 2\mu_1^4\chi_3]k + (6\chi_2 + 6C_{11} + \mu_1^4\chi_4)k^2 \quad ,$$

$$s_{12} = -[6\chi_5 + 2\mu_2^4\chi_7]k + [6\chi_6 + 6C_{21} + \mu_2^4\chi_8]k^2 \quad ,$$

$$s_{21} = -[6\chi_9 + 2\mu_1^4\chi_7]k + [6\chi_{10} + 6C_{12} + \mu_1^4\chi_8]k^2 \quad ,$$

$$s_{22} = \mu_2^4 - [6\chi_{11} + 2\mu_2^4\chi_{13}]k + [6\chi_{12} + 6C_{22} + \mu_2^4\chi_{14}]k^2 \quad ,$$

$$v_{11} = 1 - \chi_3 k \quad ,$$

$$v_{12} = v_{21} = -\chi_7 k \quad ,$$

$$v_{22} = 1 - \chi_{13} k \quad .$$

i=3:

For the three-term approximation three equations are obtained from Equation (3.59b) which can be written in the matrix form (3.64a). The elements of the two matrices are:

$$s_{11} = \mu_1^4[-6\chi_1 + 2\mu_1^4\chi_3]k + [6\chi_2 + 6C_{11} + \mu_1^4\chi_4]k^2 \quad ;$$

$$s_{12} = -[6\chi_5 + 2\mu_2^4\chi_7]k + [6\chi_6 + 6C_{21} + \mu_2^4\chi_8]k^2 \quad ;$$

$$s_{13} = -[6\int_0^1 \Phi_1\Phi_3'''d\xi + 2\mu_3^4\int_0^1 \xi\Phi_1\Phi_3 d\xi]k + [6\int_0^1 \xi\Phi_1\Phi_3'''d\xi$$

$$+ 6C_{31} + \mu_3^4\int_0^1 \xi^2\Phi_1\Phi_3 d\xi]k^2 \quad ;$$

$$s_{21} = -[6\chi_9 + 2\mu_1^4\chi_7]k + [6\chi_{10} + 6C_{12} + \mu_1^4\chi_8]k^2 \quad ;$$

$$s_{22} = \mu_2^4 - [6\chi_{11} + 2\mu_2^4\chi_{13}]k + [6\chi_{12} + 6C_{22} + \mu_2^4\chi_{14}]k^2 \quad ;$$

$$s_{23} = -[6\int_0^1 \Phi_2\Phi_3'''d\xi + 2\mu_3^4\int_0^1 \xi\Phi_2\Phi_3 d\xi]k + [6\int_0^1 \xi\Phi_2\Phi_3'''d\xi + 6C_{32} + \mu_3^4\int_0^1 \xi^2\Phi_2\Phi_3 d\xi]k^2 \quad ;$$

$$s_{31} = -[6\int_0^1 \Phi_1'''\Phi_3 d\xi + 2\mu_1^4\int_0^1 \xi\Phi_1\Phi_3 d\xi]k + [6\int_0^1 \xi\Phi_1'''\Phi_3 d\xi + 6C_{13} + \mu_1^4\int_0^1 \xi^2\Phi_1\Phi_3 d\xi]k^2 \quad ;$$

$$s_{32} = -[6\int_0^1 \Phi_2'''\Phi_3 d\xi + 2\mu_2^4\int_0^1 \xi\Phi_2\Phi_3 d\xi]k + [6\int_0^1 \xi\Phi_2'''\Phi_3 d\xi + 6C_{23} + \mu_2^4\int_0^1 \xi^2\Phi_2\Phi_3 d\xi]k^2 \quad ;$$

$$s_{33} = \mu_3^4 - [6\int_0^1 \Phi_3\Phi_3'''d\xi + 2\mu_3^4\int_0^1 \xi\Phi_3^2 d\xi]k + [6\int_0^1 \xi\Phi_3\Phi_3'''d\xi + 6C_{33} + \mu_3^4\int_0^1 \xi^2\Phi_3^2 d\xi]k^2 \quad ;$$

$$v_{11} = 1 - \chi_5 k \quad ;$$

$$v_{12} = -\chi_7 k \quad ;$$

$$v_{13} = -k\int_0^1 \xi\Phi_1\Phi_3 d\xi \quad ;$$

$$v_{21} = -\chi_7 k \quad ;$$

$$v_{22} = 1 - \chi_{13} k \quad ;$$

$$v_{23} = -k \int_0^1 \xi \Phi_2 \Phi_3 d\xi \quad ;$$

$$v_{31} = -k \int_0^1 \xi \Phi_1 \Phi_3 d\xi \quad ;$$

$$v_{32} = -k \int_0^1 \xi \Phi_2 \Phi_3 d\xi \quad ;$$

$$v_{33} = 1 - k \int_0^1 \xi \Phi_3^2 d\xi \quad .$$

APPENDIX V

REDUCED MEMBRANE AND HERRMANN-ARMENÀKAS EQUATIONS

(i) Reduced Membrane Equation

The differential operators in Equation (3.1) for the membrane theory, after neglecting terms involving $h^2/(12a^2)$, are[31]

$$L_{11} = \frac{\partial^2}{\partial s^2} + \frac{1-\nu}{2}\frac{\partial^2}{\partial \theta^2} - c_1 G\frac{\partial^2}{\partial t^2} \quad ,$$

$$L_{12} = \frac{1+\nu}{2}\frac{\partial^2}{\partial s \partial \theta} \quad ,$$

$$L_{13} = \nu\frac{\partial}{\partial s} \quad ,$$

$$L_{21} = \frac{1+\nu}{2}\frac{\partial^2}{\partial s \partial \theta} \quad ,$$

$$L_{22} = \frac{1-\nu}{2}\frac{\partial^2}{\partial s^2} + \frac{\partial^2}{\partial \theta^2} - c_2 G\frac{\partial^2}{\partial t^2} \quad ,$$

$$L_{23} = \frac{\partial}{\partial \theta} \quad ,$$

$$L_{31} = \nu\frac{\partial}{\partial s} \quad ,$$

$$L_{32} = \frac{\partial}{\partial \theta} \quad ,$$

$$L_{33} = 1 - \frac{N_\theta}{C} + c_3 G\frac{\partial^2}{\partial t^2} - \frac{N_\theta}{C}\frac{\partial^2}{\partial \theta^2} - \frac{N_x}{C}\frac{\partial^2}{\partial s^2} \quad .$$

Carrying out the reduction procedure the following equation is obtained for the beam-bending mode:

$$A_1\frac{\partial^2 w}{\partial s^2} + A_2\frac{\partial^4 w}{\partial s^4} + A_4\frac{\partial^2 w}{\partial t^2} + A_5\frac{\partial^4 w}{\partial s^2 \partial t^2} = 0 \quad , \tag{V.1}$$

where

$$A_1 = \frac{(3+\nu)(1-\nu^2)}{4}p \quad ,$$

$$A_2 = \frac{(5-4\nu-\nu^2)(1-\nu^2)}{8}P + \frac{(1-\nu)(1-\nu^2)}{2} \quad ,$$

$$A_4 = G(\frac{1-\nu}{2})(c_2 + c_3) \quad ,$$

$$A_5 = -G\{\frac{(1-\nu^2)}{4}[2c_1 + (1-\nu)c_2]P + \frac{(1-\nu)}{2}c_1 + (1-\nu^2)c_2 + (1-\nu)c_3\} \quad .$$

(ii) Reduced Herrmann-Armenàkas Equation

For the linearized Herrmann-Armenàkas theory, the differential operators, after neglecting the small terms involving $h^2/(12a^2)$, are[31]

$$L_{11} = \left(1 + \frac{N_x}{C}\right)\frac{\partial^2}{\partial s^2} + \left(\frac{1-\nu}{2} + \frac{N_\theta}{C}\right)\frac{\partial^2}{\partial \theta^2} - c_1 G\frac{\partial^2}{\partial t^2} \quad ,$$

$$L_{12} = \frac{1+\nu}{2}\frac{\partial^2}{\partial s \partial \theta} \quad ,$$

$$L_{13} = \nu\frac{\partial}{\partial s} \quad ,$$

$$L_{21} = \frac{1+\nu}{2}\frac{\partial^2}{\partial s \partial \theta} \quad ,$$

$$L_{22} = \left(\frac{1-\nu}{2} + \frac{N_x}{C}\right)\frac{\partial^2}{\partial s^2} + \left(1 + \frac{N_\theta}{C}\right)\frac{\partial^2}{\partial \theta^2} - c_2 G\frac{\partial^2}{\partial t^2} - \frac{N_\theta}{C} \quad ,$$

$$L_{23} = \left(1 + 2\frac{N_\theta}{C}\right)\frac{\partial}{\partial \theta} \quad ,$$

$$L_{31} = \nu\frac{\partial}{\partial s} \quad ,$$

$$L_{32} = \left(1 + 2\frac{N_\theta}{C}\right)\frac{\partial}{\partial \theta} \quad ,$$

$$L_{33} = 1 + \frac{N_\theta}{C} + c_3 G\frac{\partial^2}{\partial t^2} - \frac{N_\theta}{C}\frac{\partial^2}{\partial \theta^2} - \frac{N_x}{C}\frac{\partial^2}{\partial s^2} \quad .$$

Applying the reduction technique outlined in section 3.1.1 and setting n=1, one obtains an equation similar to (V.1) with the coefficients given by

$$A_1 = -\left(2(1-\nu^2)^3 P^3 + (3-2\nu)(1-\nu^2)^2 P^2 + (1-\nu)(1-\nu^2)P\right) \quad ,$$

$$A_2 = (1-\nu^2)^3 P^3 + \frac{(27-7\nu)(1-\nu^2)^2}{8}P^2 + \frac{(9-7\nu-2\nu^2)(1-\nu^2)}{4}P$$

$$+ \frac{1-\nu-\nu^2+\nu^3}{2} \quad ,$$

$$A_4 = G[2(c_2 + c_3)(1-\nu^2)^2 P^2 + (2-\nu)(c_2 + c_3)(1-\nu^2)P +$$

$$\left(\frac{1-\nu}{2}\right)(c_2 + c_3) \quad ,$$

$$A_5 = -G\{[2c_1 + \frac{3}{2}(c_2+c_3)](1-\nu^2)^2P^2 + [(2-\nu)c_1 + \frac{(11-\nu)}{4}c_2$$

$$+ \frac{(13-3\nu)}{4}c_3](1-\nu^2)P + \frac{(1-\nu)}{2}c_1 + (1-\nu^2)c_2 + (1-\nu)c_3\} \quad .$$

(iii) Solution

Letting

$$\xi = \tilde{x}/L \quad , \quad \eta = w/d \quad ,$$

Equation (V.1) may be rewritten as

$$\frac{\partial^2\eta}{\partial t^2} + \frac{A_2}{A_4}(\frac{a}{L})^4\frac{\partial^4\eta}{\partial\xi^4} + \frac{A_1}{A_4}(\frac{a}{L})^2\frac{\partial^2\eta}{\partial\xi^2} + \frac{A_5}{A_4}(\frac{a}{L})^2\frac{\partial^4\eta}{\partial\xi^2\partial t^2} = 0 \quad . \qquad (V.2)$$

To find the fundamental frequency an approximate solution is sought in the form

$$\eta = \bar{A}\Phi_1(\xi)\cos\omega t \quad . \qquad (V.3)$$

Substituting (V.3) into Equation (V.2), multiplying by $\Phi_1(\xi)$ and integrating with respect to ξ over the length one obtains

$$-\omega^2 + \frac{A_2}{A_4}(\frac{a}{L})^4\mu_1^4 + \frac{A_1}{A_4}(\frac{a}{L})^2C_{11} - \frac{A_5}{A_4}(\frac{a}{L})^2C_{11}\omega^2 = 0 \quad . \qquad (V.4)$$

Equation (V.4) may be solved to give the frequency

$$\omega = \left[\frac{A_1 (\frac{a}{L})^2 C_{11} + A_2 (\frac{a}{L})^4 \mu_1^4}{A_4 + A_5 (\frac{a}{L})^2 C_{11}} \right]^{\frac{1}{2}} .$$

APPENDIX VI

POTENTIAL ENERGY EXPRESSION FOR THE MEMBRANE THEORY

The strain-displacement relations according to the membrane theory are[31]

$$\varepsilon_x = \frac{\partial x}{\partial \tilde{x}} + \frac{1}{2}\left(\frac{\partial z}{\partial \tilde{x}}\right)^2 \quad , \tag{VI.1a}$$

$$\varepsilon_\theta = \frac{1}{a}\left(\frac{\partial y}{\partial \theta}\right) + \frac{z}{a} + \frac{1}{2a^2}\left(\frac{\partial z}{\partial \theta}\right)^2 \quad . \tag{VI.1b}$$

The middle surface curvatures κ_x and κ_θ are identical to the ones in (3.52).

Substituting the above relations into U_2 and integrating through the thickness gives

$$U_2 = \int\int \{N_x \frac{\partial x}{\partial \tilde{x}} + \frac{N_x}{2}\left(\frac{\partial z}{\partial \tilde{x}}\right)^2 + \frac{N_\theta}{a}\frac{\partial y}{\partial \theta} - \frac{N_\theta}{2a^2}\left(\frac{\partial z}{\partial \theta}\right)^2\} a d\tilde{x} d\theta \quad .$$

Assuming mode shapes given by (3.55) and applying the Rayleigh-Ritz technique (3.56) the following elements are obtained for the matrix [M] in Equation (3.57a):

$$m_{11} = (1-\nu)\int_0^1 \Phi'^2 d\xi + 2\left(\frac{a}{L}\right)^2 \int_0^1 \Phi''^2 d\xi \quad ;$$

$$m_{12} = (1-\nu)\int_0^1 \Phi'\Psi' d\xi + 2\left(\frac{a}{L}\right)^2 \int_0^1 \Phi''\Psi'' d\xi \quad ;$$

$$m_{13} = \left(\frac{a}{L}\right)\left[2\nu \int_0^1 \Phi'' d\xi - (1-\nu) \int_0^1 \Phi'^2 d\xi\right] \quad ;$$

$$m_{14} = \left(\frac{a}{L}\right)\left[2\nu \int_0^1 \Phi'' \Psi d\xi - (1-\nu) \int_0^1 \Phi' \Psi' d\xi\right] \quad ;$$

$$m_{15} = 2\nu \left(\frac{a}{L}\right) \int_0^1 \Phi'' \Phi d\xi \quad ;$$

$$m_{16} = 2\nu \left(\frac{a}{L}\right) \int_0^1 \Phi'' \Psi d\xi \quad ;$$

$$m_{21} = (1-\nu) \int_0^1 \Phi' \Psi' d\xi + 2\left(\frac{a}{L}\right)^2 \int_0^1 \Phi'' \Psi'' d\xi \quad ;$$

$$m_{22} = (1-\nu) \int_0^1 \Psi'^2 d\xi + 2\left(\frac{a}{L}\right)^2 \int_0^1 \Psi''^2 d\xi \quad ;$$

$$m_{23} = \left(\frac{a}{L}\right)\left[2\nu \int_0^1 \Phi \Psi'' d\xi - (1-\nu) \int_0^1 \Phi' \Psi' d\xi\right] \quad ;$$

$$m_{24} = \left(\frac{a}{L}\right)\left[2\nu \int_0^1 \Psi \Psi'' d\xi - (1-\nu) \int_0^1 \Psi'^2 d\xi\right] \quad ;$$

$$m_{25} = 2\nu \left(\frac{a}{L}\right) \int_0^1 \Phi \Psi'' d\xi \quad ;$$

$$m_{26} = 2\nu \left(\frac{a}{L}\right) \int_0^1 \Psi \Psi'' d\xi \quad ;$$

$$m_{31} = \left(\frac{a}{L}\right)\left[2\nu \int_0^1 \Phi \Phi'' d\xi - (1-\nu) \int_0^1 \Phi'^2 d\xi\right] \quad ;$$

$$m_{32} = \left(\frac{a}{L}\right)\left[2\nu \int_0^1 \Phi \Psi'' d\xi - (1-\nu) \int_0^1 \Phi' \Psi' d\xi\right] \quad ;$$

$$m_{33} = 2 + (1-\nu)\left(\frac{a}{L}\right)^2 \int_0^1 \Phi'^2 d\xi \quad ;$$

$$m_{34} = 2\int_0^1 \Phi\Psi d\xi + (1-\nu)\left(\frac{a}{L}\right)^2 \int_0^1 \Phi'\Psi' d\xi \quad ;$$

$$m_{35} = 2 \quad ;$$

$$m_{36} = 2\int_0^1 \Phi\Psi d\xi \quad ;$$

$$m_{41} = \left(\frac{a}{L}\right)\left[2\nu \int_0^1 \Phi''\Psi d\xi - (1-\nu)\int_0^1 \Phi'\Psi' d\xi\right] \quad ;$$

$$m_{42} = \left(\frac{a}{L}\right)\left[2\nu \int_0^1 \Psi\Psi'' d\xi - (1-\nu)\int_0^1 \Psi'^2 d\xi\right] \quad ;$$

$$m_{43} = 2\int_0^1 \Phi\Psi d\xi + (1-\nu)\left(\frac{a}{L}\right)^2 \int_0^1 \Phi'\Psi' d\xi \quad ;$$

$$m_{44} = 2 + (1-\nu)\left(\frac{a}{L}\right)^2 \int_0^1 \Psi'^2 d\xi \quad ;$$

$$m_{45} = 2\int_0^1 \Phi\Psi d\xi \quad ;$$

$$m_{46} = 2 \quad ;$$

$$m_{51} = 2\nu\left(\frac{a}{L}\right)\int_0^1 \Phi\Phi'' d\xi \quad ;$$

$$m_{52} = 2\nu\left(\frac{a}{L}\right)\int_0^1 \Phi\Psi'' d\xi \quad ;$$

$$m_{53} = 2 \quad ;$$

$$m_{54} = 2\int_0^1 \Phi\Psi d\xi \quad ;$$

$$m_{55} = 2 + (1-\nu^2)P[(\frac{a}{L})^2 \int_0^1 \Phi'^2 d\xi] \quad ;$$

$$m_{56} = 2 \int_0^1 \Phi\Psi d\xi + (1-\nu^2)(\frac{a}{L})^2 P \int_0^1 \Phi'\Psi' d\xi \quad ;$$

$$m_{61} = 2\nu(\frac{a}{L}) \int_0^1 \Phi''\Psi d\xi \quad ;$$

$$m_{62} = 2\nu(\frac{a}{L}) \int_0^1 \Psi''\Psi d\xi \quad ;$$

$$m_{63} = 2 \int_0^1 \Phi\Psi d\xi \quad ;$$

$$m_{64} = 2 \quad ;$$

$$m_{65} = 2 \int_0^1 \Phi\Psi d\xi + (1-\nu^2)(\frac{a}{L})^2 P \int_0^1 \Phi'\Psi' d\xi \quad ;$$

$$m_{66} = 2 + (1-\nu^2)(\frac{a}{L})^2 P \int_0^1 \Psi'^2 d\xi \quad .$$

The matrix [N] is identical to the one given in Appendix III for Washizu's shell theory.